EVALUATION OF WEARING SURFACE SYSTEMS FOR THE ORTHOTROPIC STEEL DECK OF THE SAN MATEO HAYWARD BRIDGE

A Thesis presented to

the Faculty of the Graduate School

at the University of Missouri-Columbia

In Partial Fulfillment

of the Requirements for the Degree

Master of Science

---

by

Ravi Sankar Chamarthi,

Vellore S. Gopalaratnam, Thesis Supervisor

December, 2012

The undersigned, appointed by the dean of the Graduate School, have examined the thesis entitled

EVALUATION OF WEARING SURFACE SYSTEMS FOR THE ORTHOTROPIC STEEL DECK OF THE SAN MATEO HAYWARD BRIDGE

Presented by Ravi Sankar Chamarthi,

a candidate for the degree of Master of Science and hereby certify that, in their opinion, it is worthy of acceptance.

Vellore S. Gopalaratnam

Sarah Orton

P. Frank Pai

EVALUATION OF WEARING SURFACE SYSTEMS FOR THE ORTHOTROPIC STEEL DECK OF THE SAN MATEO HAYWARD BRIDGE

Ravi Sankar Chamarthi

Dr. Vellore S. Gopalaratnam Thesis supervisor

ABSTRACT

Performance under static and fatigue loads are evaluated for two different wearing surfaces for possible use on the steel orthotropic deck of San Mateo Hayward Bridge in the bay area of California. The two wearing surface materials studied include a 2" thick (nominal) premixed polyester concrete (PC) and a 2" thick (nominal) epoxy asphalt concrete (EAC). Flexural specimens that comprise a "steel-plate - wearing surface" composite simulating the surfacing system and geometry specific to the orthotropic steel deck of the San Mateo Hayward Bridge are used for the static and fatigue tests. Flexural tests were conducted at different dynamic loading frequencies (0.0167, 1.0, 2.5, 5.0, 7.5, 10.0 and 15.0 Hz) and at several different temperatures (20˚F- 120˚F) to study the temperature dependency and loading rate effects. Following these tests, the fatigue tests were conducted on replicate EAC and PC composite specimens at each of room (70°F), cold (32°F) and hot (120°F) temperatures.

Both wearing surface systems performed well at the cold temperatures, surviving 10 million fatigue cycles. Both wearing surfaces experienced cracking at the room and hot temperatures prior to 10 million cycles and these cracks did not result in wearing surface delamination or local debonding. The comparative study in this exhaustive laboratory investigation has shown that the 2" thick PC material could perform equally well as the original EAC wearing surface existing on San Mateo Hayward Bridge.

ACKNOWLEDGEMENTS

I would like to greatly acknowledge the financial support from the California Department of Transportation for the research project. Also deserving of great thanks is Ric Maggenti from Caltrans for his committed interest and unstinted support for the research project. I would also like to thank ChemCo Systems Inc. and KwikBond Polymers for their assistance with placing of the epoxy asphalt concrete and polyester concrete wearing surface systems, respectively, on the steel plate for the test program. They also were generous in sharing their expertise on their respective product.

I would also like to thank Gissan Al Bahhash, Rex Gish, Richard Oberto and Brian Samuels of Engineering Technical Services at University of Missouri-Columbia for their timely assistance in the development of the test fixtures, instrumentation and electronics used for the project. Thanks are also due to Chris Novosel, Eric Schrader and Nathan Volkers our undergraduate research assistants, for their contributions to various phases of the research project.

I would like to extend special thanks to my advisor Dr. Vellore. S. Gopalaratanam for his valuable guidance, continuous support and immense patience.

Finally, I would like to thank my parents. This would not be possible without their encouragement and support.

TABLE OF CONTENTS

LIST OF FIGURES

LIST OF TABLES

LIST OF NOTATIONS

b	Nominal width of the specimens
DDR	Dynamic deflection ratio measured in the dynamic tests
d	Depth of the composite specimens
d_s	Depth of the steel plate
d_{ws}	Depth of the wearing surface
E	Modulus of elasticity of the transformed section
E_s	Modulus of elasticity of steel
E_{ws}	Apparent modulus of elasticity of the wearing surface
f	Frequency of the fatigue tests
F_{min}	Lower limit tensile fatigue load
F_{max}	Upper limit tensile fatigue load
F	Tensile load
$(I_{composite})_{steel\ basis}$	Moment of inertia of composite using steel basis
I_t	Moment of inertia of the transformed section
k	Stiffness of the composite specimen
L	Flexural span
M_{max}	Maximum design moment on the composite specimen
n	Modular ratio (E_s /E_{ws})
P	Flexural load
P_{max}	Upper limit load for the flexural fatigue tests
P_{min}	Upper limit load for the flexural fatigue tests
P_p	Tensile pull-out load
SDR	Static deflection ratio
T	Temperature
t	Time
V_o	Crack detection wire potential
$\bar{y}$	Depth of the neutral axis from top of the wearing surface
Δ	Net tensile deflection
δ	Net-deflection at the mid-span
ε	Strain
$\varepsilon_{(steel\text{-}bottom)}$	Strain at the bottom of the steel plate of the composite specimen
$\varepsilon_{(steel\text{-}top)}$	Strain at the top of the steel plate of the composite specimen
ε_s	Maximum steel strain in the composite specimen

ε_{ws}	Maximum wearing surface strain in the composite specimen
σ	Applied stress
σ_{max}	Upper limit fatigue stress
σ_{min}	Lower limit fatigue stress
σ_s	Maximum steel stress in the composite specimen
σ_{ws}	Maximum wearing surface stress in the composite specimen

1 Introduction

San Mateo Hayward Bridge is approximately 7 mile long. Opened in October 1967 it crosses the San Francisco Bay, linking the San Francisco peninsula to the East Bay. The 1.9 mile elevated navigation channel with a vertical clearance of 135 ft. is designed as an orthotropic section. It sports a 2" thick epoxy asphalt concrete wearing surface, placed in two 1" layers and bonded to the steel deck plate with an epoxy-asphalt bond coat. It covers the entire 418,000 sq. ft. of orthotropic steel deck, extending for approximately 5,500 linear feet over a width of six lanes. Orthotropic part of the bridge comprises of 14 spans of 292 ft., a main channel span of 750 ft. and two flanking cantilevered anchor spans of 375 ft. each.

Fig. 1.1 San Mateo Hayward Bridge, California (Photo by John Huseby, CalTrans)

The steel deck consists primarily of $^{5}/_{8}$" thick steel plate but is ¾" thick at higher stressed sections. It is an 80 ft. wide deck with two 12 ft. wide lanes and a 13 ft. wide lane on each side of a 2.5 ft. wide concrete median barrier. San-Mateo Hayward Bridge is a true orthotropic design because the steel plate serves as the top flange for both floor beams and for the joists that span between the beams. All the metal surfaces are coated

with self-curing inorganic zinc paint. This zinc coating is applied to protect the steel surface from corrosion before the application of wearing surface (ASCE April 1968).

Reasons for the selection of epoxy asphalt concrete as the original surfacing on San-Mateo Hayward Bridge were (ASCE April 1968):

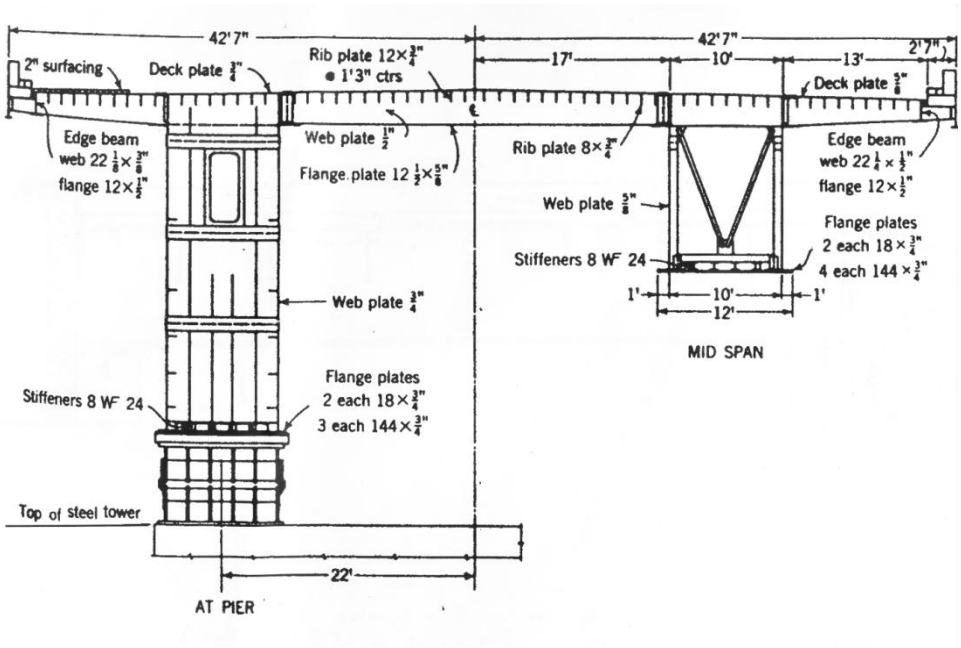

Fig. 1.2 Cross-section details of San Mateo Hayward Bridge, California

- Satisfactory adhesion to the steel deck at varying service temperatures changes and traffic loads.
- Ductility to follow changes in deck dimensions due to temperature without breaking bond.
- Sufficient fatigue resistance throughout the anticipated range of ambient temperatures to perform without cracking

- Bond strength between the epoxy asphalt and inorganic zinc exceeds 200 psi @ 77°F.

In 2002, after nearly 35 years of the service life of the bridge, fatigue cracks were observed on the wearing surface along the direction of the traffic above the welds of the longitudinal ribs to the steel decks. This prompted investigations to look for possible replacements to the wearing surface including potential reapplication of the epoxy asphalt concrete wearing surface that had performed well as the original and only wearing surface.

1.1 Research objectives

Caltrans contracted with University of Missouri-Columbia in late 2010 to undertake a systematic evaluation of two wearing surface systems including (1) an Epoxy Asphalt Concrete (EAC) and (2) a Polyester Concrete (PC) wearing system. The EAC is a modern day version of the original wearing surface system on San-Mateo Hayward Bridge that had performed well over 3 decades. The PC wearing system developed in-house by Caltrans (Maggenti, 2001) and has been extensively used on concrete bridge decks in California with great success. The University of Missouri in Columbia research program was customized to simulate the loading and environmental conditions likely to be experienced by the wearing surface materials on the San Mateo Hayward Bridge in the bay area of California. The specific objectives of this research endeavor include studies of:

1. The flexural fatigue performance of polyester and an epoxy-asphalt concrete wearing surfaces at three different test temperatures (32° F, room temperature 70°F, and 120°F).
2. The static and fatigue stiffness contributions of the two wearing surface systems to the steel deck plate at the three test temperatures and the potential reductions in deck fatigue stresses due to transverse bending and related composite action.
3. Relevant physical and fundamental mechanical properties of the wearing surfaces such as density, air void content, elastic modulus and tensile bond strength.
4. The rate sensitivity of the two wearing surface systems was established by testing the composite specimens at different fatigue test frequencies as noted in the research program (frequencies used were:1, 2.5, 5, 7.5, 10, and 15 Hz in addition to reference quasi-static rate)
5. The static failure tests to establish the strength and types of failures expected under fatigue loading in service.
6. Tensile cracking including crack initiation, crack patterns and typical maximum widths. Potential for growth of cracks due to post-cracking fatigue loads was also investigated along with qualitative measures of cracking using resistivity tests.

1.2 Organization of the report

Chapter 2 includes literature review including several other research projects completed at the University of Missouri-Columbia on wearing surfaces for orthotropic bridges. Chapter 3 provides experimental program for the research with explanations of test set-up and instrumentation used for this research. Chapter 4 details procedures used

for test program to study the influence of various parameters that influence wearing surface. Chapter 5 presents results from the research program and exhaustively details associated implications on the performance of the wearing surface systems. Chapter 6 includes conclusions and recommendations based on results presented here as well as other published information and related practical considerations.

2 Literature Review

Orthotropic bridge technology was first developed after World War II to replace the bridges destroyed during the war. The shortage of time and materials at that time provided the impetus for the development of orthotropic bridges. Such bridges are popular because they are light-weight, facilitate long spans, use materials optimally, and are economically attractive.

The term orthotropic is derived from the terms “orthogonal” and “anisotropic” (ortho-tropic). “Orthogonal” refers to properties along two directions at 90˚ with respect to each other and “anisotropic” refers to the fact that the structure has directionally dependent properties. A typical orthotropic deck comprises a steel deck plate supported on longitudinal ribs (either open ribs or closed trapezoidal ribs), which, in turn, are supported on the transverse cross beams. These elements are often welded together and act as an integral composite structure. The steel deck carries a wearing surface on top to provide comfortable ride quality, good traction, and corrosion protection for the deck. The fatigue performance of this wearing surface under service conditions poses some challenges in its design, and is the focus of the discussions to follow in this chapter.

2.1 Background and motivation

Wearing surfaces have typically faced problems with shoving, rutting, fatigue cracking, and delamination. These problems have been amplified in the recent past because of larger traffic volumes, higher permissible loads, and more severe braking and lane-changing forces. Wearing surfaces on steel bridge decks need to fulfill several

functional requirements (Seim and Ingham 2004, FHWA Manual 2012). They must provide:

- Acceptable performance over a range of temperatures encountered in service
- A skid resistant surface that uses polish-resisting aggregates (superior traction)
- Fatigue resistance against repeated dynamic loading
- Smooth ride quality, overcoming undulation of the deck weld and joints
- Good bond characteristics to the smooth steel deck
- Resistance to water infiltration, mitigating potential corrosion of the steel deck

In the past, mechanical characteristics of wearing surfaces have often been neglected in the overall structural design of such decks. The wearing surfaces have also not been engineered systematically and are used merely for their basic functional characteristics. Recent analyses and testing have demonstrated that when the composite action of the wearing surface with the steel deck plate is considered, one can reduce transverse bending stresses in the deck plate and hence extend the fatigue life of the deck plate (FHWA, 2012, and Gopalaratnam and Chamarthi, 2012).

Various wearing surface systems, such as bituminous surfacing systems, polymer surfacing systems, and concrete surfacing systems, have been developed for use on orthotropic bridges in the last several decades. Bituminous wearing surfaces are thermoplastic in nature, use asphalt as the primary binder and are typically applied thick. Gussasphalt, a poured asphalt, and mastic asphalt, which use higher binder content, are two common types of bituminous wearing systems that are applied hot. The stiffness contribution of bituminous wearing surfaces to the composite deck is influenced

significantly by temperature. Neither of the bituminous wearing surfaces mentioned earlier have been used on major orthotropic bridges in United States, although they appear to be popular in Europe. A mix of bituminous hardener and epoxy resin resulting in a thermosetting material popularly termed "epoxy asphalt" has been used quite successfully on several major orthotropic bridges in the United States, particularly in California.

Three popular types of polymer surfacing systems include: a slurry system, a multilayer broom and seed system, and a premixed concrete system. Polymer concrete wearing surface materials on orthotropic steel decks are typically of thermosetting type. Popular types of polymers include two-part epoxy resins, polyurethanes, methacrylates, and urethanes. The slurry and multilayer broom and seed systems are mostly applied as thin wearing surfaces (3/8" –1/2" thickness). Thin polymer concrete wearing surfaces do not contribute to the overall deck stiffness in any significant manner. Therefore, such surfaces do not exhibit significant variation in stiffness with temperature, even while the polymer wearing surface is temperature-sensitive. Such thin surfacing helps in keeping the dead load on the deck relatively low. Polyester Concrete (PC), a premixed system, is typically applied as thick surfacing (1 ½" - 2" thickness) and has been used extensively on various reinforced concrete bridge decks by Caltrans (Maggenti, 2001). PC is an engineered material with consistent properties providing chloride protection, smooth ride quality, high durability, and ease of placement. It can be used for a wide range of service temperatures. Textured PC, like properly engineered EA wearing surface can provide long-term skid resistance desired for good traction.

2.2 Wearing surface research at University of Missouri-Columbia

Several projects have been conducted at the University of Missouri-Columbia since the 1990's to comprehensively study the mechanical performance of wearing surfaces for steel orthotropic decks. These included research customized for the Poplar Street Bridge in St. Louis (Rigdon, 1990, Hartnagel, 1993, Cao, 1998) and the Bronx Whitestone Bridge in New York (Barret, 2003). The Poplar Street Bridge was constructed in 1967 with a wearing surface consisting of two 0.5" layers of epoxy and one 1.5" layer of rubberized asphalt concrete wearing surface (Gopalaratnam et al., 1999). The first wearing surface was serviceable until 1983, following which two other wearing surfaces had to be replaced after very short service lives. These studies at the University of Missouri, which spanned several decades, included measuring field strains on the Poplar Street Bridge, conducting regular inspections of the performance of field test-patches of various wearing surface materials on the Poplar Street Bridge, and performing extensive laboratory fatigue testing with simultaneous variations in the test temperature. These studies are briefly described in the following sections.

2.2.1 Field strain measurements

Strain gage rosettes were attached to the underside of the orthotropic deck of the Poplar Street Bridge to measure service stresses in order to study strain histograms and peak strain events on the bridge deck and consequently the wearing surface. The strain gage information recorded was used to determine the load levels to be used in the laboratory fatigue test. The gages were monitored continuously during an eight-week window (Hartnagel, 1993). The maximum steel strains measured in service were 250 με. Based on these strain measurements, an effective width of 8.5" of the tire patch (in the

longitudinal direction) was estimated. Maximum flexural stresses in the wearing surface of 1,895 psi at cold temperatures and 995 psi at hot temperatures were computed based on the experimental and associated analytical procedures used. The upper limit flexural fatigue stresses in the laboratory tests were observed to be nearly 53% in excess of the design loading per AASHTO.

2.2.2 Quality control inspections of the test patches

Test patches placed on the Poplar Street Bridge to evaluate the service performance of wearing surface systems were inspected at regular intervals. Polymer Concrete wearing surface test patches were placed in August 1992, and the inspections began in September, 1992. Several inspections were carried out to study the degradation in the performance of the wearing surface during a five year period (starting from the first month of placing of the test patches). Other companion tests of investigation include tensile pull-out tests and resistivity tests.

Pull-out load tests were performed in accordance with Appendix-A of ACI 503R. Pipe caps were glued at predetermined locations of the wearing surface using Devcon (a quick setting epoxy) and Transpo T-71 methyl methacrylate (MMA). Transpo T-71 was observed to perform well after the preliminary pull-out tests. Cores of a nominal diameter of 2" were used in the study. A pull-out device using a strain gage based load cell allowed measurement of peak pull-out loads. In most of the pull-out tests the failures were observed to be at the glue line between the wearing surface and the pipe caps. The tensile bond strength was approximately in the 500 psi range. The pull-out stress was

temperature dependent; at cold temperature the pull-out strengths were observed to be higher than those at room temperatures.

Resistivity tests were performed in accordance with ASTM D 3633-88. Soap water was allowed to penetrate the cracked wearing surfaces. Dams made from wooden frames with soap water soaked sponges inside the frames facilitated measurement of resistivity values between the top of the wearing surface and the steel deck plate of the Poplar Street Bridge. When cracks were through the thickness of the wearing surface they would record a zero resistance value. Resistance values in excess of 700,000 Ω were typically recorded, indicating that most service cracks were not through-thickness cracks.

2.2.3 Flexural fatigue tests

A series of flexural fatigue tests were performed customized to the conditions of the Poplar Street Bridge, simulating winter and summer deck temperatures on wearing surface-steel composite specimens and the rib-to-rib spacing taken as the span of the test specimens tested. Specimens of lengths 15" with five wearing surfaces, including two epoxy concretes, a methyl methacrylate concrete, a rubberized asphalt concrete, and an epoxy asphalt concrete were evaluated (Rigdon, 1990). In the thin polymer concrete wearing surface systems tensile cracking was the predominant mode of failure when simultaneously subjected to fatigue loads and very cold temperatures (~ 0ºF).

Six wearing surfaces, two asphaltic concretes and four polymer concretes, were evaluated for potential cracking and delamination (Hartnagel, 1993). The laboratory flexural fatigue tests were performed at stress levels 5% higher than the maximum values measured in the field. Test patches on the bridge were investigated for fatigue cracks. The

asphalt-based wearing surfaces exhibited shoving and rutting within a month, perhaps from not tightly controlling the construction temperatures recommended. One type of polymer concrete wearing surface (Transpo T-48) was observed to clearly perform better in both laboratory and field tests compared to the other materials tested.

Static flexural tests on polymer concrete beams (without the steel base plates) and compression tests on polymer concrete cylinders were carried out in another related study to establish the fundamental material properties (Cao, 1998). Polymer concrete beams (T-48 polymer concrete) were of 2" x 2" x 10.5" size, whereas the cylinders were 2" in diameter and 4" in length. It was observed that the modulus of elasticity, flexural strength, and compressive strength increased with decrease in temperature. The beams tested at room and cold temperatures (20°F) exhibited brittle failures, while the beams at hot temperatures exhibited softening type of failures. Polymer concrete cylinder failures were due to shear at a local level for tests at all three temperatures. As expected, it was observed that the fatigue life increased with a decrease in the upper limit flexural fatigue stress. It was observed that at all three test temperatures (cold, room and hot) increasing the loading rate increased the stiffness of the beams. Loading rate effects were observed to be significant at the higher test temperatures.

Three different repair materials/techniques, including the use of a methyl-methacrylate (Transpo MMA), an asphalt based material (cold-pour Pavon asphalt), and a bonded fiber reinforced concrete plate (SIMCON) were studied. Transpo MMA and Pavon asphalt were effective as crack sealants, but had relatively short fatigue lives. The

fatigue cracks repaired bonding precast SIMCON plates were observed to be promising even after the application of the several million fatigue cycles.

Two different types of thin polymer concrete wearing surfaces -- PolyCarb, a multi layered broom and seed type of polymer concrete wearing surface and Transpo T-48, a slurry-based polymer concrete system were evaluated for use on the Bronx Whitestone Bridge (NY, Barrett, 2003). Specimens of 15" length with a wearing surface depth of 3/8" and a base steel plate of 9/16" were used for the composite specimens. Uniform loading (a neoprene pad was used for the application of load) and concentrated loading were the two type of loading configurations used to study the differences in the associated failure patterns. Specimens tested with uniform loading did not crack or debond, but specimens loaded with a concentrated load did exhibit tensile cracking. Both wearing surfaces were flexible and demonstrated a good bond to the steel plate. Neither material contributed significantly to the overall stiffness of the composite specimens. Neither wearing surfaces exhibited measurable temperature sensitivity measured using composite stiffness characteristics, perhaps due to the minimal contribution of the thin wearing surface to the overall composite stiffness.

2.3 Stresses on the wearing surface and steel deck in orthotropic bridges

Orthotropic steel decks are typically more flexible than other types of bridge decks. Wearing surfaces are typically subjected to biaxial stress states. Wearing surface stresses due to longitudinal bending are predominantly compressive, except at the floor beams where, because of the negative moments, wearing surfaces experience tensile stresses. The stresses in the wearing surface due to the transverse bending between the

supporting ribs are also compressive. However, the stresses critical to the design of wearing surfaces are the tensile stresses in the transverse direction immediately above the longitudinal ribs. Fig. 2.1 from Wolchuck (2002) illustrates the competing effects that are likely to occur in a wearing surface-steel deck composite system.

Stresses in the wearing surfaces and steel caused by the transverse bending effects can be accurately computed using a finite strip approach instead of a more involved 3D numerical modeling of the orthotropic deck. Wearing surface-steel composite can be idealized as a multi-span continuous beam consisting of five or seven simply supported spans (Rigdon, 1990, Rigdon et al., 1991, and Gopalaratnam et al., 1993 - See also Fig. 4.2).

AASHTO LRFD design limits the depth of the steel deck plate to a minimum of 14 mm or 4% of the span between the longitudinal stiffeners (Seim, 2004). This results in stiffening of the deck plate and an increase in deflection ratio from 300 to 1200. Several bridges constructed with thin wearing surfaces showed early failures, which have resulted in changes in AASHTO, requiring thick wearing surfaces. Various changes were proposed in the fifth edition of the AASHTO LRFD Bridge Design Specifications related to orthotropic steel deck (OSD) bridges as detailed below.

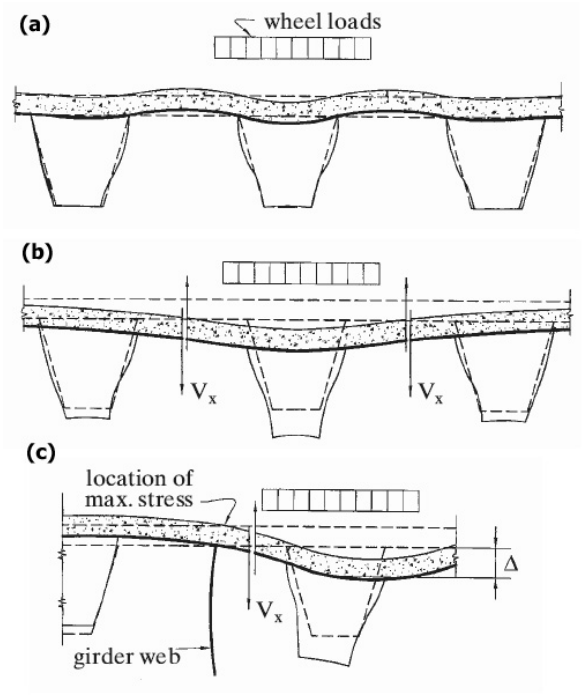

Fig. 2.1 *Flexural response and shear forces on the wearing surface-steel composites caused by relative displacements and transverse bending. (a) Closer to floor beams (b) Midway between the floor beams (c) Near the main girder (Wolchuck, 2002)*

AASHTO LRFD specifies that the 32 kip truck axle represents a tandem of two 16 kip axles separated by 4 ft. (Kozy et al., 2011). Each wheel of 16 kip axle is properly modeled as two closely spaced 8 kip wheels 4 ft. apart. The single-axle simplification is acceptable for main members not directly subjected to axle loads such as girders, floor beams and truss members. The more elaborate analysis with a distributed wheel load at the contact area is required with the elements directly loaded by wheels, such as expansion joints, and the orthotropic steel deck (including the wearing surface).

Wearing surface deterioration and cracking are influenced by the stiffness (thickness) of the steel deck plate. Thin wearing surfaces may be expected to perform better, as they are more flexible, but in contrast, thick wearing surfaces lessen the stresses

in the wearing surfaces and steel plate (Wolchuck, 1999). The influence of the thickness of the steel plate in the reduction of stresses is reported to be less significant than the influence of temperature on the wearing surface (Kolstein and Wardenier, 1997). Elastic modulus of the wearing surfaces is temperature-dependent because the resin used in most of the wearing surfaces is temperature sensitive. The variation of elastic modulus with temperature influences the stress levels in the steel deck plate as well as the wearing surface, affecting the fatigue life of both of these deck components. Different wearing surface materials popularly used for the wearing surfaces exhibit measurably different mechanical performance. Asphalt surfacings are more temperature sensitive than the polymer concrete surfacing. Wolchuck R. (1999) has compiled data on the variation of elastic modulus with temperature for various wearing surface composites (Fig. 2.2). Many wearing surfaces used with the steel deck plate are also typically viscoelastic in nature. They act in a linear elastic manner only when they are rigid at cold temperatures (where viscous effects are less significant). At room and hot temperatures they exhibit viscoelastic characteristics. Most wearing surfaces also often exhibit loading rate sensitivity.

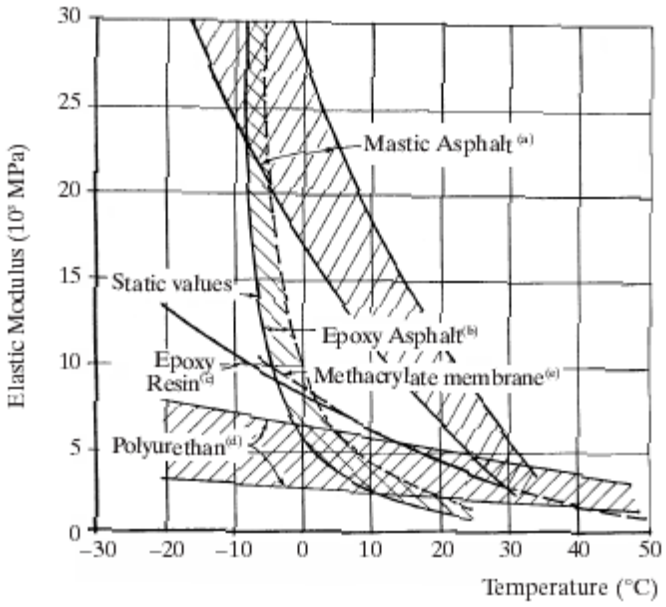

Fig. 2.2 Elastic modulus of various wearing surfaces obtained from tests of composite specimens (Wolchuck, 2002)

Modulus of the epoxy asphalt wearing surface back calculated from static tests was observed to be in the 48-72 ksi range and those from dynamic tests (5Hz) was observed in the 49-92 ksi range in flexural tests conducted by the California Department of Transportation (1981 Report to Caltrans). These room temperature tests were completed to evaluate the fatigue performance of epoxy asphalt mix for use in the renovation of the Golden Gate Bridge project. The composite specimens used comprised a 4" x 15" x 7/16" steel base plate with a 2" thick epoxy asphalt wearing surface.

Results from four point bend tests performed on steel-wearing surface composites of epoxy asphalt, stone mastic asphalt (SMA), and steel fiber reinforced high performance concrete (SFRHPC) are reported by Sugioka (2009). He used composite specimens with a wearing surface depth of 40 mm (1.57") and steel depth of 6 mm (0.24"). Specimen length of 420 mm (16.54") and a width of 50 mm (1.97") were used to study the influence of loading rate and temperature. Stress reduction factors (SRF) were

reported to decrease with a decrease in temperature and with an increase in loading frequency. SRF was defined as the ratio of steel stress from a composite specimen with wearing surface to steel stress on a specimen without the surfacing.

Bo et al. (2011) report that composite response is viscoelastic even while the steel base plate does not exhibit viscoelastic behavior in room temperature test. Based on 3-point flexural tests on composite specimens of epoxy asphalt (50 mm wearing surface depth, 2" nominal) bonded to a steel plate(14mm depth, 0.55") of plan dimensions 380 mm (15" nominal length) and a 100 mm (4" nominal width) they report that the strain distribution was linear. Strains in their tests were measured using foil gages glued along the composite specimen depth.

Dynamic tests were performed by Smith and Cullimore (1987) on a section of steel deck plate of vee-stiffener using a 20 mm thick rubber disc to simulate loading from heavy vehicle tires. 50 mm thick mastic asphalt wearing surface on the steel plate was subjected to loads applied at several different loading rates in their tests. Strain gages glued at several locations on the stiffener were used to measure stress reduction factors in the 64-84% range at room and hot temperatures and 84-98% at cold temperatures (steel stress in the composite specimen compared to the bare steel plate). No recommendations for stress reduction rules for OSD's were made, as Smith and Cullimore acknowledge the wide ranges of service parameters that affect operating temperature and loading rate.

Composite action of the wearing surface and the steel deck plate play a major role in the reduction of stresses in both wearing surfaces and steel-deck plate. Medani (2001) has compiled a fairly comprehensive review of composite action between asphalt

surfacing and orthotropic steel decks. The bonding layer or the waterproofing membrane used between the wearing surface and the steel deck plate has been reported by some researchers to influence the composite characteristics. The temperature sensitivity of the low modulus bond or tack coat, as well as its thickness, play a role in the overall composite response as well (FHWA Manual, 2012). In such cases, wearing surfaces can be subjected to lower strains, and in some cases, poor bond could result in wearing surface and the steel plate independently resisting bending. Fig. 2.3 illustrates experimentally measured strains (Hemeau et al., 1981) along the depth of the wearing surface, steel deck plate, and bonding layer exhibiting the nonlinear strain distribution and shear lag effects.

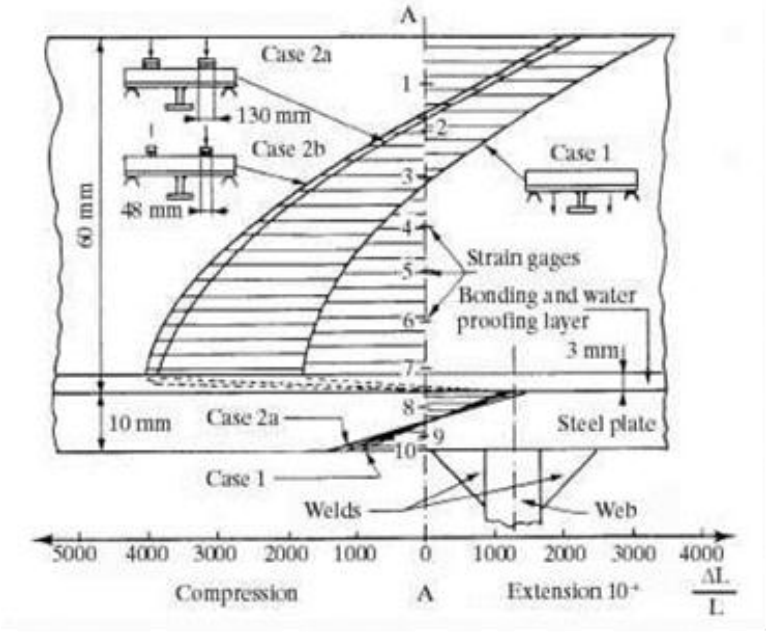

Fig. 2.3 *Strains measured along the depth of the wearing surface using strain gages in thick mastic aspahlat for differernt loading cases exhibiting nonlinear strain distribution (Hemeau et al., 1981)*

Stress reduction on the orthotropic deck due to composite action was studied (Sugioka, 2009) on three different wearing surface composites (epoxy asphalt with an expanded metal lath, epoxy asphalt without the expanded metal lath, and a stone mastic asphalt without the reinforcing lath).

Three different methods were used to estimate the percent of composite action. (1) The "Linear Elastic" model estimates composite action as a ratio of the difference between the experimentally obtained stiffness of the composite specimen and the bare steel stiffness to the difference between the theoretically calculated composite stiffness and bare steel stiffness. The composite action percentages Sugioka obtained from this approach were very low (13% in some cases), and speculated that assuming asphalt to have linear distribution may not be accurate. (2) In the "Steel Strain Comparison Method", Sugioka compared the strain at the top and bottom of the steel plate, and observed that if these strains are equal in magnitude but opposite in signs, there is no composite action. The ratio of the difference between the top and bottom strains of the bare steel plate to the strain at the bottom of the steel plate has been used to compute percent composite action.

Composite action= $\frac{\varepsilon_{(steel-bottom)}-\varepsilon_{(steel-top)}}{\varepsilon_{(steel-bottom)}}$

This equation would imply that for full composite action (left hand side value = 1), $\varepsilon_{(steel-top)}$ equals 0. This implies that the neutral axis of the composite specimen has to be located at the wearing surface-steel interface, a condition which is unrealistically restrictive. (3) In the third method, termed by Sugioka as the "Slip" method, composite action is quantified as the ratio of the difference between slip between the wearing

surface and the steel plate (when acting as a composite) and slip when no composite action is present to the slip when no composite action is present. Since values of slip were not practically measurable in Sugioka's experiments, this third method to quantify composite action remains largely conceptual.

Detailed analytical and experimental analyses on composite action have been presented by Gopalaratnam (2009) and Gopalaratnam and Chamarthi (2012) for a range of wearing surface moduli and depths, test temperatures, and loading frequencies. Composite action in polyester concrete wearing surface on steel deck plate has been experimentally documented where the strain distribution along the depth of the composite specimen has been reported to be linear in the service load levels (uncracked elastic behavior) with no slip at the bond coat interface at all test temperatures (cold 32^{o}F, room 70^{o}F and hot 120^{o}F temperatures). This is unlike measurements reported for asphaltic wearing surface systems by Hemeau et al. (1981) and Smith and Cullimore (1987) where interface slip have been reported or where nonlinear strain distribution has been reported (Hemeau et al., 1981, Fig. 2.3). Gopalaratnam and Chamarthi (2012) have also studied the strain distribution characteristics in a room-temperature static failure test on a polyester concrete steel composite system, where progressive tensile cracking and its influence on progressive degradation of composite stiffness has been documented.

Fatigue problems of orthotropic bridges at the deck/rib junctions and rib/floor beam junctions are complicated in geometry and material characterizations, and therefore pose challenges to analytical and numerical modeling. For major bridges, a service life of 20 to 30 years is required. Assuming 10,000 vehicles/day/lane pass over the bridge, a

theoretical value of 10 to 15 million fatigue cycles is obtained for the service life of 20 to 30 years (Seim and Manzanarez, 2004). Fatigue design is often completed based on a combination of laboratory testing, actual service experience, and engineering judgment. The full potential of OSD bridges in United States can be exploited (Kozy et al., 2011) with proper design and detailing, well-executed fabrication, and quality construction.

3 Experimental Program and Test Set-Up

3.1 Scope of the experimental program

The primary motivation for the research reported here was to evaluate the mechanical performance of two different wearing surfaces for possible use on the orthotropic steel deck of the San Mateo – Hayward Bridge. Flexural specimens that typically comprise of a "steel-plate - wearing surface" composite simulating the surfacing system on the orthotropic steel bridge deck were used for the static and fatigue tests. Different types of tests as detailed in this section were completed to accomplish the overall research objective.

Flexural tests were performed on wearing surface-steel composite specimens at static and dynamic loading rates and at different temperatures to compare the composite stiffness as influenced by temperature and loading rate. Flexural fatigue tests were carried out to evaluate the fatigue performance of the wearing surfaces. Static failure tests were performed to study the potential types of failures. Composite specimens of Polyester Concrete were placed by Kwik Bond polymers at University of Missouri-Columbia and Epoxy Asphalt Concrete were placed by ChemCo systems at their facility. All the specimen of Polyester Concrete (24) and Epoxy Asphalt Concrete (22) were numbered to match with the numbers provided by the manufacturers. Apart from the flexural tests, quality control tests were performed to evaluate the tensile bond strength of the wearing surface to the steel plate. Post-test crack detection and resistivity tests were also carried out to further map crack characteristics (crack widths, lengths, distributions and patterns).

Static flexural tests were conducted to measure the stiffness of the composite specimens. The elastic load-deflection behavior was observed under slow (0.0167 Hz) sinusoidal loading unloading tests. Values of the modulus of elasticity, static deflection ratio, stress in the steel plate and the stress in the wearing surfaces were calculated from the measured stiffness assuming uncracked elastic composite behavior. These tests were conducted at temperatures in the range of 120°F to 20°F in nominal steps of 10°F. Table 3-1 shows the specimens used for the static flexural tests. (Table A1 in the appendix shows the physical properties of all EAC and PC specimens fabricated)

Dynamic tests were performed to study the loading rate sensitivity of the wearing surface-steel composite specimens. Dynamic tests were carried out at several different loading rates (1 Hz, 2.5 Hz, 5 Hz, 10 Hz, and 15 Hz in addition to the earlier mentioned static tests conducted at a loading rate of 0.0167 Hz). Modulus of elasticity, dynamic deflection ratio, stress in the wearing surface and stress in the steel plate were calculated from the measured stiffness values assuming elastic composite action. Dynamic tests were also performed at the prescribed test temperatures (identical to those used in the static flexural tests). Table 3-1 shows the specimens used for dynamic flexural tests.

Table 3-1 Specimens used in the various tests (non-fatigue test configuration)

Specimen Numbers	Static flexural tests1	Dynamic flexural tests2	Static flexural failure tests3	Tensile pull-out tests2	
Epoxy Asphalt Concrete (EAC)	4, 5	6, 7	Reused after static tests 4, 5	1, 2, 3	Reused after dynamic tests 6,7
Polyester Concrete (PC)	8, 9	10, 11	Reused after static tests 8, 9	6, 7	Reused after dynamic tests 10

1 Conducted at temperatures in the range of 20°F to 120°F in nominal steps of 10°F
2 Conducted at controlled temperatures of 32°F, 70°F and 120°F
3 Conducted at room temperature of 70°F

Static flexural failure tests were performed to study the types of failure and failure patterns in the wearing surface. Composite specimens were tested to failure at room temperature to study the load-deflection behavior and potential types of failure. Cracks on the wearing surface were monitored using the crack detection wire. Potential delamination between the wearing surface and the steel plate was monitored using end-slip gages. Two specimens of each wearing surface were used for the static flexural failure tests (Table 3-1). As noted in Table 3-1 the specimens used for the static flexural tests were reused for the static failure tests. These specimens were neither cracked nor damaged in any manner prior to the static failure tests.

Table 3-2 Specimens used for flexural fatigue tests

Specimen Numbers	Wearing Surface Temperatures		
	Room (70°F)	Cold (32°F)	Hot (122°F)
Epoxy Asphalt Concrete	10, 11, 17, 18, 19	12, 13, 14, 15	20, 21, 22
Polyester Concrete	16, 17, 18, 19	11, 12, 14, 15	13, 20, 21, 22, 23, 24

Flexural fatigue tests were carried out to evaluate the fatigue performance of the two wearing surface materials. Cracks in these tests were monitored using crack detection wire. Potential delamination between the wearing surface and the steel plate was monitored using end slip gages. Stiffness was monitored during the fatigue test. These tests were conducted at the three prescribed temperatures. Although nominally four specimens were to be tested at each temperature, the actual number of specimens tested varied due to constraints in test schedule and availability of virgin specimens. Table 3-2 shows the specimens used in the flexural fatigue test.

Tensile pull-out tests were performed to study the tensile bond strength between the wearing surface and the steel plate. These tests were also performed at three prescribed temperatures.

Cracking characteristics were studied post-test for all specimens that exhibited wearing surface cracking (static failure as well as flexural fatigue tests). Crack widths, length, distribution and pattern were documented using a template with grid pattern to facilitate crack mapping.

Following crack mapping, a sampling of specimens of each wearing surface was subjected to a resistivity test. Detergent was added to water to reduce the surface tension and allow water to infiltrate even the finest cracks. Electrical resistivity was measured between the top of the wearing surface and the steel plate at hourly intervals after initial saturation (Explained in detail in section 4.8). Results from this test (1) identify through thickness cracking and (2) provide a qualitative estimate of the severity of cracking in the wearing surface material. Low resistance (in the ohm range) indicates the wearing surface had a crack through the thickness of the wearing surface. Resistance in the mega-ohm range (even after several hours the cracked specimen is ponded with water) represents a crack that is not through the depth.

3.2 Specimen fabrication

3.2.1 Fabrication of steel plates

Steel plates were fabricated at University of Missouri-Columbia. A36 hot rolled steel with nominal yield strength of 36 ksi was used for the base plate material for all the specimens (Epoxy Asphalt Concrete (EAC), Polyester Concrete (PC) and bare steel (BS)

specimens). This grade of steel is identical to that used on the San Mateo Hayward Bridge. Steel plates were fabricated using 0.625" thick stock with plan dimension of 18" x 4". As the longitudinal ribs on the bridge were spaced center to center at a distance of 15" the specimens were fabricated at a length of 18" to facilitate space for the supports. Two steel tabs were welded one on each end of the steel plate. These tabs act as supports to four rollers that transmit the reactions on to the upper crosshead of the test machine. Steel plate tabs with dimensions of 6" x 2" x 0.625" were welded at a distance of 1.5" from the length of the edges of the steel specimens. Fig. 3.1 illustrates the plan schematic of the steel plate template on which the wearing surfaces were placed.

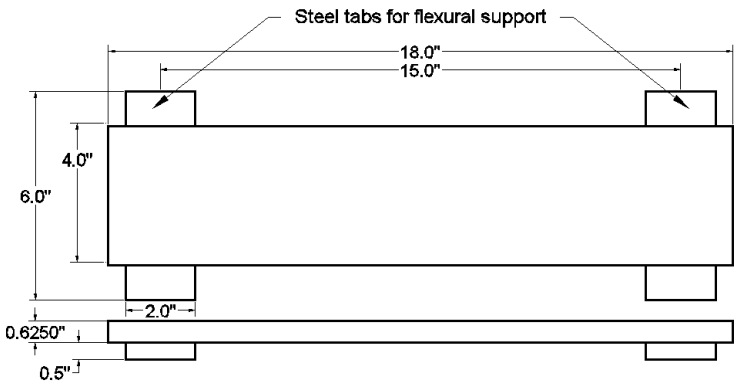

Fig. 3.1 *Plan view schematic of the steel plate template used for fabricating composite specimens.*

3.2.2 Fabrication of Epoxy Asphalt Concrete specimens

Steel plates fabricated at the University of Missouri-Columbia were sent to ChemCo Systems for placement of the Epoxy Asphalt Concrete wearing surface. Details of the placement of EAC wearing surface was obtained through personal communication from ChemCo Systems. Steel molds were used in the placement of the EAC wearing surface (Fig. 3.2a).The steel plates were coated with an inorganic zinc coating named Hempadur zinc 15360 after they were sand blasted to near white metal finish as per SSPC

SP-10. A Type B1d (ChemCo systems) bond coat and binder mix was spread on to the steel plate at a rate of 0.66 L/m^2 (Fig. 3.2b) using a paint brush. The EAC mix was made with the same 3/8" minus dense graded mix using 100% crushed basalt aggregate. Two heated components of epoxy resin were properly metered and mixed with aggregate to achieve the mix. The binder to stone ratio of 6.5% (by weight) was used for the EAC mixture. The EAC specimens were prepared in a steel mold at 121°C. The wearing surface was placed in two 1" lifts, first a leveling course and next a finish course. Another bond coat and binder layer at a rate of 0.33 L/m^2 was sprayed after the leveling course was compacted using a 4"x4" plate attachment (Fig. 3.2d). The finish course was placed next and compacted as described above to achieve the 2" wearing surface. After an accelerated cure of 4 hours at 121°C, the specimens were removed from the mold and weights were measured by water displacement.

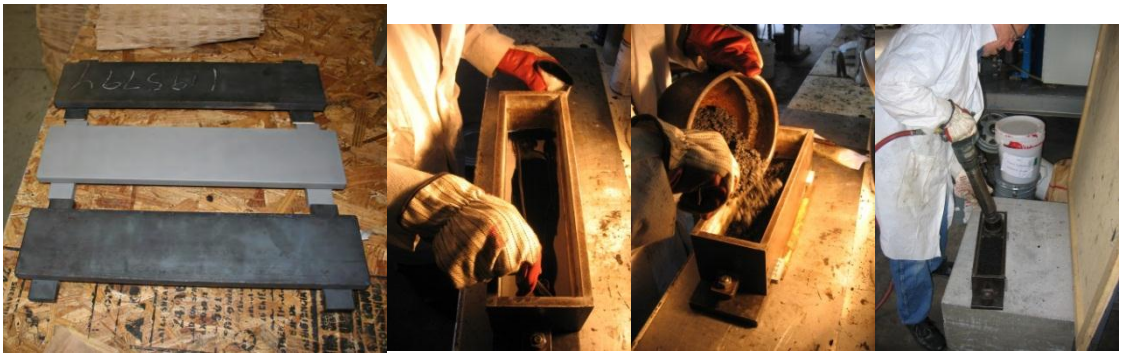

Fig. 3.2 *(a) Comparison of the sand blasted near white surface to the actual base plate (b) Base steel plate with a steel mold and a spread of inorganic zinc primer (c) Pouring of Epoxy Asphalt Concrete mix in to the steel mold (d) Compaction operation using a 4" x 4" plate*

3.2.3 Fabrication of Polyester Concrete specimens

Polyester Concrete wearing surfaces were placed on the blank steel templates at University of Missouri-Columbia by Kwik Bond Polymers. Steel templates were sand

blasted using industrial quartz sand, the night before placing the wearing surface. Sand blasting was done in a closed chamber to give the steel surface a white metal finish (Fig. 3.3a) in accordance with SSPC SP-10. A 6 micron layer (nominal) of primer made up of 15 parts zinc primer resin (made of neat resin and 1.5% of DDM9 catalyst) and 85 parts zinc powder (6 micron particle size) was applied (Fig. 3.4a) on the steel templates before the pouring of the polyester concrete. DDM9 is peroxide catalyst Methyl Ethyl Ketone peroxide (MEKP). Wooden molds were used for the polyester concrete placement (Fig. 3.4b).

The concrete mixture was prepared using a mixture proportion of 12.125 lbs. of polyester to 100 lbs. of aggregates (2 parts of B11 sand and 1 part of B39 aggregate) 1.5% (by weight of polyester resin) of the catalyst DDM9 was also added to the mixture. A heavy duty mechanical drill was used to mix the polyester binder and aggregates. The polyester concrete mixture was placed into the molds in two 1" lifts and vibrated on a table vibrator in order to drive out trapped air bubbles (Fig. 3.4c). Care was taken to ensure that the primer coat was not fully cured when the polyester concrete was placed. The polyester concrete wearing surface was allowed to set and gain strength before removing the wooden molds (after approximately an hour and a half of curing time).

Fig. 3.3 (a) Sand blasted steel templates; (b) Sand blasting chamber

Four batches of polyester concrete mix were made to fabricate the 24 specimens used in this investigation. The first batch of the polyester concrete specimens were placed using relatively thin Plexiglas molds which upon vibrating provided poor control over dimensional tolerances (particularly specimen width due to mid-span bulging). As a result this first batch of specimens were only used for pull-out load tests as the varying width of the specimens do not affect the bond strength between the steel and wearing surface, unlike in a flexural test where the varying width poses problems. Table A4 includes details of mix proportions for various batches used in fabrication process.

Fig. 3.4 *(a) Application of 6 micron layer of zinc polyester primer; (b) Finishing of the Polyester Concrete specimens; (c) Vibration of Polyester Concrete specimen on a vibrating table*

3.3 Customized instrumentation developed for wearing surface research

Custom transducers were used to measure net-deflection, load and end slips in the composite specimens. Fig. 3.5 shows a load transmission bar attached at mid-span to transfer the load uniformly along the specimen width, end slip fixtures to measure potential slip at the end of the specimens between the wearing surface and the steel plate and a net deflection fixture to accurately measure the deflection at specimen mid-span.

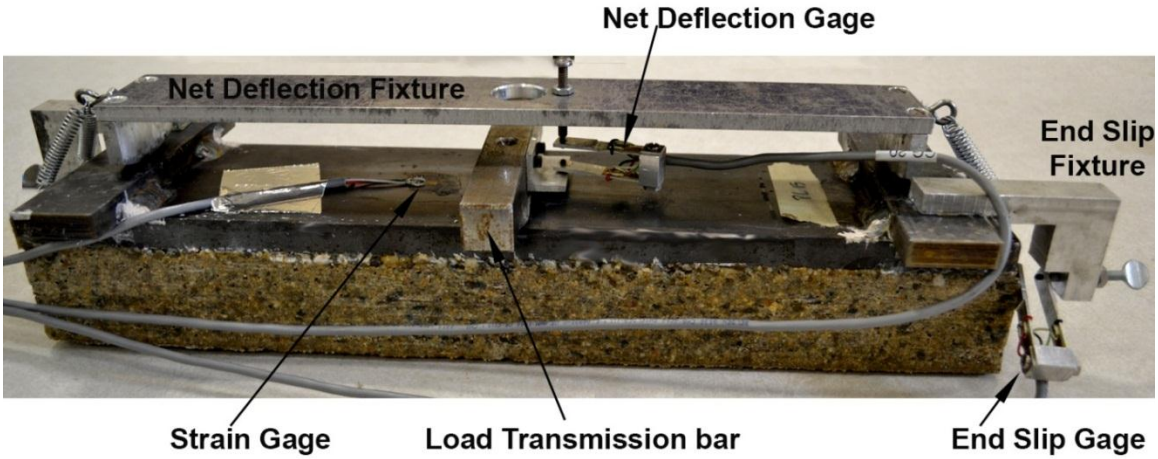

Fig. 3.5 Composite specimen with displacement measurement and loading fixtures attached

3.3.1 Load cells for flexural tests

Load cells were fabricated using fatigue rated steel with a yield strength of 50 ksi. A three point bend configuration was used for the load cells. Four 350 Ω foil type strain gages were used at the load-cell midspan in a full Wheatstone bridge configuration. Two strain gages were used on the top in compression and two strain gages in tension were used at the bottom of the steel plate. A height adjustable hemispherical stub mounted on a frame atop the load cell (Fig. 3.6 and Fig. 3.7) allowed fine adjustments of specimen preload in the flexural tests. As the test setup was designed to test four flexural specimens simultaneously, four load cells (one each for a flexural specimen) were fabricated and used during the tests. Load cells were supported on roller supports and each load cell was able to be individually positioned to avoid potential eccentric loading. A 10 V D.C. power supply was used to excite the full bridge transducer. Load cells were calibrated using a compression load cell in a temperature control chamber at three different

temperatures and at different loading rates ranging between 0.01 to 10 Hz (Appendix Table A5).

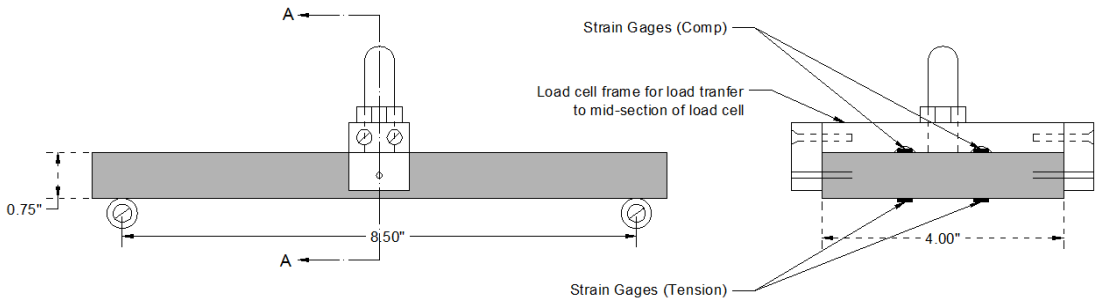

Fig. 3.6 Schematic of load cell used for the flexural tests

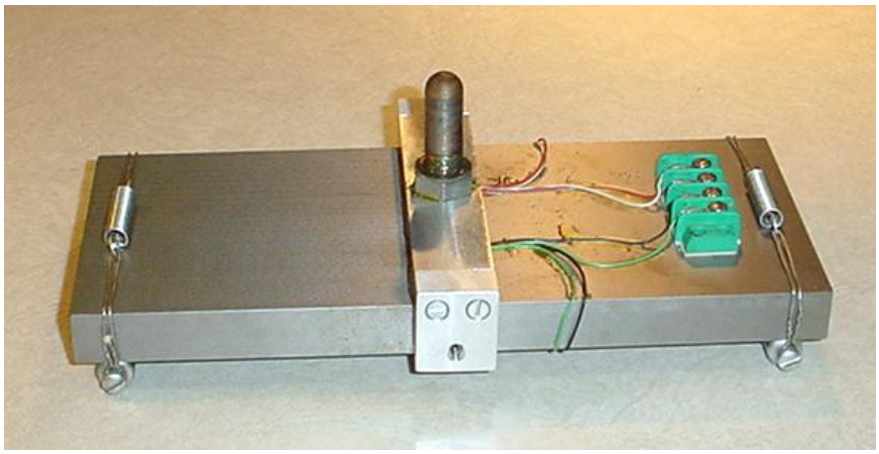

Fig. 3.7 Load cell used for the flexural tests

3.3.2 Clip gages for deflection and end slip measurements

Three clip gages were used with each specimen during the flexural tests. One gage was used for measuring net deflection (Fig. 3.5). Two clip gages were used, one at each end of the specimen to measure the relative shear displacement between the wearing surface and the steel plate (monitoring end slip, representing potential shear delamination, Fig. 3.5). All the clip-gage designs were identical and used a twin

cantilever beam configuration. The two legs and the separator block were made using fatigue rated aluminum. Four 350 Ω foil type strain gages were used in the full Wheatstone bridge configuration. Two strain gages which were glued inside of the cantilever legs were typically subjected to compression and the two outer gages were subjected to tension (Fig. 3.8 and Fig. 3.9). The clip gages were excited with a 10 V D.C. from Vishay conditioners, one conditioner dedicated to each clip-gage. Two dummy resistors facilitated bridge balance operation to achieve desired displacement ranges. In order for the clip gages to properly function in different environments, they were calibrated at different frequencies and temperatures. Clip gages were placed in the temperature control chamber and the chamber was allowed to reach the temperatures used in the research 32°F, 70°F and 122°F. Initially the clip gages are wrapped with silicone tubing around the clip gauge to protect the strain gages from external environment. The loading rate dependability on the measured calibration factors was observed to be minimal at all the three temperatures but the temperature dependability on the measured calibration factors was observed to be significant and is investigated to be caused because of the silicone tubing around the strain gauge legs. As the silicone tubing used is temperature complaint it was removed and the clip gages were found to work temperature independent. So, the calibration were performed at room temperature (72°F) (Appendix A Table A6).

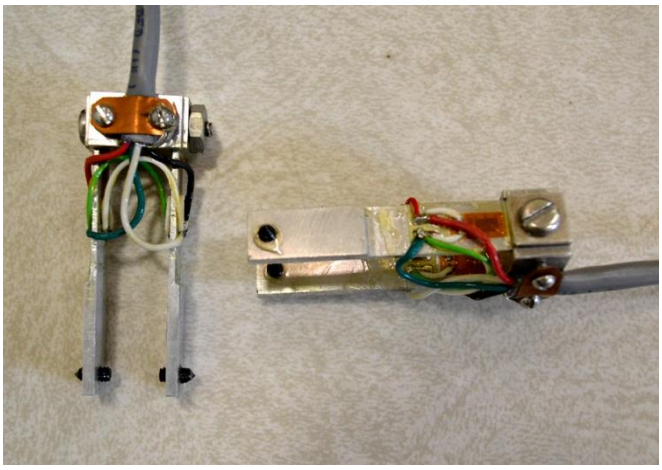

Fig. 3.8 Clip gages used for the flexural tests

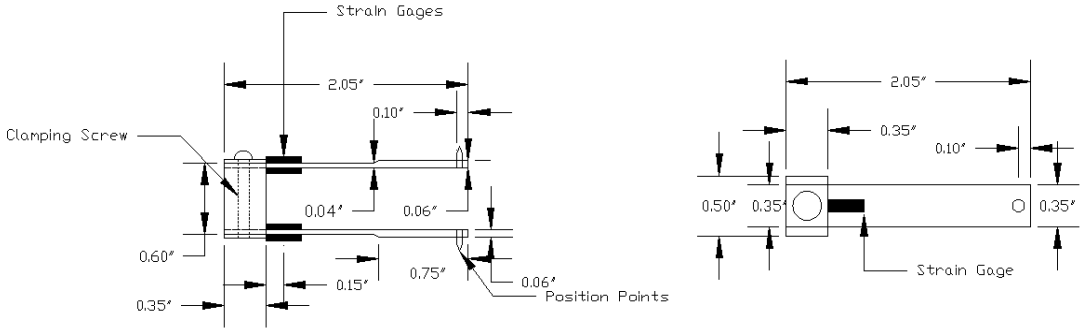

Fig. 3.9 Schematic of clip gage used for the flexural tests

3.3.3 Load cell for tensile pull-out tests

Load cell used for tensile pull-out tests was made of steel. A round steel specimen with flared shoulders at two ends and tapered at the middle to a constant diameter (0.5") was used as the load measuring device for the pull-out tests. Four 350 Ω strain gages were used is a full Wheatstone bridge configuration. Two foil type strain gages were affixed longitudinally in tension and other two in compression in the transverse direction. Both ends of the pull-out load cell were threaded so one end could be fixed to the pull-out load fixture and other end to the pipe cap (Fig. 3.10).

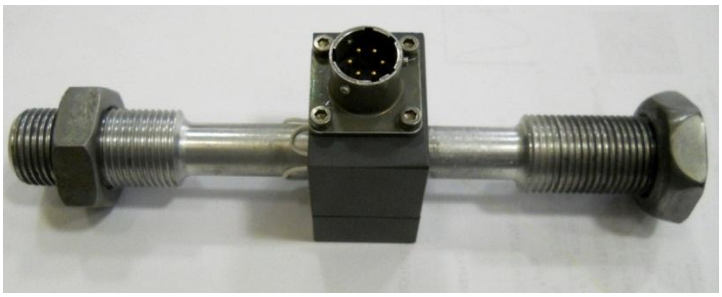

Fig. 3.10 Load cell used for the tensile pull-out load tests

3.3.4 Net-deflection fixture

Net deflection was measured using a custom designed aluminum yoke (Fig. 3.11 and Fig. 3.12). It measures the deflection of the composite specimen at midspan (offset by 1" to allow midspan loading) with respect to the specimen end supports. A hole in the yoke fixture allowed a cylindrical load application stub attached to the load cell to pass-through the fixture for load application. Two springs were used on each end to keep the net deflection fixture in place at the bottom of the specimen. A screw attached to the net deflection gage was used to zero the clip gages (Fig. 3.11). Measured net deflection values were analytically adjusted to account for the offset in the measurement location from mid-span.

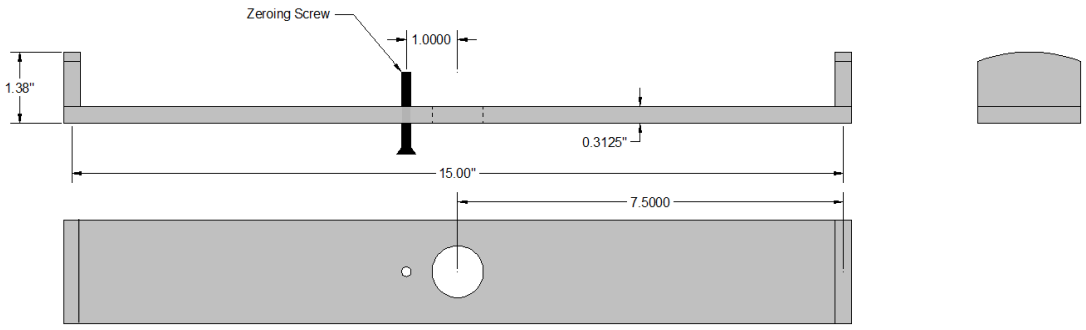

Fig. 3.11 Schematic of Net-deflection fixture attached at the bottom of the specimen

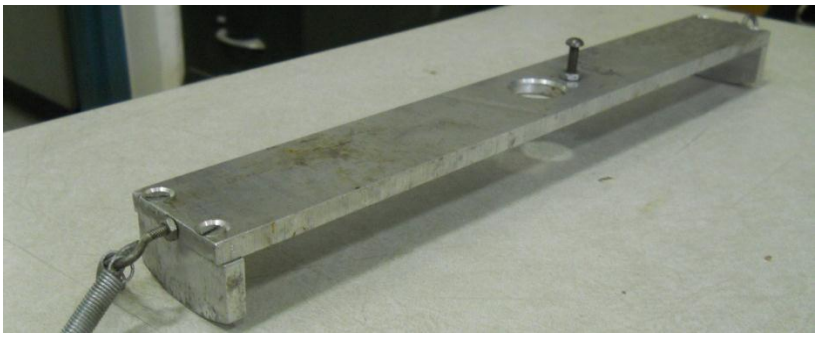

Fig. 3.12 Schematic of Net-deflection fixture attached at the bottom of the specimen

3.3.5 End slip fixtures

Potential delamination of the wearing surface from the steel plate was monitored using one clip gage at each end of the composite specimen along its span. These gages measure the relative shear deformation between the wearing surface and the steel plate and are termed “end-slip” gages. The fixture that facilitated mounting and zeroing of the end-slip gages was made from aluminum and was glued (with a quick-setting epoxy) to the bottom of the specimen (Fig. 3.5). One leg of the clip gage was supported by the wearing surface and the other leg was supported by the zeroing screw attached to the steel plate, thus measuring the relative lateral displacements of the two materials in the composite flexural specimen.

3.3.6 Support rockers

The composite specimen was supported on 4 rockers (Fig. 3.13) made of steel (one on each side along the span and on each side of the specimen along the width). In order to simulate a roller type of support, the rockers were rounded at the contact points touching the support tabs. The 4.5" tall rockers allowed adequate clearance to mount and deflect the composite flexural specimens which had a total nominal depth of 2 5/8 " (steel plate depth of 5/8 " and the nominal wearing surface depth of 2").

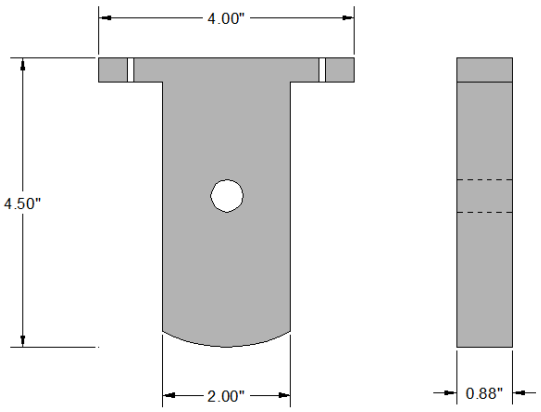

Fig. 3.13 Schematic of the rocker used for various flexural tests

3.3.7 Thermocouples

Six thermocouples of T type were used for measuring the temperatures inside the test chamber. Four of these were directly attached to the top surface of the wearing surfaces using aluminum foil tape. One thermocouple was placed at the middle of the chamber and measured the air temperature in the chamber. This thermocouple was used to control test chamber temperature. The other thermocouple was placed at the cooling inlet of the chamber, primarily for monitoring purposes. All the thermocouple wires were directly connected to the data acquisition card ("NI USB-6255") thereby not needing cold junction compensation (CJC).

3.3.8 Crack detection wire and associated set-up

One approach used to detect cracks on the wearing surface of the composite flexural specimens was to monitor the continuity of a surface bonded fine wire (0.005" diameter copper armature wire). The thin armature wire was glued on the wearing surface using a quick setting epoxy. The gluing operations were a multi-step process to ensure that the wire was held taut and as close to the extreme tension face as possible. Crack initiation on the tension face of the wearing surface would immediately result in a

discontinuity in the crack detection wire. Fig. 3.14 shows the schematic of the electrical circuit used to monitor cracking in the wearing surface during static as well as flexural fatigue tests. The voltage across the resistor in series, V_o, is monitored using the data acquisition system. When there are no cracks (i.e. the circuit is intact), the crack detection system output equals 5 V.D.C. When the wearing surface cracks, the resultant discontinuity in the crack detection wire is recorded by a drop in V_o to 0 V.D.C. Since the data acquisition protocol in the fatigue tests (described later) calls for signal averaging for compact data storage, and the discontinuity in the crack detection wire is sometimes intermittent (loading/unloading) for very small crack sizes, crack detection system voltages between 0 and 5 V.D.C. were recorded (any voltage below 5 V.D.C. represents a crack in the wearing surface).

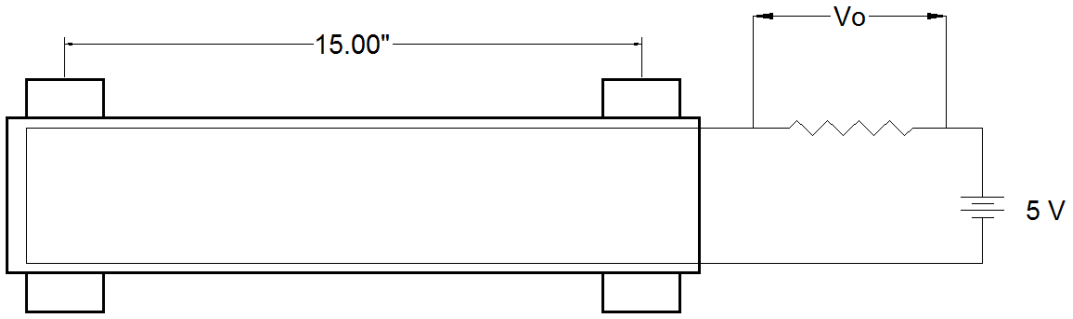

Fig. 3.14 Circuit used in the crack detection

3.4 Test chamber and temperature control

Static and flexural fatigue tests reported here were performed in a temperature controlled chamber insulated with foam. A conventional cooling unit and resistance heater were used in conjunction with a programmable PID controller to control the temperature inside the chamber.

3.4.1 Overall test set-up

The overall test set-up used for the flexural fatigue and static tests is shown in the Fig. 3.15. The cooling unit on the left of the photograph has a capacity to cool the test chamber to 10°F. The proportional–integral–derivative (PID) controller used to control the cooling and heating of the chamber is capable of turning on and off the cooling unit, the heater and associated duct fans needed to deliver desired constant test chamber temperatures. The cooling and heating ducts independently loop the test chamber so as to simplify temperature control routines. The temperature chamber is built around the MTS test frame and has outside dimensions of (33" x 33" x 22" width, depth and height, respectively). A 2" layer of Styrofoam insulation is placed on the inside of the sheet metal temperature chamber. Ram displacement of the MTS test frame is used for test control in the electro-hydraulic servo controlled testing machine. The photograph also shows the test control electronics and associated instrumentation comprising banks of amplifiers and PC-based data acquisition systems (DAQ). An USB based data acquisition card (“NI USB-6255” as described later in the section on Test control and data acquisition) was used for data acquisition.

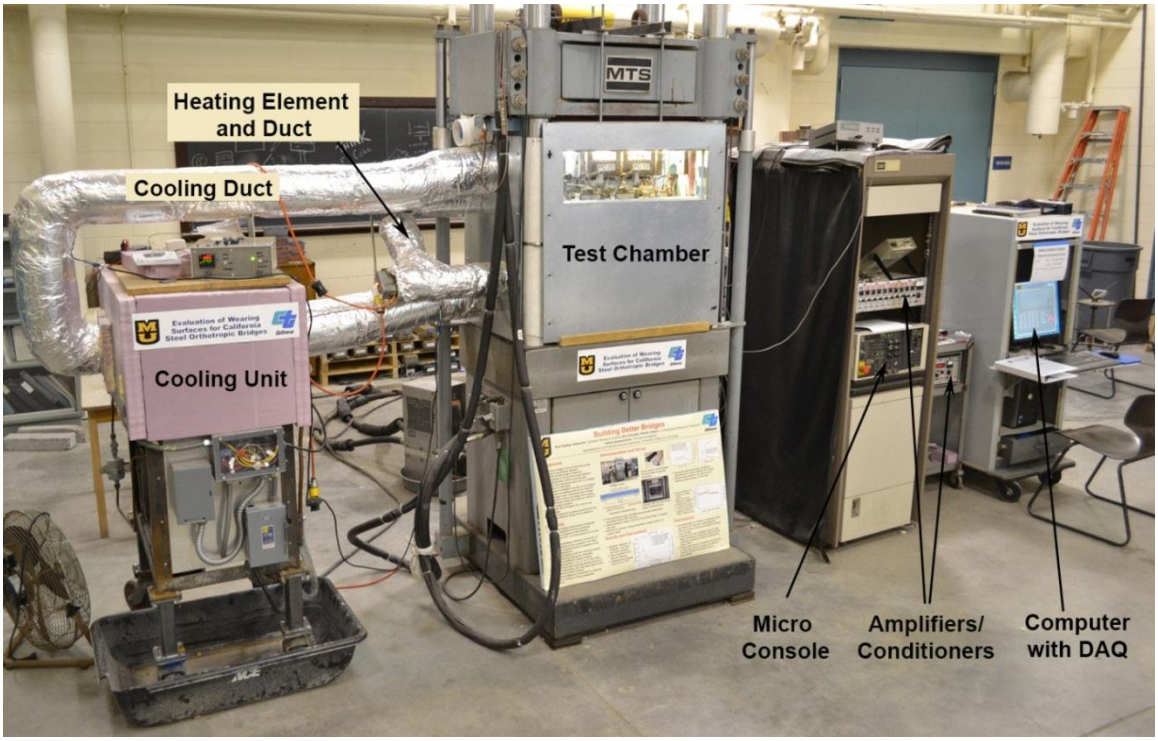

Fig. 3.15 Overall fatigue test set-up

3.4.2 Test chamber

Tests on four specimens of the same wearing surface type were simultaneously performed so that replicate data could be obtained giving insights into the statistical scatter that can be typically expected from such wearing surface materials (Fig. 3.16). Even while loads and net midspan deflections were measured individually for each of the test specimen, they were simultaneously loaded under ram displacement control so as to achieve desired minimum and maximum flexural loads. The four load cells were supported on a very stiff custom designed steel box beam which was connected to the hydraulic ram of the test machine. Each load cell had an adjustable loading stub that allowed equalize loads as needed. All four specimens tested simultaneously were of the same wearing surface type so that their stiffness characteristics were similar. The stiff box beam was engineered with a “lower limit support” so that even when the hydraulics

was shut off, the loading stubs from the four load cells did not travel out of the spherical seating designed for load application. This feature allowed restarting the fatigue test without the need to open the temperature controlled test chamber to reposition the load cells when it was sometimes necessary to shut off the hydraulic system.

The test chamber was designed to operate at prescribed constant temperatures (cold, room or hot temperatures). As described earlier, the test chamber comprised four sheet metal sides insulated with 2" Styrofoam sheets. The two machine crossheads served as the top and bottom faces of the test chamber. These were also insulated with 2" thick Styrofoam insulation. In addition, the hydraulic ram which moves within the chamber was also wrapped with mat insulation so as to mitigate potential cooling losses. Two of the side faces of the test chamber were fixed and were used to run wires to all transducers from the DAQ terminals and to run the heating and cooling ductwork loops (Fig. 3.15). The front and back faces of the test chamber were designed to be removable so as to facilitate mounting and removing of the specimens and instrumentation in to and out of the test chamber. Each of these two faces had a Plexiglas window to facilitate occasional visual monitoring of the test as needed. The top crosshead of the test machine supported a rigid 1" thick steel plate with a recess of 3" to allow for the camera tray (described later in section 3.5). The recess was designed using two stiff box beams so that specimen supports were non yielding. The 1" thick steel plate carried loads from the sixteen support rockers (four supports used for each specimen as noted earlier). Four 2" diameter holes in the 1” thick steel plate positioned right over the four specimen midspan locations provided direct access to the digital camera lenses for visual crack monitoring. These holes had a clear acrylic sheet cover to prevent air leaks from the temperature controlled

environment. Four cameras were mounted immediately above these visual monitoring ports. Fig. 3.16 shows the open test chamber.

Fig. 3.16 Chamber showing the steel beam and specimens mounted

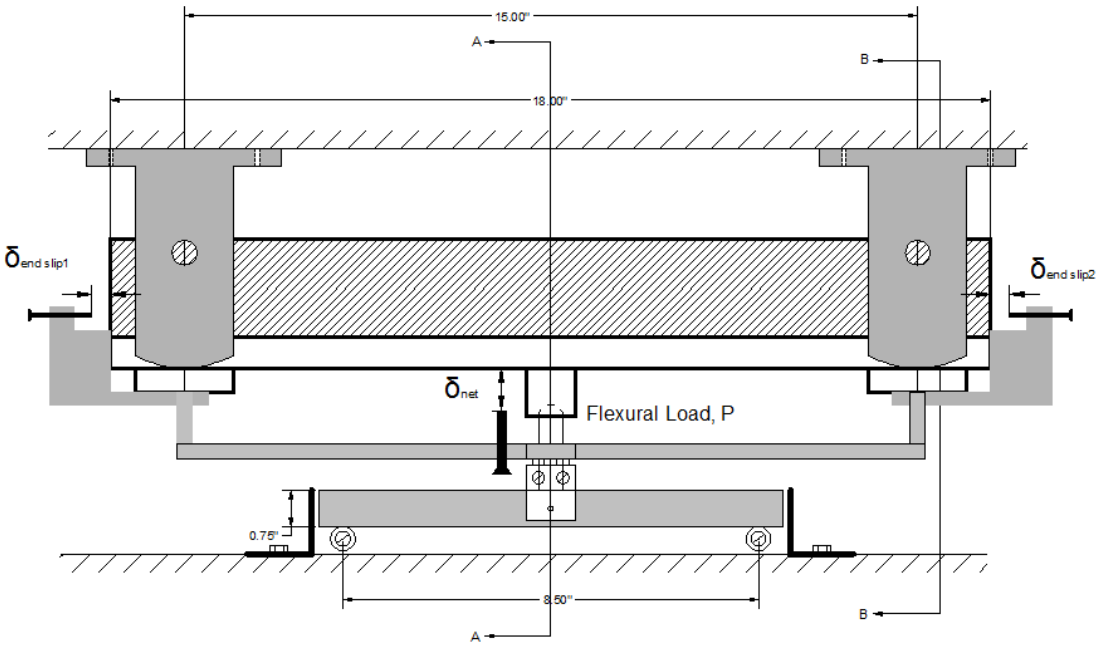

Fig. 3.17 Schematic of the flexural test configuration (see sections AA and BB in Fig. 3.18)

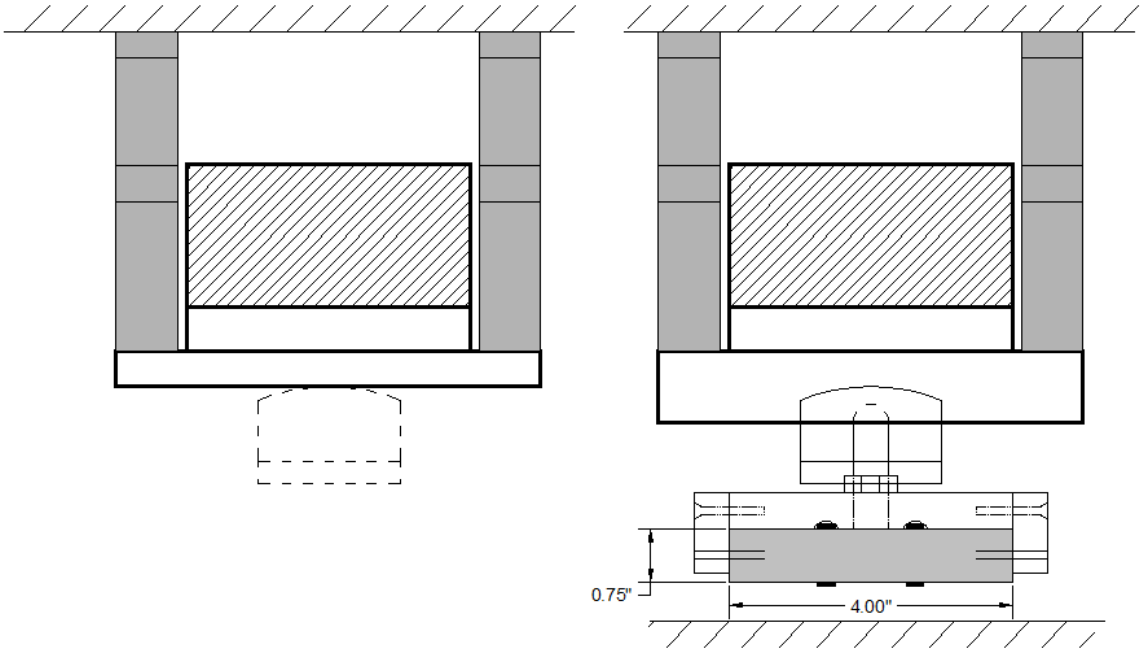

Fig. 3.18 (a) Section B-B of the flexural test set-up (b) Section A-A of the flexural test set-up

3.4.3 Specimen configuration for flexural tests

The orthotropic section of the San Mateo Hayward bridge comprises a steel deck plate of thickness 0.625" and a wearing surface of thickness 2" wearing surface on top. Steel deck plate is supported on open ribs and transverse floor beams. The open ribs used for San-Mateo Hayward Bridge were 8" x 0.75" and were placed at a distance of 15" center to center distance. In order to simulate the conditions on the bridge the specimens were designed to obtain a 15" span between the supports. A three point bend configuration was used for various flexural tests. Specimens of 18" length were fabricated with support tabs welded at a distance of 1.5" from the ends. This has resulted in obtaining a clear span of 15" between the supports. Fig. 3.17 demonstrates the three point bent set up with support tabs and all other fixtures used for the tests.

3.4.4 Cooling and heating units

Two independent ductwork loops, one for cooling and the other for heating the test chamber were used. R416A was used as the refrigerant in the cooling unit to maintain the chamber temperature at 32°F for the cold temperature tests. Duct fans in the cooling loop and in the test chamber were used in the efficient movement of cold air through the test chamber. A resistance heater in the heating ductwork loop along with a duct fan facilitated controlled heating of the test chamber. Temperature in the test chamber was maintained at prescribed levels for each test using a proportional, integral and derivative (PID) controller. P depends on error present, I depend on accumulation of past error and D is the prediction of future error. Weighted sum of all these actions is used to adjust the cooling and heating process. A thermocouple placed in the middle of the chamber (measuring air temperature) was used as the temperature reference for the test chamber temperature control.

In initial cooling tests the automated PID control resulted in frequent on and off switching of the cooling units. Since this frequent switching of compressor was considered undesirable, an alternate control approach was used. In this approach, the cooling system was operated continuously to achieve test chamber temperatures well below the desired cold temperature (wearing surface temperature of 32°F) with automated defrost cycles every 6 hours to maintain its cooling efficiency. The heater was operated in a PID control mode to maintain the desired wearing surface temperature.

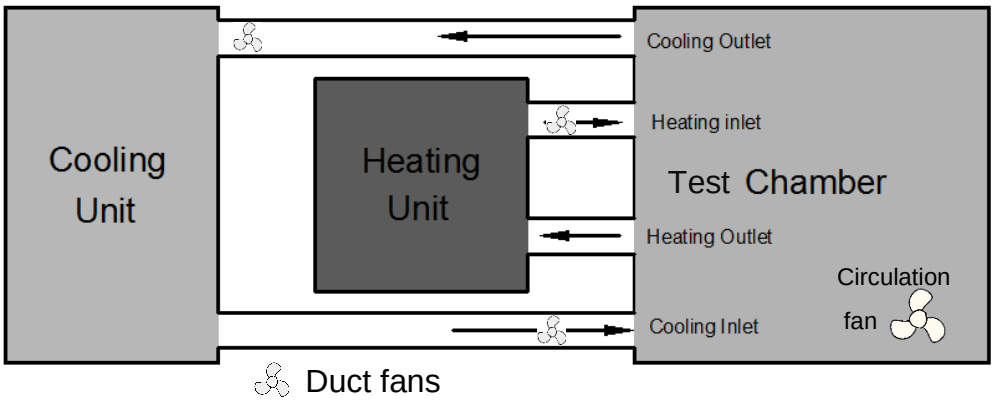

Fig. 3.19 Schematic of the temperature control features of the test chamber.

3.5 Automated digital imaging system

Four digital cameras were used to take photographs of the tensile face of the wearing surface specimens during the fatigue tests. These cameras were each mounted above the midspan of the specimens with their lenses positioned to capture potential surface cracks on the top of the wearing surface. The cameras were located in a camera chamber above the test chamber, separated by a 1" thick steel plate, with circular holes as viewing ports for the digital cameras. A 0.25" thick clear acrylic sheet covered the four viewing ports to protect the cameras and isolate the test chamber from convective losses. The cameras were positioned using Velcro straps on an upside down u-shaped wooden tray (Fig. 3.20). The tray makes for easy maintenance of the digital imaging system. The camera chamber was insulated adequately even while allowing removal of the camera tray for routine maintenance as and when needed.

Four Canon Powershot G2 cameras were chosen for their ability to be remotely controlled from a computer. The lenses were approximately 3" away from the tension face of the wearing surface, when the lenses were deployed allowing them to focus

sharply in macro mode. The field of view for each camera was 4" (entire specimen width) by 2.75" (length, along specimen span right at the midspan section). Two “under-cabinet” style low-profile fluorescent strip lights illuminated the test chamber to facilitate the auto focus features of the digital cameras and to produce good quality digital photographs.

The photographs themselves were taken sequentially on each of the four specimens, on an 10 minute loop. Thus, each 10 minutes, one photograph was taken of each specimen, with approximately 2.5 minutes between photographs of consecutive specimens (Fig. 3.22). BreezeSystems’ PSRemote (v2.1.1) software which allowed complete remote control of these cameras through an USB cable was used in conjunction with LabVIEW 2010 software for the digital imaging system. LabVIEW 2010 (v10.0), outputted command signals to a power relay, sequentially switching on one camera at a time. LabVIEW also sent command prompts to PSRemote, then to the cameras via the USB connections, to remotely control the cameras. Thus, for each camera, LabVIEW controls the following sequence of operations: power the camera, connect the camera to PSRemote via command prompt, capture a photograph in auto-focus mode using PSRemote via command prompt, wait allowing the photograph to download to the computer, disconnect the camera from PSRemote via command prompt, then power down the camera via the DAQ. This sequence is then repeated for the next camera. After each of the four specimens were photographed, the program cycles continuously until interrupted manually. The photographs taken by the cameras were downloaded directly to the computer via PSRemote, and stored on an external hard drive. The latest photograph taken of the specimen is displayed on the front panel allowing near real-time monitoring the condition of the specimen surface during the test. Fig. 3.21 shows the front panel of

the program displaying photographs of the specimens. Fig. 3.22 shows the sequence of steps involved in the program used for automated digital imaging system. The automated imaging system was designed to operate independently of the main data acquisition system.

Fig. 3.20 Tray with Velcro mounted array of four digital cameras

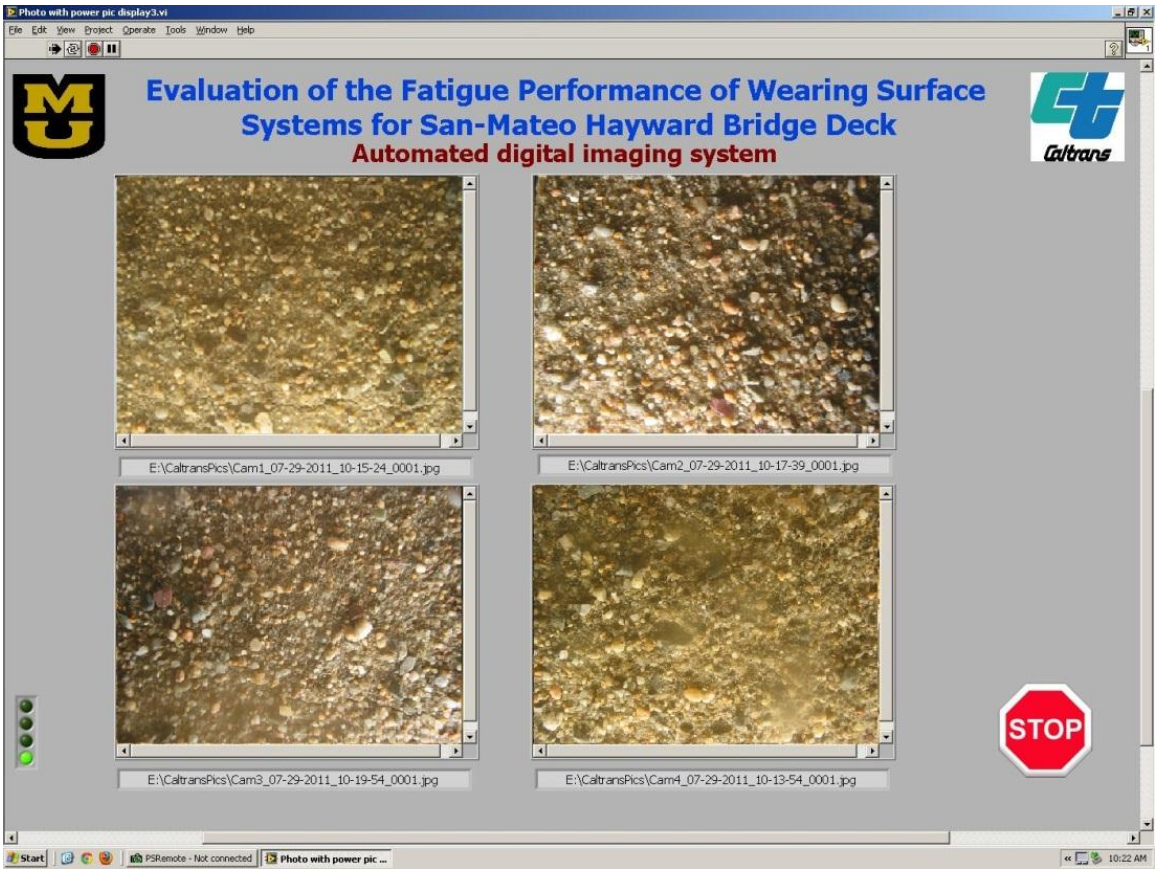

Fig. 3.21 Front panel of the automated digital imaging system

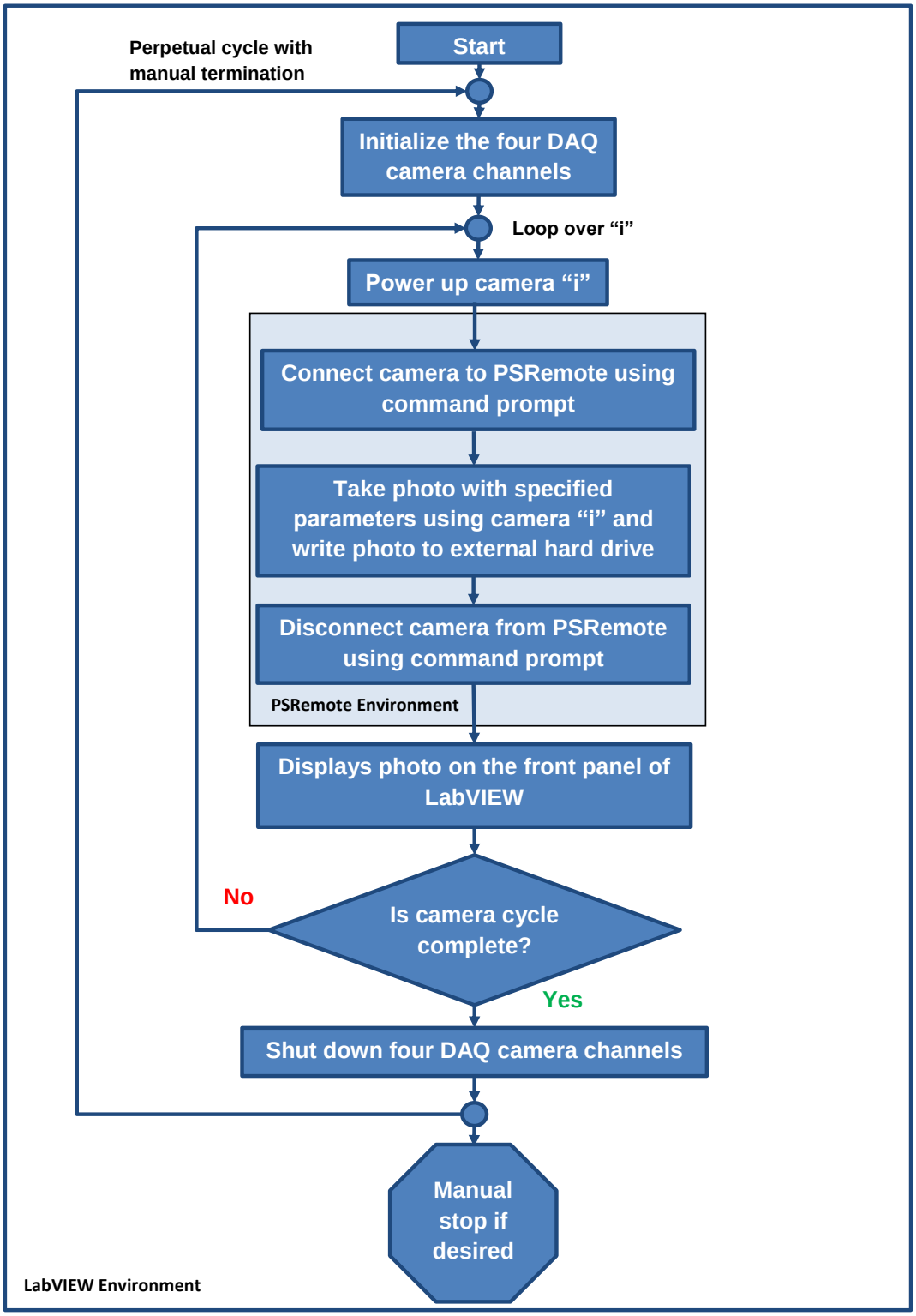

Fig. 3.22 Flowchart illustrating various steps involved in camera program

3.6 Test control and data acquisition

An USB based data acquisition card “NI USB-6255” was used as noted earlier in Section 3.4.1. The card is capable of measuring 40 differential and 80 single ended channels. A differential configuration was used for all the channels measured. This configuration provides robust high level signals (externally pre-amplified) that are “noise free” and “grounding issue free“. A mass termination type DAQ card was connected to custom designed terminal panel via two SCB 68 shielded input/output connector blocks. The custom terminal panel had convenient operator access and served as a junction for all transducer connections (load cells and clip gages). All thermocouples were directly connected to one of the “SCB-68” connector blocks to avoid the use of a cold junction compensation (CJC) correction (necessary if electrical wires are used in series with thermocouples). A total of 16 channels were required for load, net-deflection and end-slip measurements as each specimen was monitored using three clip gages (one for net-midspan deflection, and two for end-slips at each specimen end) and one load-cell. Vishay conditioners/amplifiers were used for the signal amplification for all these 16 channels. Additional channels of information recorded included “crack detection wire” signals from each specimen, thermocouples (wearing surface temperature) from each specimen, thermocouples measuring air temperature at two locations within the test chamber, ram displacement, and command signal.

Custom LabVIEW programs were used developed for each type of flexural test. These LabVIEW programs established two-way communication with the MTS microconsole by sending and receiving appropriate control strings using RS-232 protocol for these communications. The LabVIEW programs thus passively controlled the MTS

servo-controlled test machine (by sending the test control parameters) at the start of a test. Once started, the MTS Microconsole controlled the flexural test independently, only permitting pause/stop features from the LabVIEW program. This configuration allowed LabVIEW programs efficient and uninterrupted data acquisition operations. Details of the various LabVIEW programs are described in Chapter 4 on Test Procedures.

3.7 Remote monitoring of fatigue tests

Flexural fatigue tests conducted at 10 Hz typically took approximately 12 days to complete 10 million fatigue cycles. The fatigue tests were monitored on a bi-hourly basis by direct "in-lab" inspections involving several research personnel. In addition, automated monitoring capability using the Internet was also designed so as to allow redundancy and more flexibility in the conduct of fatigue tests. Instead of streaming video of the LabVIEW front panel displaying test results in real time (bandwidth intensive), a static screen-shot of the front panel display was posted every 10 minutes to an Internet file sharing site (Dropbox). This allowed all research personnel remote access to the fatigue test results every 10 minutes. When necessitated, research personnel could visit the lab for direct inspection based on results from this remote monitoring feature.

3.8 Static failure test set-up

Due to the significantly larger loads expected from a static failure test, this test was performed using a different test machine using a comparable test configuration as the other flexural tests. The set up for the static failure test comprised a very stiff support mechanism just like in the flexural fatigue tests (Fig. 3.23). The main difference was that instead of using a flexural load cell (which had limited load capacity of approximately

4,000 lbs), a compression load cell already mounted on the test machine (also a MTS test frame like in the fatigue tests) was used. The loading configuration test instrumentation and LabVIEW and monitoring features were identical to those used for the fatigue tests.

Fig. 3.23 *(a) Set-up with top steel plate and other fixtures used for the static failure tests (b) MTS machine used for static failure tests*

3.9 Test set-up used for crack detection and mapping

Cracking characteristics were studied post-test for all specimens that exhibited wearing surface cracking (static failure as well as flexural fatigue tests). The test set up for post-test crack detection (Fig. 3.24) allowed application of deflections identical to the maximum deflection imposed on the specimen during the actual test (so as to open cracks in an identically loaded condition). The fine cracks on the specimens were not visible to the naked eye when the specimen was not loaded. This detection of cracks necessitated because while the specimens were being fatigue tested they could not be photographed or inspected at high enough magnifications or from several different directions.

Crack detection was undertaken using a set-up consisting of a rigid steel platform, C-clamps and precisely machined rods with diameter simulating maximum deflections

from the static and fatigue tests. Composite specimens were mounted on the steel platform and the rod is placed in between composite specimen and the steel platform. C-clamps were used to apply loads symmetrically to the four ears of the composite specimen. Procedures used to detect and map crack patterns are described in section 4.7.

Fig. 3.24 Post-test crack detection set-up

3.10 Resistivity test set-up

Following crack mapping, a limited number of representative specimens of each wearing surface were subjected to a resistivity test. Resistivity tests were performed on the wearing surface composites according to ASTM D3633 – 98 (Reapproved 2006). This method "Electrical Resistivity of Membrane-Pavement Systems" is used for the wearing surface composites to qualitatively measure cracking in the wearing surfaces. The test (Fig. 3.25) consists of constructing a dam on top of the wearing surface with plywood along the rectangular edges. Silicone rubber caulking was used around the edges to prevent water from reaching the steel plate. Once the caulk was set up, a detergent and water mixture was placed on the surface of the specimen. Detergent was added to minimize the surface tension, thus allowing the water to penetrate fine cracks (often

invisible to the naked eye), which might be present in the specimen. A copper plate was attached to a sponge, which was allowed to soak in the soap water mixture. This “probe” was attached to one lead of an ohm meter; the other lead was attached to the steel plate of the composite specimen.

Electrical resistivity measured between the wearing surface and the steel plate provides a qualitative estimate of the severity of cracking in the wearing surface material. Resistivity test procedures are discussed in section 4.8.

Fig. 3.25 *(a) PC Specimen with dam constructed and caulk applied (b) EA specimen with dam constructed and caulk applied (c) Specimens with sponge placed with copper plates and ready to test*

3.11 Tensile pull-out test set-up

Tensile pull-out test is adapted from methods to quantify the tensile bond of epoxy concrete overlays on concrete (ACI 503R-93). Tensile pull-out test in this study offers measures of the tensile bonding of the wearing surface systems to the steel deck plate and also insights into potential type of pull-out failure. Results from small tests provide an effective quality control tool that can be used to ensure proper wearing surface placement and for detecting potential delamination while in service.

Cores of 2" in diameter were drilled in the wearing surface until the depth reached the steel plate. Core drill was secured on a level table (Fig. 3.26a) and care taken to

ensure accurate vertical coring. Seven cores were drilled on each of the composite specimens as shown in the Fig. 3.26b to allow for multiple tests from each specimen. Pipe caps were glued on the cores using an adhesive. The pipe cap was connected to a tripod loading and monitoring device (Fig. 3.26c) using a threaded rod connection. The device allowed manual application of tensile loads required to pull out the wearing surface core from the steel plate. It was also equipped with an electrical load cell (Fig. 3.10) that facilitated recording of the load-time history along with the maximum pullout load. Procedures used to conduct the tensile pullout test are included in section 4.9

Fig. 3.26 *(a) Coring operation (b) Cores drilled on composite specimens (c) Set-up used in Tensile Pull-out test*

4 Test Procedures

4.1 Introduction

Procedures used for various tests on the wearing surface composites fall broadly into two categories: flexural tests and other supporting tests. Flexural tests include; static flexural tests, dynamic flexural tests, flexural fatigue tests and static failure tests. With the exception of the static failure tests which were conducted at room temperature, all the other flexural tests were conducted at several test temperatures ranging from 20°F to 120°F. The other supporting tests include; tensile pull-out tests, crack detection and mapping effort, and resistivity tests.

All the flexural tests were conducted using a servo-controlled electro-hydraulic testing machine interfaced with a PC-based system for test control, data acquisition and real-time monitoring. The static failure tests were performed in ram displacement control mode using a ramp command function (linear function of time). These tests were performed one specimen at a time. For all the other flexural tests (static, dynamic and fatigue), replicate specimens (2-4, depending upon the type of test) were tested under ram displacement control, producing desired upper and lower limit loads. The command signal in these flexural tests was sinusoidal, with the frequencies depending upon the type of test (static at 0.0167 Hz, fatigue at 10 Hz, and dynamic at constant frequencies in the range 0.0167 – 15 Hz). Details of the computations of the upper limit load used for these flexural tests are included in Section 4.2. Discussions of the test procedures used for the flexural tests are included in Sections 4.3 – 4.6.

The tensile pull-out test, crack detection and mapping effort, and resistivity tests were conducted with the custom set-up designed for these tests, as described earlier in Chapter 3. Details of the test procedures used for these other supporting tests are included in Section 4.7 – 4.9.

4.2 Load limits for flexural tests

The upper limit fatigue load for all flexural tests (static, dynamic and fatigue) was computed based on provisions for design loads for orthotropic decks (AASHTO T-14, and detailed in Kozy et al., 2011). Wearing surfaces in this research were analyzed for design loads. With factors that account for multiple presence and impact factor for local analysis and design of orthotropic decks, AASHTO T-14 has approved treating the design truck as a five axle vehicle. Fig. 4.1 illustrates the five axle loading considered. Front axle of 8 kips and each of the four rear axles of 16 kips were considered in the calculation of the loading for wearing surfaces. The patch areas per the AASHTO T-14 are 10"x10" for the front axle and 20"x10" for the rear axle. Tire pressure calculated based on the load and the areas is obtained as 40 psi (4,000 lbs. /100 in^2 for front axle and 8,000 lbs. /200 in^2 for rear tires) is same for both rear and front axles. Using a multiple presence factor of 1.2 and impact factor of 1.33 the design tire pressure is obtained as 63.84 psi. A 1" strip is considered in the analysis of the wearing surface. Different cases of loadings considered were

Case A: Two rear axle tires placed right above the rib such that the 10" of loading is on each side of the rib. (Fig. 4.2a)

Case B: Two rear axle tires centered over two adjacent ribs. (Fig. 4.2b)

Case C: Single tire front axle placed between adjacent ribs. (Fig. 4.2c)

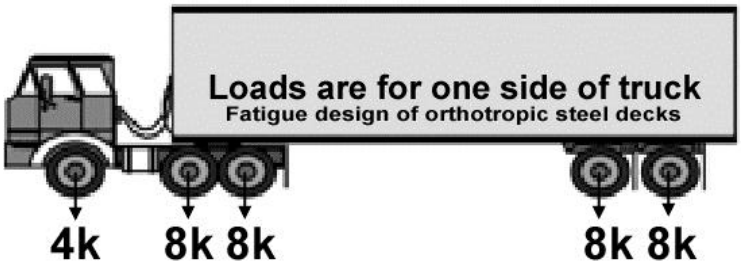

Fig. 4.1 Refined design truck loads for fatigue design of orthotropic decks (AASHTO T-14 and Kozy et al., 2012)

Analysis of the above cases has shown that the critical case for the design is Case-A. The transverse bending analysis was carried out using RISA-2D. The ribs were idealized to be non-yielding simple supports. This is more conservative for determining flexural stress than yielding supports which is more representative of service performance. It should also be noted that the tire pressure assumed in this analyses are higher than the actual local pressures due to the actual load distribution typical in a 2" deep wearing surface. A 45° pressure distribution often assumed through the depth of the wearing surface would result in pressure patches of 24"x14" and 14"x14" for rear and front tires respectively on the steel deck instead of the 20"x10" and 10"x10" patches assumed. So the pressures assumed in these analyses are approximately 70% (rear tires 336 in^2/200 in^2) and 96% (front tires 196 in^2/100 in^2) larger than if the tire loads were distributed over the larger patch (accounting for the wearing surface depth).

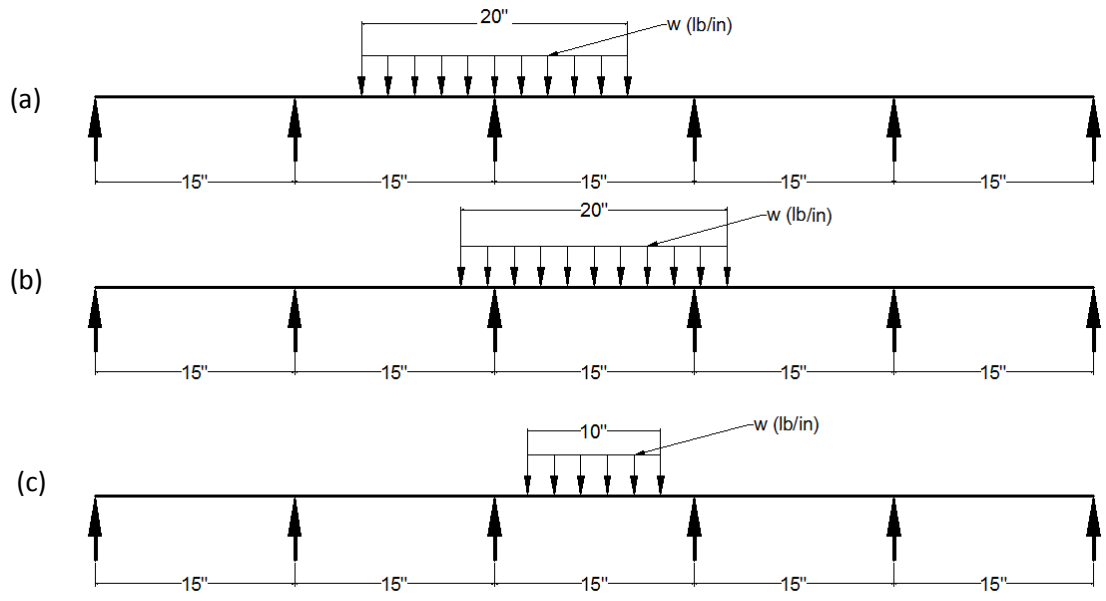

Fig. 4.2 *Design truck loading configurations evaluated to produce maximum negative moment over ribs (a) Loading Case A (b) Loading Case B and (c) loading Case C*

For convenience, all transverse bending analyses reported in this section have been carried out for a standard uniform distributed load of 100 lb./in. on a 1" finite strip (along the longitudinal or traffic direction). Moment diagrams thus generated are used to compute moments for actual design truck tire pressure (64 psi as described earlier) and design lane load of 64 lb./ft. for a 10 ft. lane (equivalent pressure of 0.44 psi).

The maximum negative moment due to design truck (loading case A) =-1,970 x64/100=1,261 lb-in. (for a 1" strip along traffic direction). The maximum negative moment due to lane loading (loading case D) = -2,362x0.44/100=-10.4 lb-in. (for a 1" strip along traffic direction).

For the 4" wide laboratory flexural specimens, the maximum moment to be generated is M_{max}=-(1,261+10.4)x4=-5,086 lb-in.

At a span of 15", the upper limit fatigue load equal P_{max}=4M/L=1,356 lbs. A nominal upper limit load of 1,350 lbs. was used in the static, dynamic and fatigue tests on flexural specimens (BS, EAC and PC composite specimens).

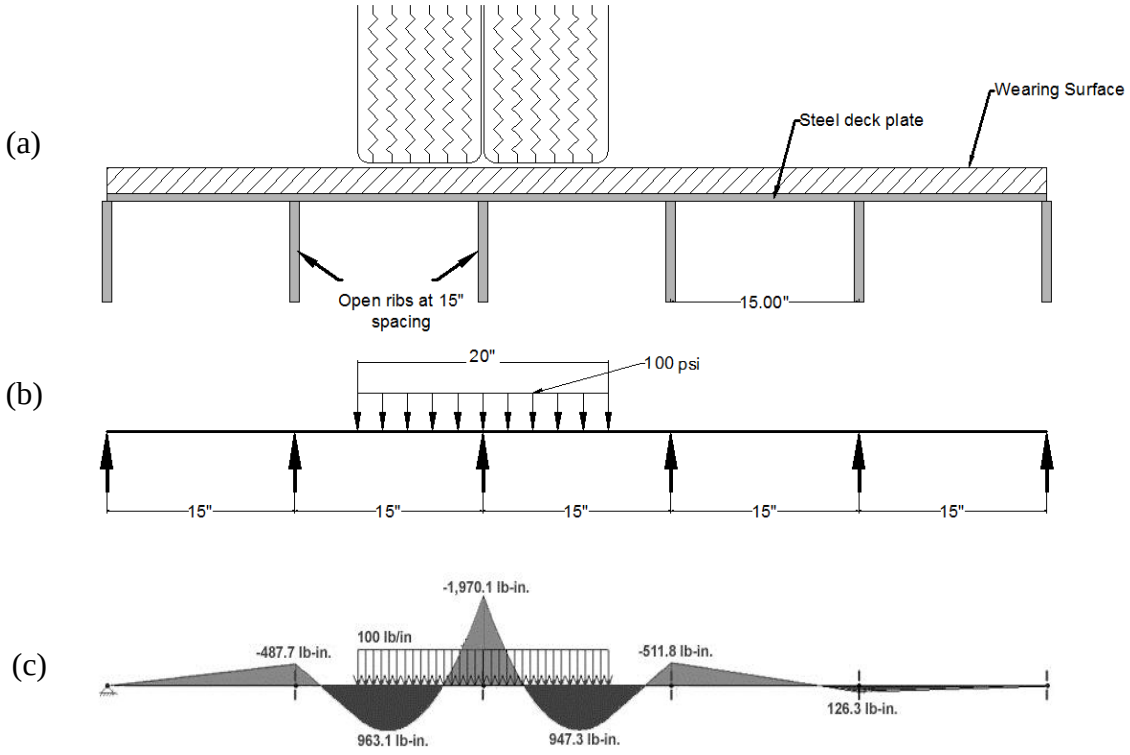

Fig. 4.3 *(a) Placement of the tire of design truck for the critical case (Case A) (b) Idealization of loading conditions for the purpose of analysis (C) Bending moment diagram due to the application of design truck load.*

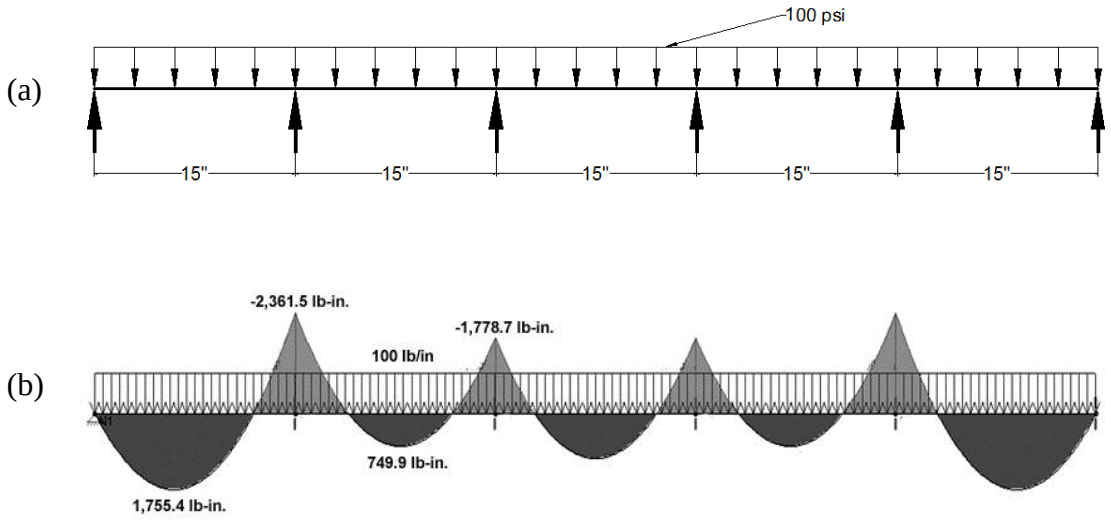

Fig. 4.4 *(a) Lane load placed along the continuous rib spans (Loading Case D) (b) Bending moment caused due to the lane load.*

4.3 Static flexural tests

Static tests comprised 3 sinusoidal loading/unloading cycles between the upper and lower limit flexural loads (1,350 lbs. and 200 lbs., respectively) as described in the previous section. These tests were carried out at a test frequency of 0.0167 Hz (one cycle per minute). Two replicate specimens of each type (BS, EAC and PC composite specimens) were tested under static conditions. The tests were servo-controlled using ram displacement signal to achieve the prescribed upper limit load. Tests were performed at constant temperatures ranging from 20°F to 120°F, in nominal temperature increments of 10°F. A LabVIEW program customized for the static flexural test incorporated test control, data acquisition, and real-time monitoring features. This program is somewhat similar to the "program module" used for the "slow cycle" component of the fatigue test described later in Section 4.5. The test-control feature of the programs used for this research project was designed to hand over control to the MTS Microprofiler via a RS-

232 serial interface once the test commenced. Thereafter the LabVIEW program only retained pause/restart and stop functions, allowing the computer based system to be dedicated exclusively to data acquisition and real-time monitoring of the test.

Parameter histories monitored during the test for each specimen included: flexural load, net-deflection, two end slips, wearing surface temperature and steel strain. Custom transducers used to measure load, net-deflection, end-slip and temperature were described earlier in detail in Chapter 3. Steel strain in these tests was measured using a 120 Ω foil strain gage bonded to the compression face of the specimens. These gages were bonded as close to the midspan as possible (to avoid boundary effects from the load distribution bar at midspan) along the span and exactly at specimen mid-width. Steel strain at midspan was analytically computed from the measured strains using simple mechanics.

Among the important performance parameters and properties obtained from the static flexural test included: the load deflection response, composite stiffness, and apparent elastic modulus. The variation of these properties with temperature was also integral to a better understanding of the wearing surface performance.

The task of starting a new test series involved careful gluing of the load distribution bar and the end-slip measurement fixtures on each specimen, mounting of the replicate specimens in the test chamber, adjustment of the load cells and loading stub height, mounting of the net-deflection fixture, and fixing and zeroing of the net-deflection and the two end-slip gages. Thermocouples were also affixed on to the top of the wearing surfaces using aluminum foil tape. A transparent grid printed on plastic sheet was also taped on to top of the wearing surface so as to provide visual maps of cracking during the

test. This grid was within the field of view of the digital camera dedicated to each specimen (which was a part of the automated digital imaging system described in Section 3.5. The static flexural tests were conducted at temperatures from 120°F to 20°F in (approximately) 10°F steps. Logistically, it was convenient to start the static tests at the hottest temperature and gradually cool the test to 20°F. At each desired temperature, the temperature controller was programmed to hold the temperature for 2+ hours so that the specimen and fixtures could attain steady state temperature before the static flexure test was conducted. Prior to each series of test, the preload was adjusted to the prescribed value of 100 lbs. This readjustment at each temperature was necessary to account for linear thermal expansion/contraction of the test fixtures and specimens within the chamber.

The start of each test involved the synchronous initiation of the automated systems for temperature control, mechanical loading and data acquisition, and digital imaging. For the static flexural tests, data was acquired at the rate of 1 sample per second. This allowed 60 samples for each of the three cycles of loading/unloading.

During the test, the load, net-deflection, the two end slips, steel strain and wearing surface temperature were displayed for each specimen. In addition, the ram displacement and test chamber temperature at two locations (air temperature in the middle of the test chamber and cold inlet) were also displayed. Real-time plots of the load deflection response from each specimen were also displayed on the screen (Fig. 4.5). The flowchart illustrated in Fig. 4.6 highlights the steps involved in data acquisition and processing for the static flexural tests.

4.4 Dynamic flexural tests to study potential loading rate effects

Dynamic flexural tests were performed to study the loading rate sensitivity of wearing surface materials. Dynamic tests were conducted at different constant frequencies: 0.0167, 1.0, 2.5, 5.0, 7.5, 10.0 and 15.0 Hz and at three different wearing surface temperatures (32°F, 70°F, and 120°F) to understand the combined effect from temperature and loading rate. The instrumentation, the configuration of the specimen and test procedures used were identical to those used for the static flexural tests. The LabVIEW program for data acquisition used in the case of dynamic flexural tests was modified to allow faster rates of acquisition (300 samples per second for each parameter measured) for the faster tests and to efficiently process the raw data for on-screen display during the test and for writing the complete data set to file for post-test analysis.

Every second the 300 samples for each parameter were written to file. The maximum and minimum of the load and net-deflection were computed from these points and the screen plot of the maximum and minimum was refreshed. This allowed real-time monitoring to ensure the prescribed maximum and minimum load was accurately controlled. This process was repeated for the 30 second test duration at each of the test frequencies. The flowchart illustrated in Fig. 4.7 highlights the steps involved in data acquisition and processing for the dynamic flexural tests.

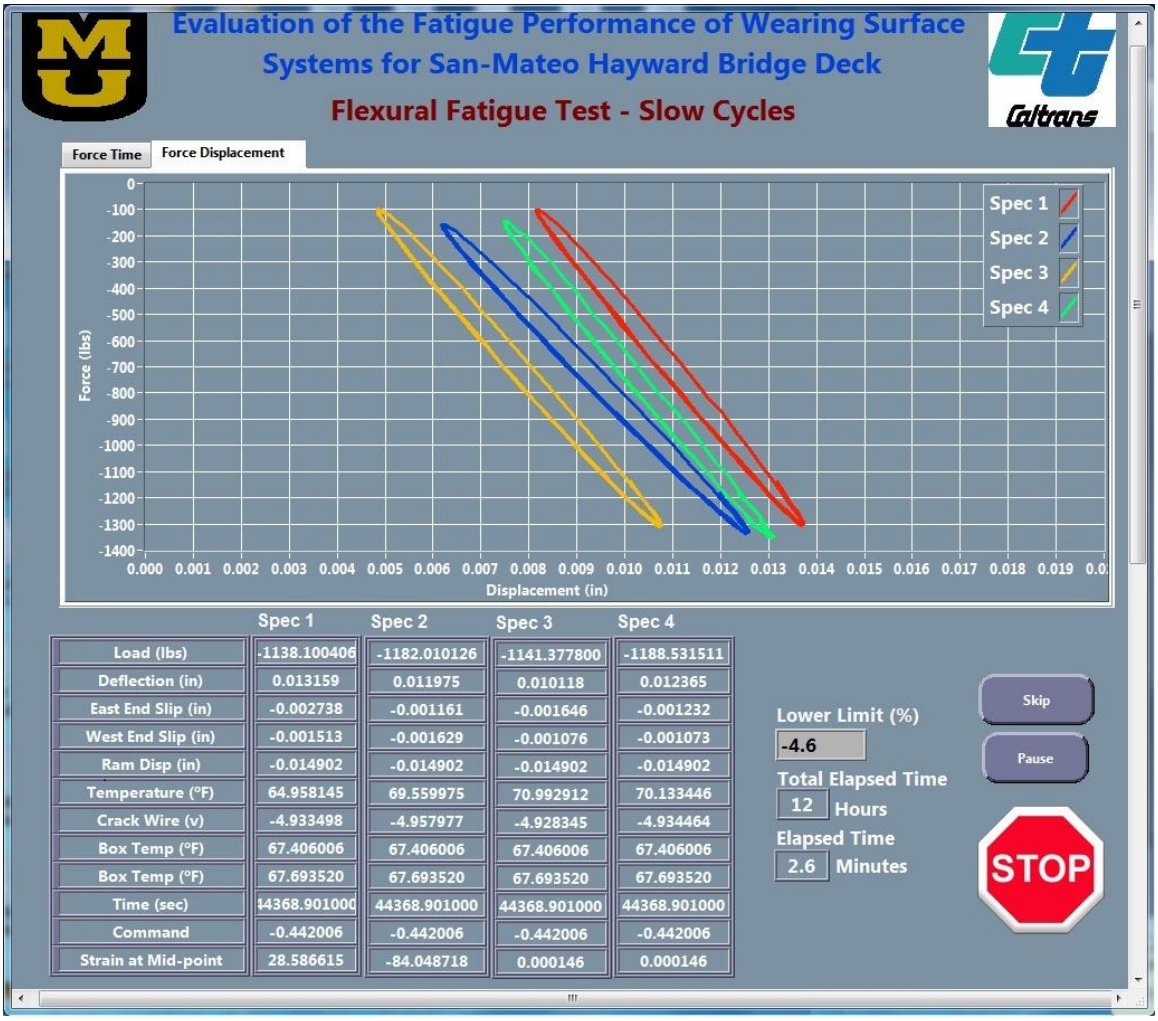

Fig. 4.5 Front panel of slow cycle

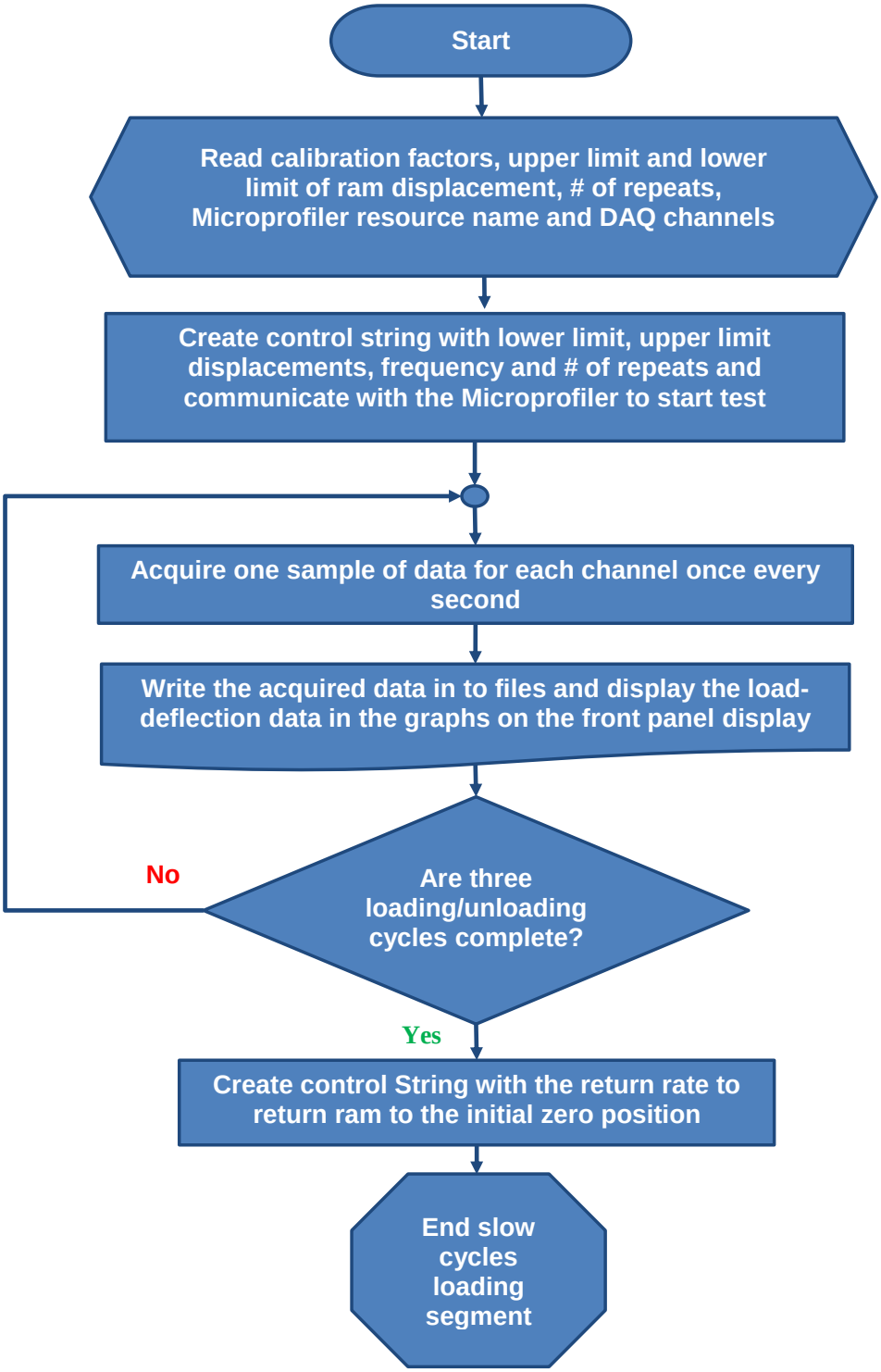

Fig. 4.6 Various steps involved in static flexural tests or slow cycles

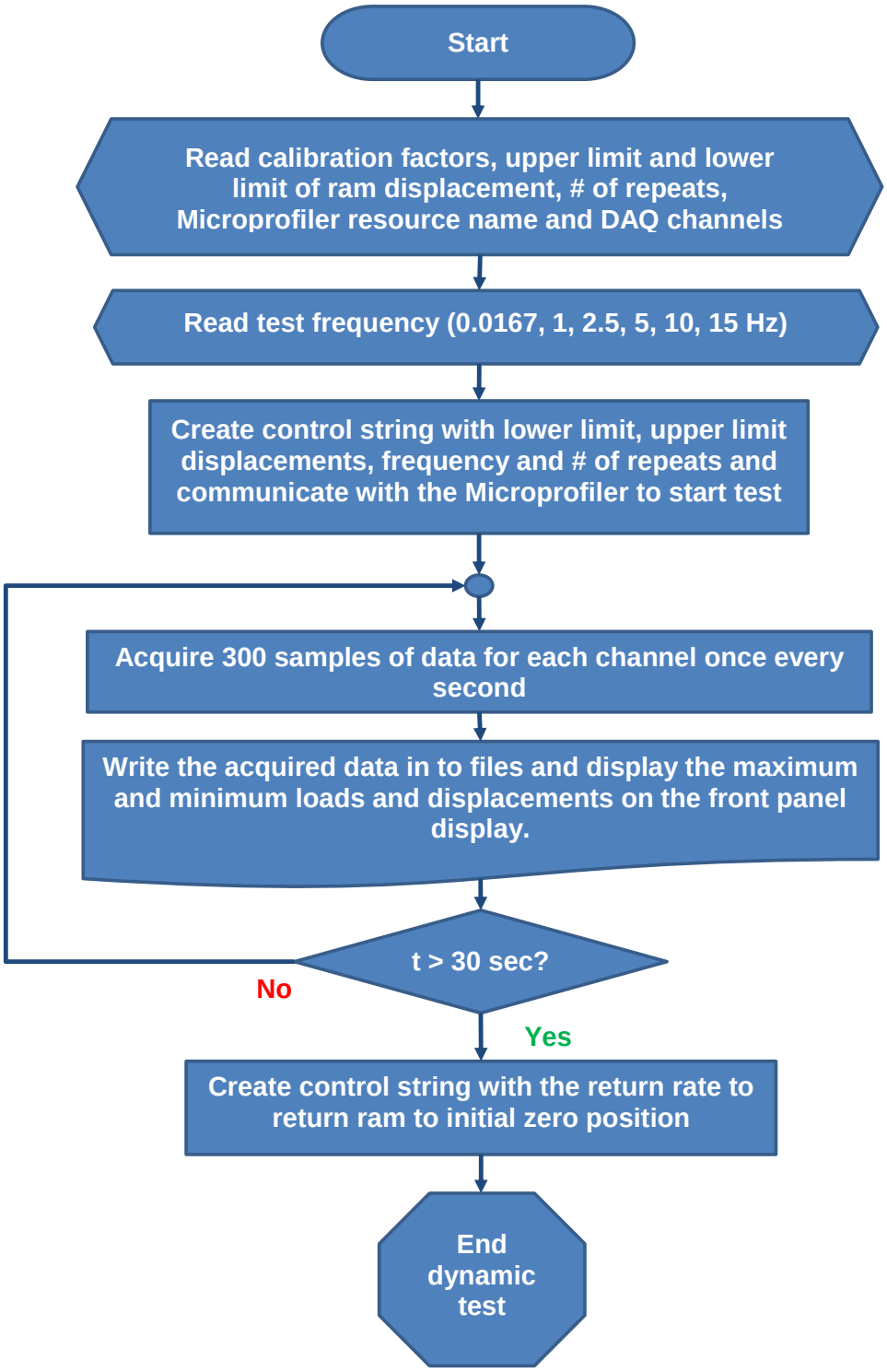

Fig. 4.7 Various steps involved in dynamic tests

4.5 Flexural fatigue tests

Flexural fatigue tests comprised alternate segments of "slow cycles" and "fast cycles" loading. Slow cycle loading was identical to static flexural test in that it was conducted at a loading rate of 1 cycle per minute (0.0167 Hz).

The slow cycle segment comprising three loading/unloading cycles, allows recording of the complete load deflection history and facilitates monitoring of gradual degradation of stiffness with fatigue loading. The fast cycle loading segment runs for two hours at 10 Hz (a total of 72,000 cycles). The fatigue tests were run up to 10 million cycles (approximately 11.5 days). Tests where specimen cracking occurred early were terminated earlier than 10 million cycles. Even for these specimens, fatigue tests were continued well beyond initial cracking so that progressive growth in cracks (distribution and severity) under additional fatigue could be studied

Data acquisition features in the slow cycle loading of the fatigue test were identical to that described earlier for the static flexural tests in Section 4.3. Data acquisition features in the fast cycle loading of the fatigue test were optimized so that the volume of data stored from the extended length, high speed acquisition, focused on retaining critical aspects of information in deference to relatively less important information from the test. Data was acquired at the rate of 300 samples per second for each parameter monitored. A minimum and maximum value for each sinusoidal varying test parameter was determined for the 10 Hz loading for the 300 sample window. The process was repeated 30 times during the 30-second window. The values of the 30 minimum and maximums were averaged and stored to file and also updated on the on-

screen plots. Real time stiffness value, computed from ratio of the difference between maximum and minimum load to the difference between maximum and minimum net deflection, was also plotted along with maximum and minimum loads and deflections from each specimen. Stiffness was also monitored from direct linear regression of the complete load deflection response (not based on the maximum and minimum values). Non-sinusoidally varying parameters (such as wearing surface temperature, crack detection wire signal etc.) were averaged during the data acquisition window. All of these raw as well as computed parameters were written to file and updated in the on-screen plots every 30 seconds (Fig. 4.11). The 30-second data acquisition and processing sequence was repeated during the 2-hour fast cycle loading segment.

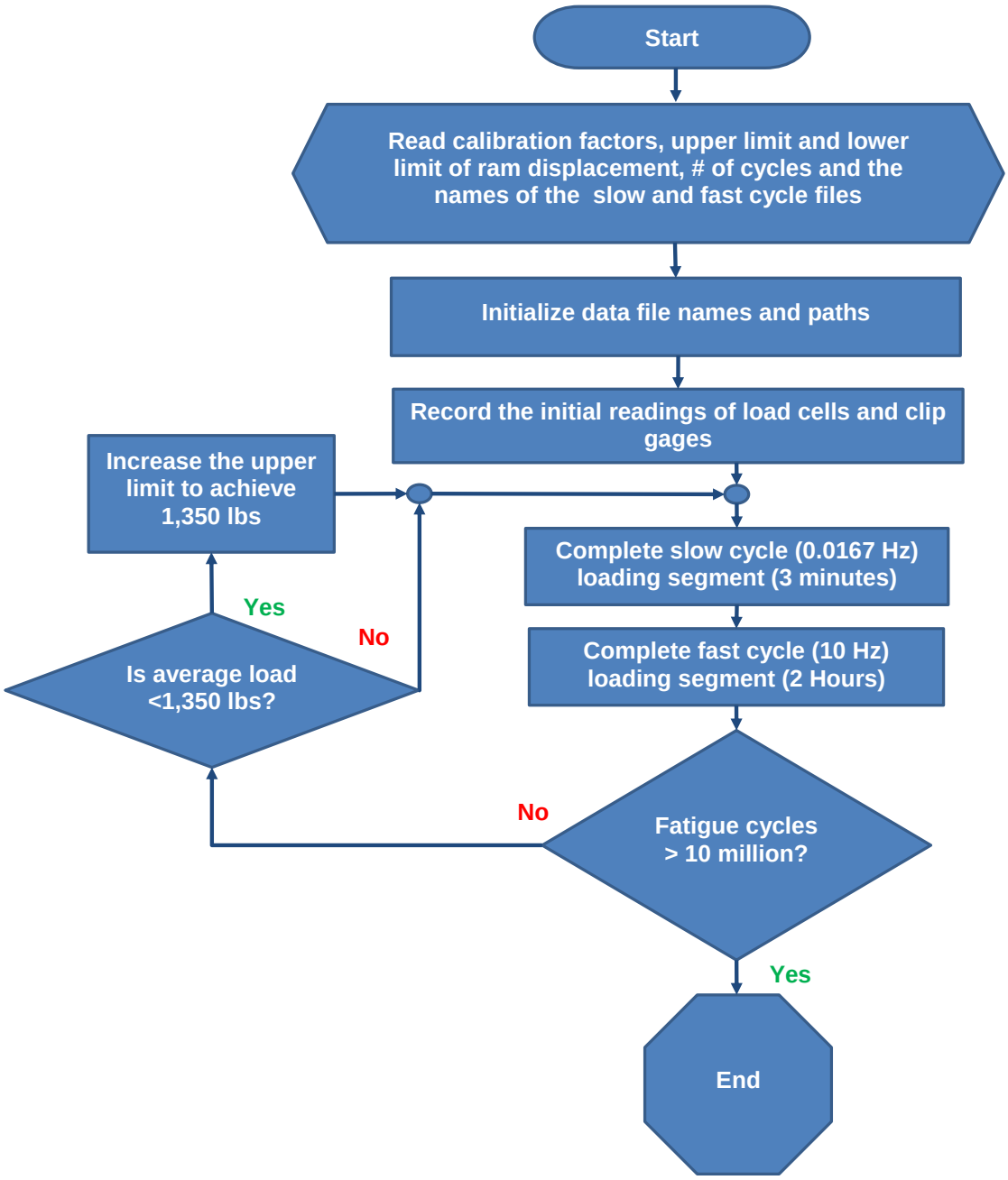

Fig. 4.8 Various steps involved in Overall fatigue tests

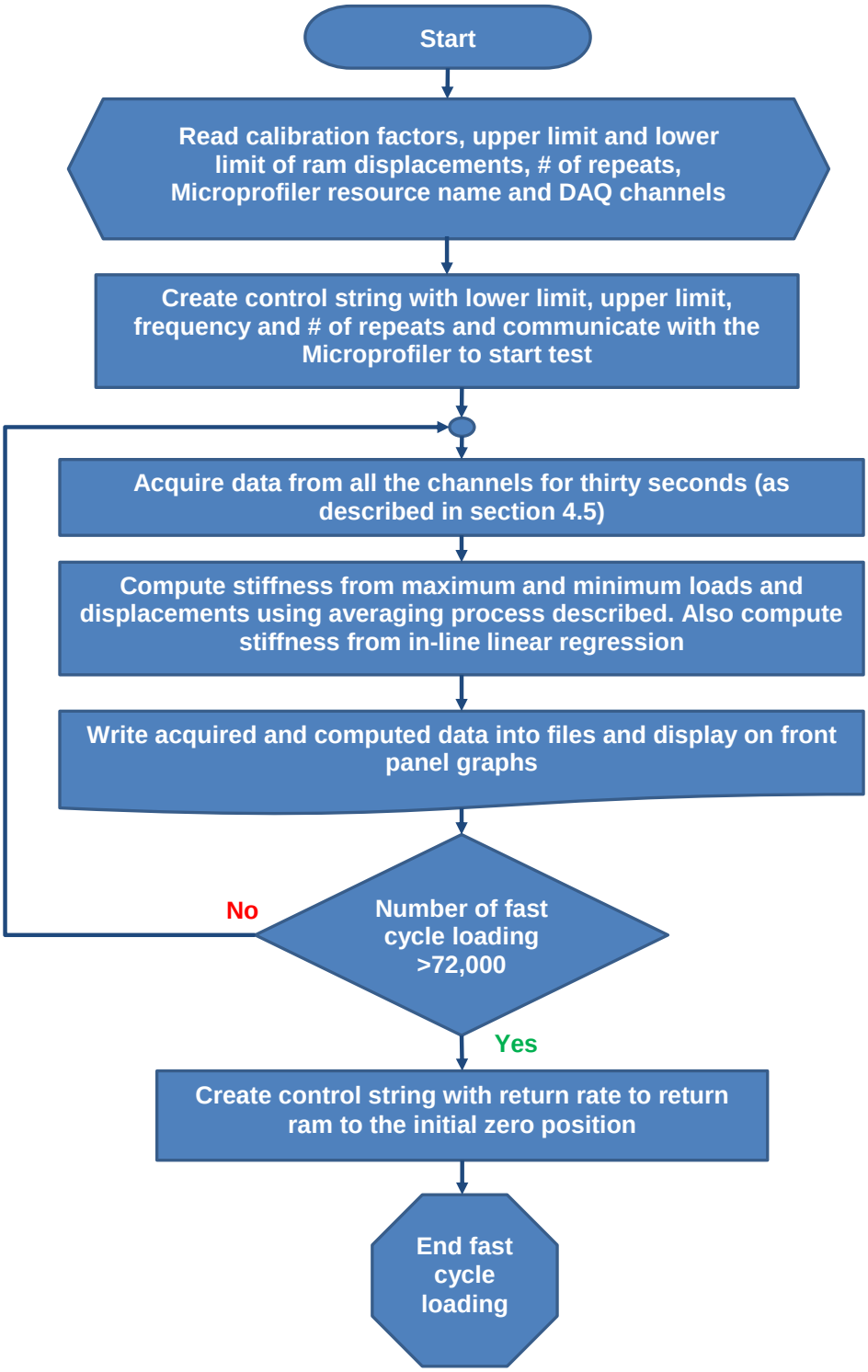

Fig. 4.9 Various steps involved in Fast cycles

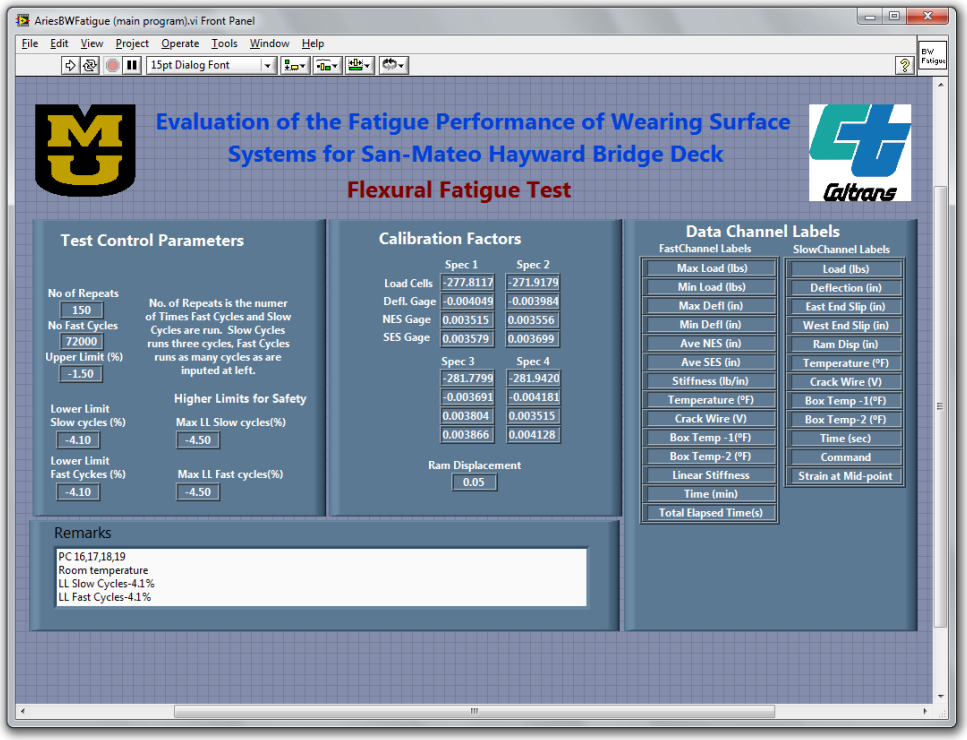

Fig. 4.10 Front panel of fatigue test

4.5.1 Active readjustment of maximum load

Since the fatigue tests were conducted on several specimens simultaneously, ram displacement control was used to apply prescribed fatigue loads to all the specimens. Viscoelastic materials when subjected to fatigue tend to exhibit relaxation with number of loading cycles, resulting in small drop in maximum load with fatigue cycles. The LabVIEW program for fatigue testing was automated to correct for this small drop in maximum load with each segment of fast cycle loading. The upper limit ram displacement was increased incrementally until the sustained upper limit load was at the prescribed value of 1,350 lbs. One of the replicate specimens recording the highest maximum load was used as the control specimen for these automated load adjustments. The incremental adjustment technique developed using actual maximum load

measurements allowed control of maximum load within ±75 lbs. Fig. 4.8 describes steps involved in the conduct of the overall fatigue test. Fig. 4.9 illustrates the steps involved within the fast cycle loading segment of the fatigue test.

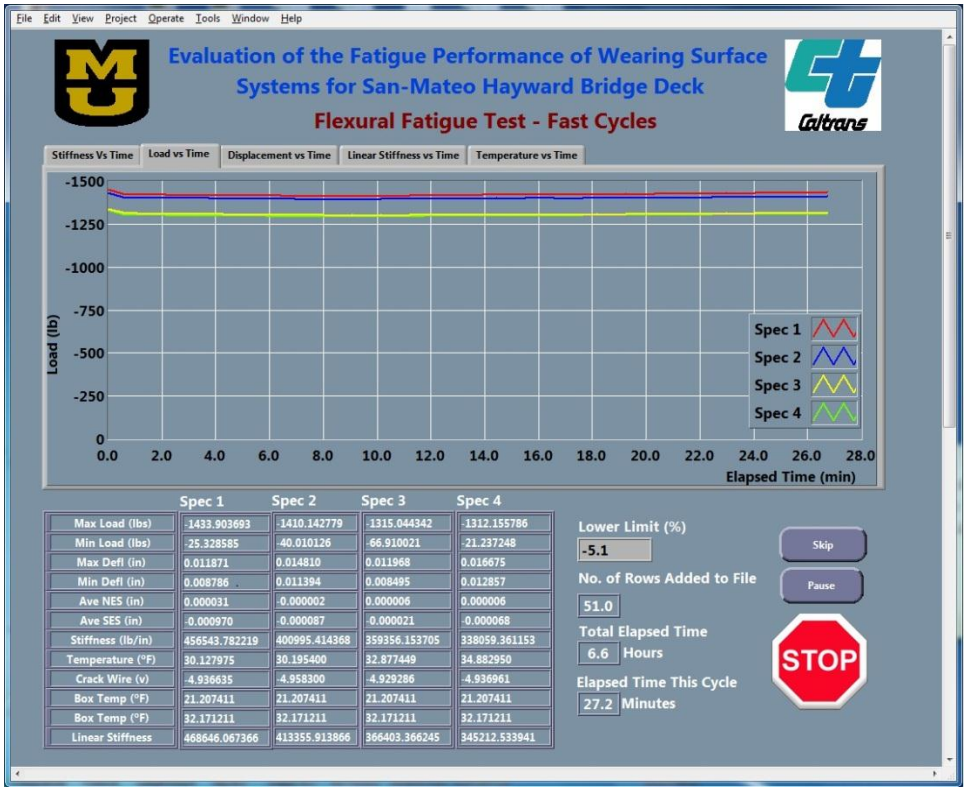

Fig. 4.11 Front panel of fast cycle

4.5.2 Input to the LabVIEW fatigue test program

As noted earlier, the flexural fatigue tests comprised alternate "slow cycle loading" and "fast cycle loading". Fig. 4.10 shows the front panel of the customized LabVIEW fatigue test program showing the input parameters required. The middle panel includes cells where calibration factors for the load cells, net-deflection and end-slip gages as well as the RAM displacement can be entered. Default values of these are stored in these cells. The input cells in the left panel comprise parameters used to control the test. The cell labeled "No. of Repeats" represents the number of repeats desired of a set of

slow and fast cycle loading segment (default of 150) and allows input of the limiting number of fatigue cycles (150 x 72,000 greater than 10^6 cycles). The cell labeled "No. Fast Cycles" allows input of the number of fast cycle loading in each segment (at 10 Hz, a two hour test interval results in 72,000 cycles). The lower limit of the ram displacement used was 1.5% which results in a load of approximately 200 lbs retained at the lower limit. This lower limit load ensures there is no unseating or slack in the loading train. Two different upper limits were used for slow and fast cycle loading to achieve the same upper limit fatigue load. This results from the loading rate sensitive behavior of the composite specimens. As described earlier, the LabVIEW program was designed to automatically adjust the upper limit of the ram displacement between the cycles to maintain the design load of 1,350 lbs. A cap on the upper limit displacement was also designed to ensure against accidental overloads.

The right panel (Fig. 4.10) contains column labels used in the data files for all the individual specimens. Other unchanging input like the frequencies used in the slow cycle loading (0.0167 Hz) and fast cycle loading (10 Hz) were hard-coded in the Lab VIEW program.

4.6 Static failure tests

Static failure tests were performed at room temperature, testing one specimen at a time. Among the parameters that were monitored during the test were flexural load, net deflection, two end slips, crack detection wire signal, steel strain, ram displacement and command signal used for test control. Tests were completed on a bare steel specimen as well as two EAC and PC composite specimens each.

Prior to the test, the test specimen was prepared by gluing the crack detection wire on the wearing surface in a multi-stage process to ensure tautness of the wire. This facilitated detection of crack as soon as it initiated on the wearing surface. The two end slip measurement fixtures as well as the midspan load distribution bar were glued on to the specimen using a quick setting epoxy. The test specimen was mounted in place using all the spring-loaded support fixtures (Fig. 3.23). All clip gages, the load cell, steel strain and ram displacement signals were zeroed. The ram was moved up until the loading stub was seated in the spherical seating of the load distribution bar glued to the specimen. A preload of approximately 100 lbs. was applied to ensure that all slack was removed from the loading train.

Static failure test was conducted using a linear ramp command signal using the ram displacement as the control parameter. Loading was applied at the rate of 0.0175 in./s. The ramp signal had a large enough termination limit (displacement limit of 0.50") so that the test could be stopped by the user on the failure of the composite specimen (due to any number of potential failure such as tensile cracking of the wearing surface, delamination of the wearing surface or yielding of the steel plate). A custom LabVIEW program facilitated test control, data acquisition as well as test monitoring. Data was acquired at a sample rate of one point per second from each of the channels recorded. Data was written to an output file once every second along with updates to multi-tab front panel plots of load, net deflection, end slip, ram displacement and steel strain signal histories. On user termination of the test, the ram was returned to its initial location at a specified “return to zero” rate. On some later tests (PC composite specimens) the

procedure for termination of the test was modified to allow data acquisition during the "return to zero" segment. This allowed a record of the unloading response.

4.7 Post-test crack detection and mapping effort

Cracking characteristics was studied post-test for all specimens that exhibited wearing surface cracking (static failure as well as flexural fatigue tests). The test set up for post-test crack detection (Fig. 3.24) allowed application of deflection identical to the maximum deflection imposed on the specimen during the actual test (so as to open cracks in an identically loaded condition). The crack detection set-up facilitated crack mapping outside of the test chamber where cracks could be viewed in better lighting and under magnification. Crack widths, length, distribution and pattern were documented using a template with grid pattern. All crack detection and mapping were undertaken in a room temperature environment.

Flexurally tested composite specimens were mounted, one at a time, on the steel platform designed for crack detection and mapping. C-clamps were used to sequentially load the four loading tabs in a calibrated manner using digital calipers while the specimen midspan was propped up with a precisely machined steel rod. This arrangement allowed reloading the specimen to the maximum deflection it had experienced during the flexural tests. At this level of deformation, cracks could be detected using a lighted magnifying glass. Table 4-1 includes the magnitudes of deflections recorded for the wearing surface composite specimens at the different test temperatures. Crack distribution patterns on the top and the two sides of the wearing surface were recorded in templates with grid

patterns. A crack width gage was also used to record widths at significant locations. Close-up photographs were also recorded under these loaded conditions.

Since the cracks were typically very fine, in addition to detecting cracks under load and under well-lit magnified views, it was often necessary to resort to additional crack enhancement techniques. This included dusting the cracked wearing surface with chalk dust, and cleaning the surface, thereby enhancing the visibility of the crack (white dust lodged in the cracks of a black wearing surface). Another enhancement technique involved wetting the cracked wearing surface with a fine spray of water to infiltrate cracks and enhance the contrast.

Table 4-1 Maximum deflection magnitudes used for wearing surfaces at different temperatures

Wearing Surface	Maximum midspan deflections			
	Fatigue (Cold)	Fatigue (Hot)	Fatigue (Room)	Static failure (Room)
EAC	0.0006	0.0300	0.0130	0.1700
PC	0.0007	0.0250	0.0120	0.0600

4.8 Resistivity tests

Following crack mapping, a limited number of representative cracked specimens of each wearing surface for each type of test were subjected to a resistivity test. Resistivity tests were performed on the wearing surface composites according to ASTM D3633 – 98 (Reapproved 2006). This method "Electrical Resistivity of Membrane-Pavement Systems" is used to provide a qualitative measure of the extent and nature of cracks in the wearing surface.

The test (Fig. 3.25) consisted of constructing a dam on top of the wearing surface with a plywood box along the rectangular edges. Silicone caulking was used around the

edges to prevent water from reaching the steel plate except through the top cracked surface of the wearing surface. Once the caulk had cured for a day, water containing a small amount of detergent was ponded on the surface of the specimen (using a supersaturated sponge). Detergent was added to minimize the surface tension, thus allowing the water to penetrate even very fine cracks (often invisible to the naked eye). A copper plate was placed atop the sponge, which was allowed to soak in the detergent water mixture. This "probe" was attached to one lead of an ohm meter; the other lead was attached to the steel plate of the composite specimen. When a reading was desired, the probe was taken from the soap water and placed on top of the specimen and the ohm meter was read immediately. Readings were typically taken at regular intervals (instantaneous, 1 hour, 2 hours and 3 hours after the specimen had been saturated with the detergent water mixture). The top of the specimen was sprayed afresh with the detergent-water mixture before each reading was taken. This ensured no evaporative drying of the top surface. With time, the measured resistance usually decreases. Results from this test provide a qualitative estimate of the severity of cracking in the wearing surface material. Low resistance (in the Ohm range) indicates the wearing surface had a crack through the thickness of the wearing surface. Resistance in the Mega-ohm range represents a crack that is not through the depth.

4.9 Tensile pull-out test

Several virgin composite specimens were reserved for the tensile pull-out tests. 2" diameter cores were drilled in the wearing surface until the core depth reached the steel plate. Up to 7 cores could be drilled in one composite specimen (plan area 18" x 4"). This allowed multiple pull-out tests on each specimen.

The top of the core was roughened in the case of EAC composite specimens to enhance the bonding to the pipe cap. The surface of the PC composite specimens already provided an aggregate rich surface for good bonding. 2" pipe caps were glued on to the cores using different types of glues (rapid setting as well as slow-curing). In the case of EAC, where failure of the cores was often at this glue-line rather than at the steel-wearing surface interface, the glue was additionally complemented with mechanical anchors (sleeve anchor, wedge anchor etc.).

After requisite curing of the glue (that was used to bond the pipe cap), the composite specimen was placed in the temperature controlled test chamber for 3+ hours so that it attained steady state temperature (either cold at 32°F or hot at 120°F). Pull-out tests were carried out as soon as the specimen was removed from the test chamber (often within 2-3 minutes). Pull-out tests were conducted in a room temperature environment. Those specimens that were intended for room temperature tests did not require the heating/cooling treatment.

The tensile pull-out test procedure involved placing the pull-out specimen under a steel platform supporting the wearing surface. A 3" diameter hole in the platform allowed the pipe cap glued to the core to be tested to be accessible for testing. The tripod device with the pull-out loading and measurement capability was threaded on to the pipe cap. A strain gage based load cell described earlier in Section 3.3.3 was used in series with the pull-out device. One end of this load cell was secured to the pipe cap using an adaptor and the other end was attached to the tripod loading frame. The load cell was connected to the conditioner /amplifier. The output of the amplifier was connected to the DAQ card.

Load was applied at a steady rate using the loading arm that applied tensile load on the pipe cap. As the pipe cap was pulled up the load cell signal was monitored and written to file using a custom LabVIEW program for the tensile pull-out test. As soon as the core was pulled out (or alternate type of failure was observed), the program was terminated.

5 Results and Discussions

5.1 Introduction

The sections in this chapter are organized based on results from the various types of tests described earlier in Chapter 3 on Experimental Program and Test Set-up and on Chapter 4 Test Procedures. Some sections bridge one or more of the topics of interest (e.g. Static Flexural Tests and the Effect of Temperature on Wearing Surface Properties). Analyses of the raw and processed results are discussed within the appropriate sections with references to how observations from this investigation may relate to service performance of the wearing surfaces studied.

5.2 Physical properties of test specimens

Prior to mechanical testing, the dimensions of each specimen were measured using digital calipers and weighed both in air and water. This allowed determination of the wearing surface density. These values are tabulated in Tables A1 and A2 (Appendix A) for the Epoxy Asphalt Concrete (EAC) and the Polyester Concrete (PC) composite specimens, respectively. As can be observed from these tables, the coefficient of variation of computed densities for the PC composite specimens is larger than that for the EAC composite specimens. This variation perhaps is reflective of the levels of consistency in the fabrication process. Comparable variations in results from the mechanical testing described in this chapter are also observed.

5.3 Static flexural response of composite specimens

5.3.1 Flexural load deflection response from static loading/unloading tests

As noted earlier in Chapter 4, static flexural tests were conducted on bare steel (BS), Epoxy Asphalt Concrete (EAC)-steel and Polyester Concrete (PC)-steel composite specimens at room, cold and hot temperatures. All static flexural tests comprised 3 sinusoidal cycles between the upper and lower limit loads used for the flexural fatigue tests (P_{max}, nominally 1,350 lbs. and P_{min}, 100 lbs., respectively) at a frequency of 1 cycle per minute (0.0167 Hz). Fig. 5.1 shows typical load-deflection plots for BS, EAC and PC wearing surface composite specimens conducted at room temperature. The slope of the load-deflection plots represents the flexural stiffness of these specimens. The contribution of the wearing surfaces to the flexural stiffness of the composite at room temperature is readily obvious when one compares the stiffness of bare steel to those of the two composite specimens. Also, at room temperature, it was observed that the PC wearing surface had typical apparent modulus value (the prefix "apparent" used only because these were not directly measured but "back calculated" from the composite load deflection responses assuming uncracked elastic transformed section analysis-discussed in more detail in section 5.3.3.3) between 6-8 fold that of the EAC wearing surface (average values of 479 ksi versus 57 ksi, respectively).

Table 5-1 includes summary results from static flexural tests conducted at room temperature. Data in the table also includes results from virgin "slow-cycle tests" conducted at the start of the flexural fatigue test series at room temperature. The virgin "slow-cycle" component of the fatigue tests is identical to the loading protocol used for the static flexural tests. The larger pool of results provides a more practically

representative database while also highlighting the statistical scatter of mechanical properties one could expect in typical field

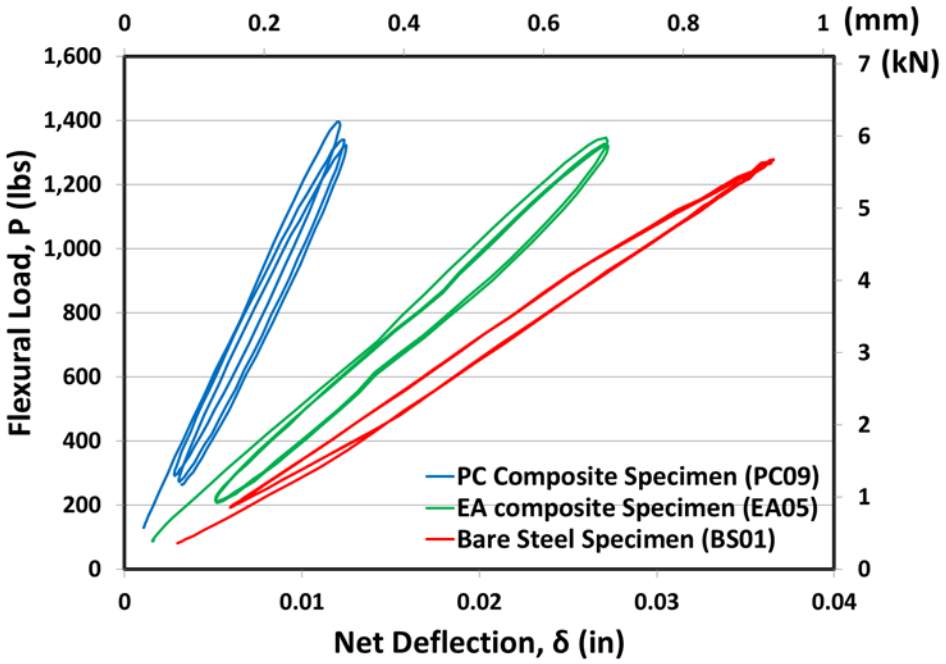

Fig. 5.1 *Static load-deflection responses for bare steel and composite specimens at room temperature (Nominal 70°F)*

applications of these materials. It should be noted that scatter in the properties of the PC specimens were typically larger than those recorded for the EAC specimens (coefficient of variation for apparent modulus values of 35% and 15% respectively). The binder content in the PC specimens was 12.5% (by weight) compared to those in the EAC specimens of 6.5%). The typical variation in elastic properties observed in this limited laboratory investigation can be attributed to variations in actual binder content from specimen to specimen.

Fig. 5.1 also highlights hysteresis observed due to the viscoelastic behavior of the thick wearing surface materials. At room temperature, the EAC-steel composite specimen

exhibits more hysteretic behavior compared to the PC-steel composite specimen. The small amount of apparent hysteresis observed in the steel response is attributed to an artifact of the net-deflection measurement set-up. Notice the distinct sharp tips of the steel cyclic loading/unloading response unlike the typically well-rounded response of composite specimens exhibiting hysteresis.

Table 5-1 Summary of results from static flexural tests conducted at room temperature

Room Temperature, 70°F		EAC Specimen	PC Specimen	BS Specimen
Apparent Elastic Modulus[1], E (ksi)	Range[2]	48-67	288-731	30,000
	Average	57	479	30,000
$\sigma_{s(max)}$ (ksi) at load of 1,350 lbs	Range[2]	14-15	3.7-6.9	19
	Average	14.5	5	19
$\sigma_{ws(max)}$ (ksi) at load of 1,350 lbs	Range[2]	0.17-0.22	0.45-0.58	NA
	Average	0.20	0.51	NA
$\varepsilon_{s(max)}$ (μstr) at load of 1,350 lbs	Range[2]	467-513	123-231	648
	Average	487	172	648
$\varepsilon_{ws(max)}$ (μstr) at load of 1,350 lbs	Range[2]	3,337-3,649	664-1,547	NA
	Average	3,487	1059	NA

[1] *Modulus values for the wearing surfaces were back calculated from flexural stiffness of the composite specimens assuming elastic analysis of the transformed cross-section*

[2] *Includes data from static flexural tests as well as virgin "slow cycle" results from fatigue tests*

Typical static flexural responses of the bare steel and composite specimens (PC and EAC) at cold temperature (Nominally 32°F) are compared in Fig. 5.2. Summary values from these series of tests are listed in Table 5-2. At the cold temperature, both wearing surfaces contribute significantly to composite flexural stiffness. Also the relative difference between stiffness values of the EAC and PC composites is marginal. It can also be observed that at the cold temperatures, the hysteretic behavior of the both types of composite specimens is greatly reduced.

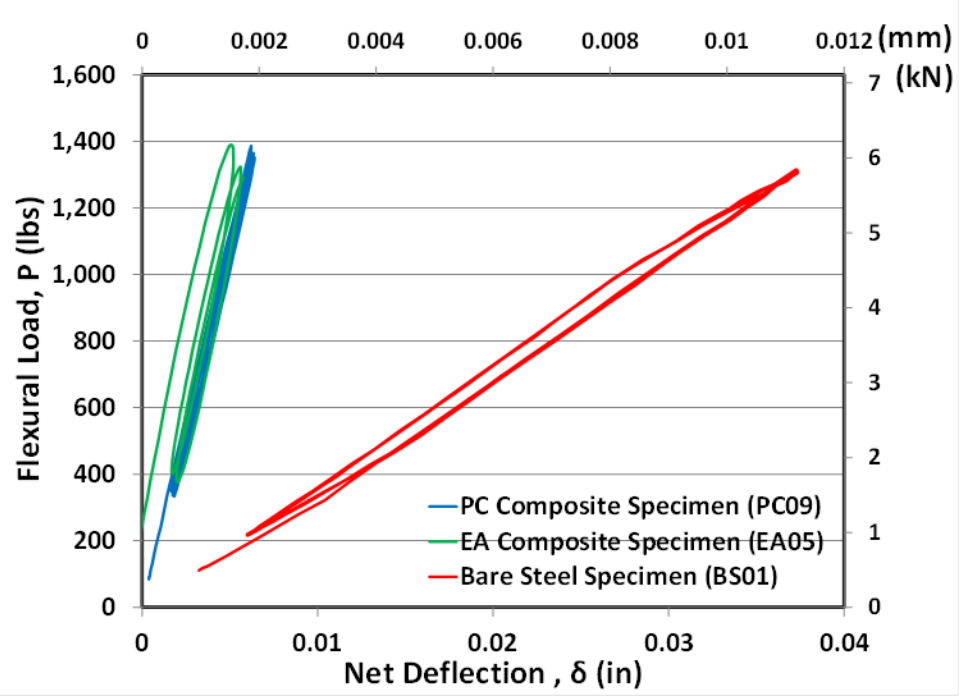

Fig. 5.2 Static load-deflection responses for bare steel and composite specimens at cold temperature (Nominal 32°F)

Table 5-2 Summary of results from static flexural tests conducted at cold temperature

Cold Temperature, 32°F		EAC Specimen	PC Specimen	BS Specimen
Apparent Elastic Modulus[1], E (ksi)	Range[2]	882-1,304	714-1,428	30,000
	Average	982	988	30,000
$\sigma_{s(max)}$ (ksi) at load of 1,350 lbs	Range[2]	3.3-4.1	2.7-4.1	19.4
	Average	3.9	3.5	19.4
$\sigma_{ws(max)}$ (ksi) at load of 1,350 lbs	Range[2]	0.61-0.66	0.55-0.65	NA
	Average	0.63	0.58	NA
$\varepsilon_{s(max)}$ (μstr) at load of 1,350 lbs	Range[2]	111-138	91-137	648
	Average	130	116	648
$\varepsilon_{ws(max)}$ (μstr) at load of 1,350 lbs	Range[2]	504-699	407-766	NA
	Average	654	592	NA

[1] *Modulus values for the wearing surfaces were back calculated from flexural stiffness of the composite specimens assuming elastic analysis of the transformed cross-section*

[2] *Includes data from static flexural tests as well as virgin "slow cycle" results from fatigue tests*

Hysteresis is associated with material viscosity in viscoelastic materials like EAC and PC. Although direct measurements were not made to determine the viscous characteristics of the wearing surface materials tested, it is reasonable to assume that both

materials exhibit significantly larger viscosities (reduced time-dependent characteristics) at the cold temperature compared to those at room temperature, resulting in the reduced hysteresis observed for the cold temperature static tests.

Static flexural responses of the bare steel and composite specimens (PC and EAC) at hot temperature (Nominally 120°F) are compared in Fig. 5.3. Summary values from static and virgin slow-cycle fatigue tests are included in Table 5-3 from the tests at hot temperatures. It can be readily observed from Fig. 5.3 that the contribution of the wearing surfaces to the composite

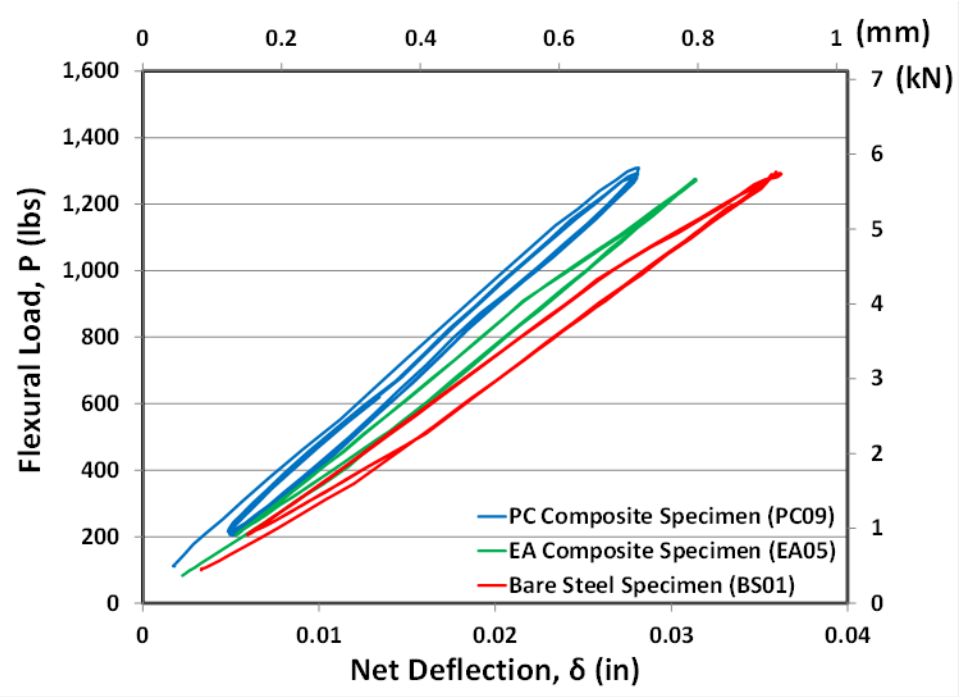

Fig. 5.3 *Static load-deflection responses for bare steel and composite specimens at hot temperature (Nominal 120°F)*

stiffness for both EAC and PC specimens are relative modest when compared to their respective cold and room temperature responses. This results largely from the significantly lower modulus of these wearing surface materials at the hot temperature. The variation of elastic moduli of the wearing surfaces with test temperatures is discussed

in greater detail later while presenting results from a test series where a more exhaustive range of test temperatures have been used for static flexural tests. Even while the stiffness values are comparable, PC composite specimens were observed to exhibit marginally higher values of flexural stiffness compared to EAC composite specimens at hot temperatures.

Table 5-3 Summary of results from static flexural tests conducted at hot temperature

Hot Temperature, 120°F		EAC Specimen	PC Specimen	BS Specimen
Apparent Elastic Modulus[1], E (ksi)	Range[2]	21-48	24-51	30,000
	Average	32	42	30,000
$\sigma_{s(max)}$ (ksi) at load of 1,350 lbs	Range[2]	15.0-17.3	14.3-16.6	19,440
	Average	16.3	15.0	19,440
$\sigma_{ws(max)}$ (ksi) at load of 1,350 lbs	Range[2]	0.86-1.74	0.10-1.82	NA
	Average	1.23	1.56	NA
$\varepsilon_{s(max)}$ (μstr) at load of 1,350 lbs	Range[2]	497-578	478-554	648
	Average	544	501	648
$\varepsilon_{ws(max)}$ (μstr) at load of 1,350 lbs	Range[2]	3,575-4,154	3,601-4,188	NA
	Average	3,938	3,810	NA

[1] *Modulus values for the wearing surfaces were back calculated from flexural stiffness of the composite specimens assuming elastic analysis of the transformed cross-section*

[2] *Includes data from static flexural tests as well as virgin "slow cycle" results from fatigue tests*

One would expect larger hysteresis in the static loading/unloading response from the composite specimens at hot temperatures given the observation that the viscosity of the wearing surface materials decreases with temperature. However this is not the case as observed in Fig. 5.3(compared to Fig. 5.1). This behavior is easily explained while considering composite action and the temperature dependent viscous behavior of the wearing surface materials. Even while these materials exhibit lower viscosities at the hot temperature, their contribution to composite stiffness at the hot temperatures is reduced due to the lower modulus of elasticity values (Table 5-3).

5.3.2 Static deflection ratio

One parameter that provides insights into the relative contribution of the wearing surface to composite action at the different test temperatures is the Static Deflection Ratio, SDR, a non-dimensional parameter. SDR is defined as the ratio of the span to the static deflection of the flexural specimen at a prescribed flexural load. Fig. 5.4 shows the plot of SDR as a function of test temperature for BS, EAC-composite and PC-composite specimens at test temperatures ranging from 20°F to 120°F in increments of approximately 10°F. The prescribed load at which the SDR values have been computed for Fig. 5.4 is 1,350 lb.

Fig. 5.4 clearly shows that BS does not exhibit temperature dependent stiffness characteristics (constant SDR values). Results from the composite specimens show the contribution to composite stiffness is obviously temperature dependent. While at hot temperatures, these materials do not change the stiffness characteristics of the composite specimens significantly; at the cold temperatures (~20°F) they increase the SDR by 800-1,000%.At both the extreme temperatures (20°F and 120°F), the SDR values of EAC and PC composite specimens are comparable. However in the temperature range 30-80°F, PC composites exhibit SDR values that are 2-4 times higher than the EAC composite specimens.

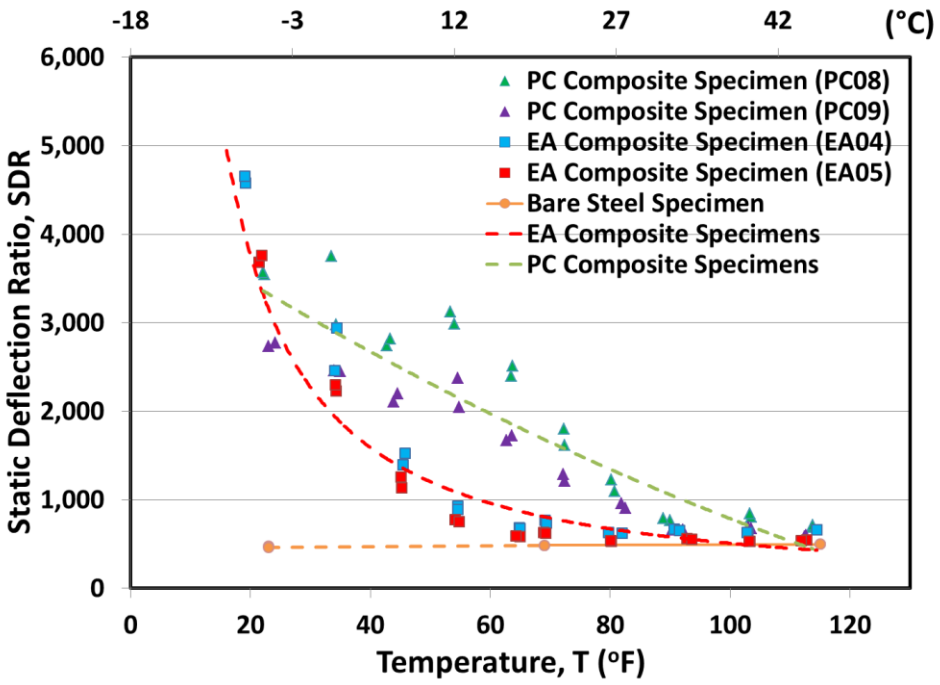

Fig. 5.4 Static deflection ratio of wearing surfaces and bare steel specimens

This difference in performance has implications with regard to service stresses on the wearing surface and steel deck plate as discussed in later sections of this chapter. The trend lines plotted using dashed lines in Fig. 5.4 also show that the temperature dependence of SDR in PC composite is flatter and somewhat linear compared to that observed for EAC composite specimens, which exhibits a steep concave upwards response.

5.3.3 Influence of temperature on viscoelastic charateristics of wearing surface materials

5.3.3.1 Load deflection response

Temperature plays an important role in influencing the mechanical properties of the two wearing surface materials studied. Of particular significance is the influence of temperature on the elastic modulus, although influences on tensile strength and corresponding strain, and viscous characteristics are also relevant to the service

performance of these materials on the bridge deck. Direct measurement of these influences was beyond the scope of this investigation, although indirect computations of elastic modulus are discussed in detail in this section. Wherever relevant, observations have been made on the viscous characteristics as well as strains at cracking. Fig. 5.5 and Fig. 5.6 illustrate the static load-deflection response of EAC and PC composite specimens, respectively, at various test temperatures. These figures highlight the loading unloading behavior including composite stiffness and hysteretic behavior. As noted earlier, composites made with both wearing surfaces show increased stiffness with decrease in the test temperature. At hot temperatures, the contribution of the wearing surface stiffness to overall composite stiffness is very minimal (see also Fig. 5.3), whereas the wearing surface contribution to composite stiffness at cold temperatures is very significant. This contribution has been shown in later sections to dramatically reduce stresses in the steel deck from transverse bending and can result in its improved fatigue performance (particularly as it relates to the potential for fatigue cracking of the steel plate over the longitudinal stiffeners). Also, as observed earlier, both wearing surfaces exhibit more hysteresis the temperature range 50-80°F (in the vicinity of the room temperature of 70°F) than at cold temperatures (20-30°F). The least hysteresis for the composite specimens was observed at hot temperatures (110-120°F) even while one would expect the lowest viscosities for the wearing surface material at the hot temperature (and consequently most hysteresis). This is attributed to the relatively marginal contribution of the wearing surface to overall composite stiffness at the hot temperature. The room temperature hysteresis of EA composite specimens is very pronounced compared to the hysteresis exhibited by the PC composite specimens.

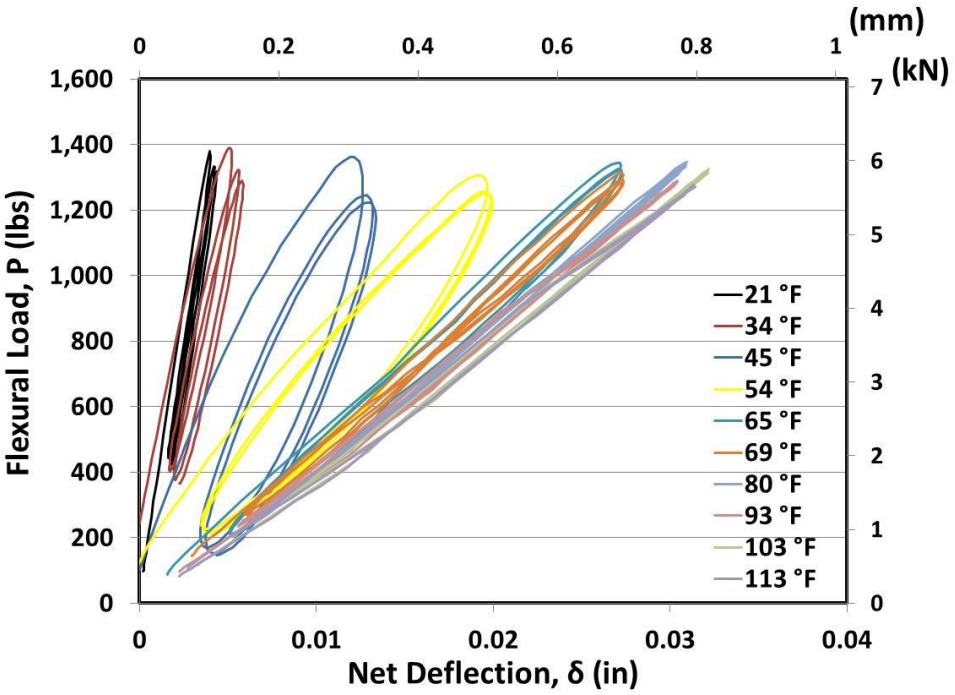

Fig. 5.5 Static flexural response of Epoxy Asphalt Concrete specimen (EA05)

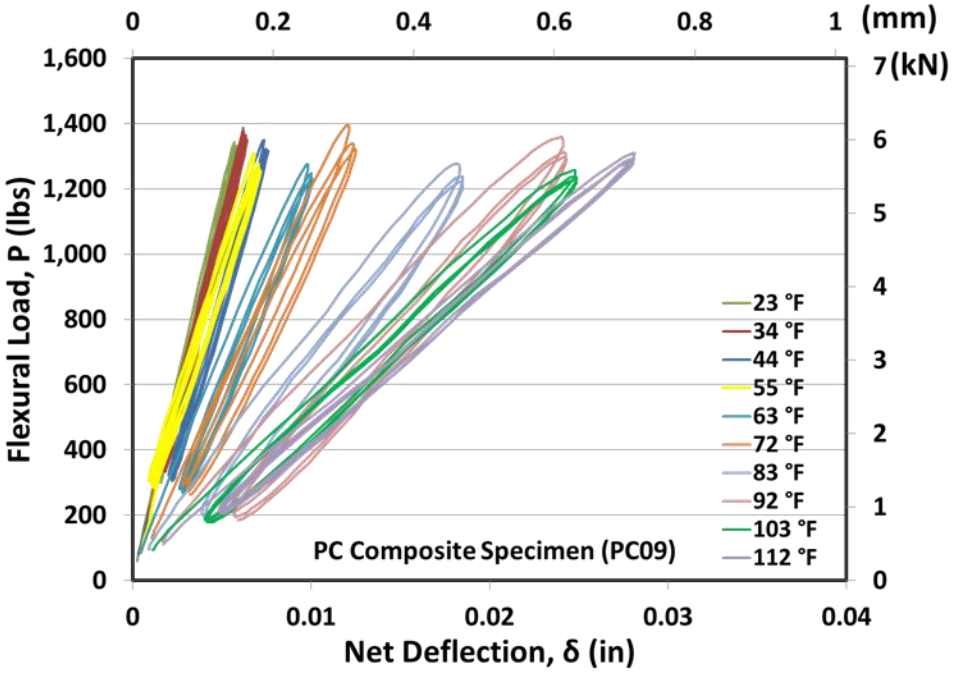

Fig. 5.6 Static flexural response of Polyester Concrete composite specimen (PC09)

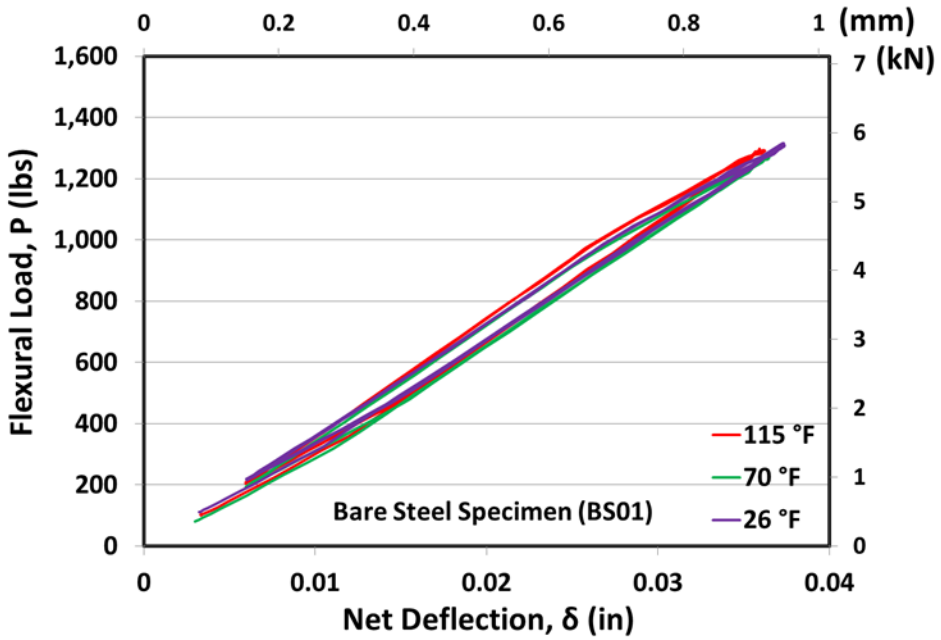

Fig. 5.7 Static flexural response of bare steel specimen (BS01)

Fig. 5.7 shows the loading-unloading response of the bare steel specimen subjected to the three different temperatures, essentially highlighting a temperature-independent behavior. The small amount of apparent hysteresis observed in the steel loading-unloading response is attributed, as earlier, to an artifact of the net-deflection measurement set-up. The stiffness values recorded for the bare steel specimens (approximately 37,000 lb./in) is marginally lower than those obtained for the EA and PC composite specimens tested at the hot temperature (approximately 45,000 lb/in at 120°F), clearly highlighting the relatively small contribution of the wearing surface at these temperatures to composite section. The influence of test temperature to both the elastic modulus and wearing surface viscosity, and as a result, on contributions to composite action of the wearing surface at different temperature is phenomenologically highlighted in the next section.

5.3.3.2 Phenomenological temperature dependent behavior from rheological model

The mechanics of the temperature-related viscoelastic response has, in principle, been demonstrated using a standard solid rheological model (Fig. 5.8) of the composite specimens.

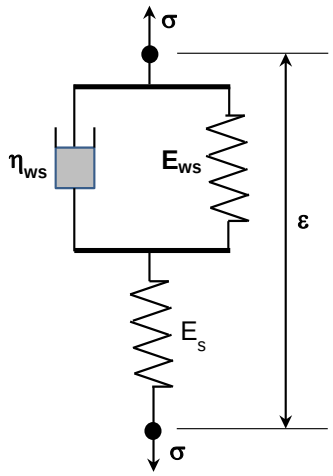

Fig. 5.8 *Schematic of a standard rheological model representing the wearing surface-steel composite subjected to tension*

The wearing surface is represented as a Kelvin-Voigt model (elastic modulus, E_{ws}, and viscosity, η_{ws}) exhibiting both elastic and viscous behavior and the steel plate as an elastic solid (elastic modulus, E_s). The governing differential equation for this standard solid is given by:

$$\frac{d\varepsilon}{dt}\eta_{ws} + \varepsilon E_{ws} = \frac{d\sigma}{dt}\left(\frac{\eta_{ws}}{E_s}\right) + \sigma\left[1 + \frac{E_{ws}}{E_s}\right] \qquad 5.1$$

where σ is the applied stress and ε is the resultant displacement. Even while this simple tension model for the σ-ε response does not adequately characterize the more complicated flexural behavior of the composite specimen, it is nevertheless very useful in understanding the influence of temperature on the viscoelastic behavior of the wearing

surfaces (both EAC and PC composites exhibit viscoelasticity). Solutions obtained using MATLAB for the strain based on a loading function of the type used (Eq. 5.2, Fig. 5.9) is plotted in Fig. 5.10.

$$\sigma(t) = \left(\frac{\sigma_{max} - \sigma_{min}}{2}\right) \sin \omega t + \sigma_{static} \qquad 5.2$$

Nominally, the cross-section area A and length L have been assumed to be unity for the plots in Fig. 5.9 so that σ directly represents the applied tensile load, F (time dependent sinusoidal function), and ε directly represents the resultant time-dependent tensile displacement, Δ, for convenience of the illustration.

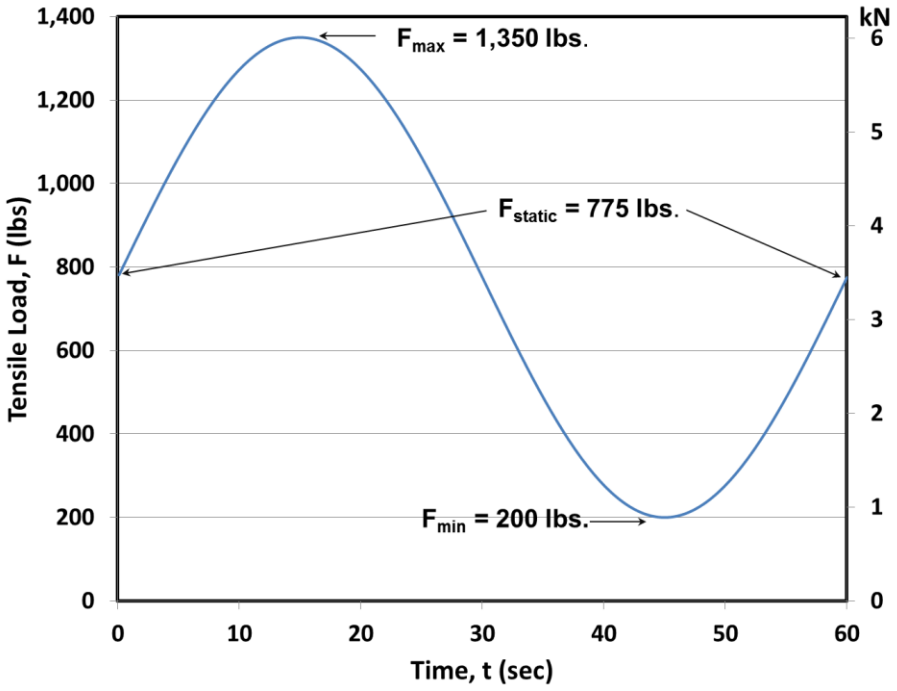

Fig. 5.9 *Tensile fatigue load history applied to the Kelvin-Voigt rheological model showing fatigue load range as well as the static load*

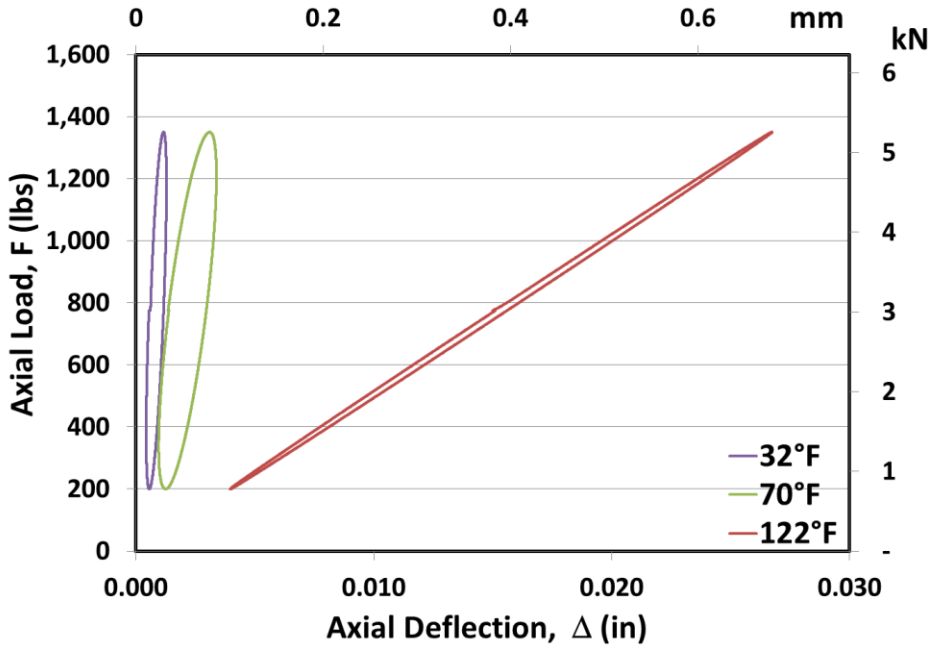

Fig. 5.10 *Tensile load-displacement response predicted by the governing differential equation of the Kelvin-Voigt model (Eq. 5.1)*

Fig. 5.10 illustrates the same coupled influences of variation in the elastic modulus and viscosity of the wearing surface materials as a function of test temperature observed in the static flexural tests reported earlier (Fig. 5.5 and Fig. 5.6) and the resultant effects on the composite stiffness and hysteresis characteristics observed at the cold, room and hot temperatures.

5.3.3.3 Temperature dependent apparent elastic modulus of the wearing surface

The term "Apparent Elastic Modulus" is used to refer to the elastic modulus of the wearing surface back-calculated from the stiffness obtained from static flexural tests on the composite specimens conducted at various temperatures ("Apparent" only because it was indirectly computed and not directly measured). The temperatures were obtained for each specimen by attaching a thermocouple to the tension face of the wearing surface. An

uncracked-elastic transformed section analysis of the wearing surface – steel plate composite was adopted for the calculation of temperature dependent elastic modulus of the wearing surface. The bond between the wearing surface and steel plate was assumed to be perfect. The steel-basis effective moment of inertia of the transformed composite (simply supported flexural specimen subjected to midspan concentrated load) is given by:

$$(I_{composite})_{steel\ basis} = \left(\frac{P}{\delta}\right)\frac{L^3}{48E_s} \tag{5.3}$$

where: δ = net midspan deflection, P = flexural load, L = span between support rockers, E_s = elastic modulus of steel (assumed as 30,000 ksi)

The stiffness of the composite specimen, (P/δ), was computed from a regression analysis of the experimentally recorded load-deflection response. The neutral axis (from the tension face) for the transformed section of the wearing surface steel plate composite is given by:

$$\bar{y} = \frac{\frac{bd_{ws}^{\ 2}}{2n} + d_s b\left(d_{ws} + \frac{d_s}{2}\right)}{\frac{d}{n}d_{ws} + d_s b} \tag{5.4}$$

and the moment of inertia of the composite section (steel basis) is obtained as:

$$I_t = \frac{b}{n}\frac{d_{ws}^{\ 3}}{12} + \frac{b}{n}d_{ws}\left(\bar{y} - \frac{d_{ws}}{2}\right)^2 + b\frac{d_s^{\ 3}}{12} + bd_s\left(d_{ws} + \frac{d_s}{2} - \bar{y}\right)^2 \tag{5.5}$$

where $\bar{y}$ = neutral axis depth from the tension face, b = width of the steel base plate (4”), d_{ws} = depth of the wearing surface (nominally 2"), d_s = depth of the steel base plate (5/8"), n = modular ratio= E_s/E_{ws}, and $(I_{composite})_{steel\ basis}$ = moment of inertia of the composite (steel basis), I_t=Moment of inertia from the transformed section properties (steel basis)

Substituting Equation (5.4) into (5.5) provides $(I_{composite})_{steel\ basis}$ as a function of the unknown modular ratio, n.

$$(I_{composite})_{steel\ basis} = I_t(n) \qquad 5.6$$

The value of n can be uniquely solved by determining the root of Equation 5.6. The elastic modulus of the wearing surface, E_{ws}, can be computed assuming the modulus of the steel plate, E_s as 30,000 ksi. Fig. 5.11 highlights the apparent elastic modulus computed at the various test temperatures for the EA and PC wearing surface materials. At temperatures around 32°F and 120°F, the apparent modulus of EA and PC are comparable (~850 ksi and 50 ksi, respectively).

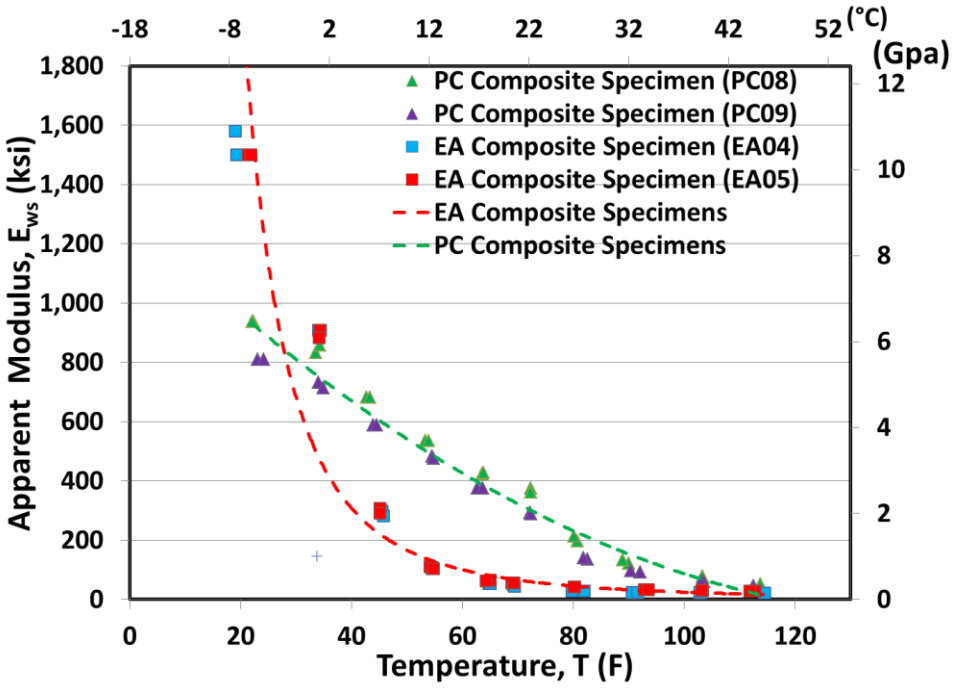

Fig. 5.11 *Apparent elastic modulus as a function of wearing surface temperature from composite EA and PC specimens.*

In the 60°-80°F temperature range, the apparent elastic modulus of PC is approximately 6-8 fold that of EA. At the coldest temperatures (~20°F), the EA exhibits

elastic modulus in the 1,500 ksi range. EA exhibits relatively less variation in elastic modulus in the 60°-120°F temperature range (45-80 ksi) and very steep stiffening at temperatures below 40°F. PC exhibits a relatively linear dependence of elastic modulus on temperature, with no steep stiffening at temperatures below 40°F. The temperature dependent performance of the wearing surface is likely to have significant practical impact on stresses from transverse bending of the orthotropic deck, both in the wearing surface as well as the steel deck plate. These issues are analytically explored and discussed in detail in the next section.

5.3.3.4 Wearing surface and steel stresses as a function of temperature

Flexural stresses at the extreme fibers of the steel plate (compressive) and the wearing surface (tension) were computed using an uncracked elastic analysis of the transformed composite specimen at the maximum applied loads (1,350 lbs. static tests) and apparent elastic modulus of the wearing surface reported earlier. They are plotted in Fig. 5.12 for the EA composite specimens and in Fig. 5.13 for the PC composite specimens. In both these figures, the primary ordinate axis (red axis title and associated scale) is used to plot the maximum compressive stress in steel and the secondary ordinate axis (blue title and associated scale) is used to plot the maximum tensile wearing surface stress. Wearing surface temperature is plotted on the abscissa. Plots are from two replicate specimens in each case. The trend lines show nonlinear regression relationships between stresses and wearing surface temperatures. In general, as the test temperature increases, the wearing surface stress decreases, resulting from the lower elastic modulus of the wearing surface and associated reductions in the composite flexural stiffness.

Two distinct differences can be observed while comparing Fig. 5.12 for EA composite specimens with Fig. 5.13 for the PC composite specimens.

(1) The shape of the stress-temperature plots have opposite curvatures for the two types of wearing surface materials. Wearing surface stress-temperature relationship in EA composite specimens exhibits a "concave upwards" response with stress magnitudes approaching a low value (of approximately 100 psi) at the high temperatures. At the colder temperatures the wearing surface stress magnitudes exhibit increasing values (approaching 800 psi at 20°F). For the PC composite specimens, this relationship is "concave downwards" with stress magnitudes at the cold temperatures asymptotically approaching 600 psi at 20°F. At the hotter temperatures the wearing surface stress magnitude continues to reduce. The steel stress-temperature profiles in contrast in both cases follow opposite trends in curvature and asymptotic magnitudes.

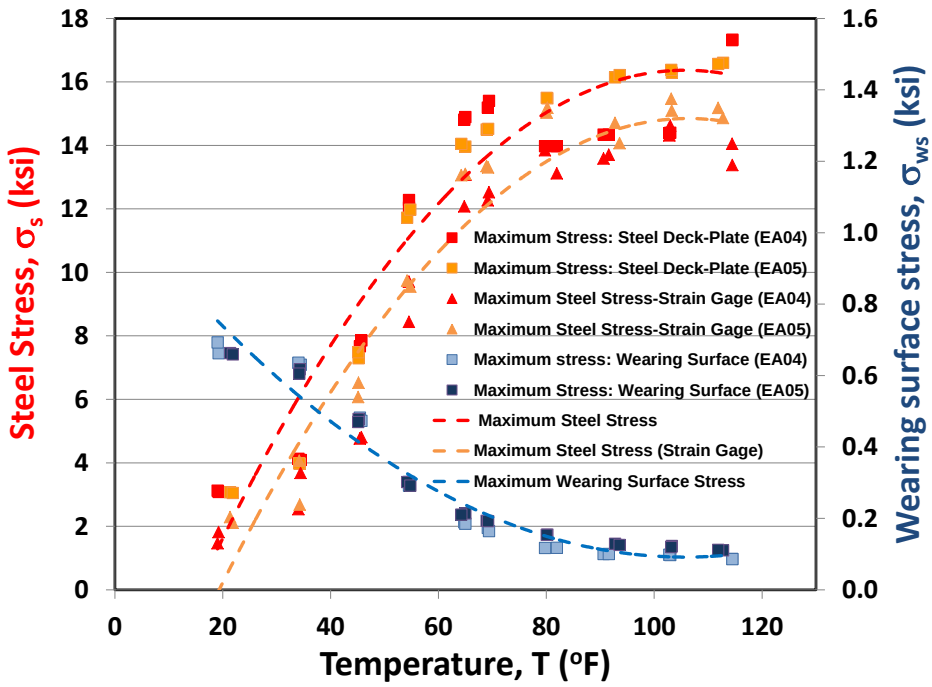

Fig. 5.12 *Steel and wearing surface stress as a function of wearing surface temperature (from EA composite specimens evaluated at the maximum load of 1,350 lbs.).*

(2) Due to the larger apparent elastic modulus values in much of the range of temperatures tested, the steel stress magnitudes in the PC composite specimens is smaller than steel stresses at comparable temperatures for the EA composite specimens. This may have implications with regard to fatigue performance of the steel deck plate, as lower stress levels result in longer fatigue lives of the deck plate (this observation is confined to transverse bending effects only). Due to the same effect, the magnitude of the wearing surface stresses are marginally larger for the PC composite specimens compared to the EA composite specimens in much of the range of the temperatures tested. This observation may also affect the fatigue performance of the wearing surface, as larger stress levels result in lower fatigue lives.

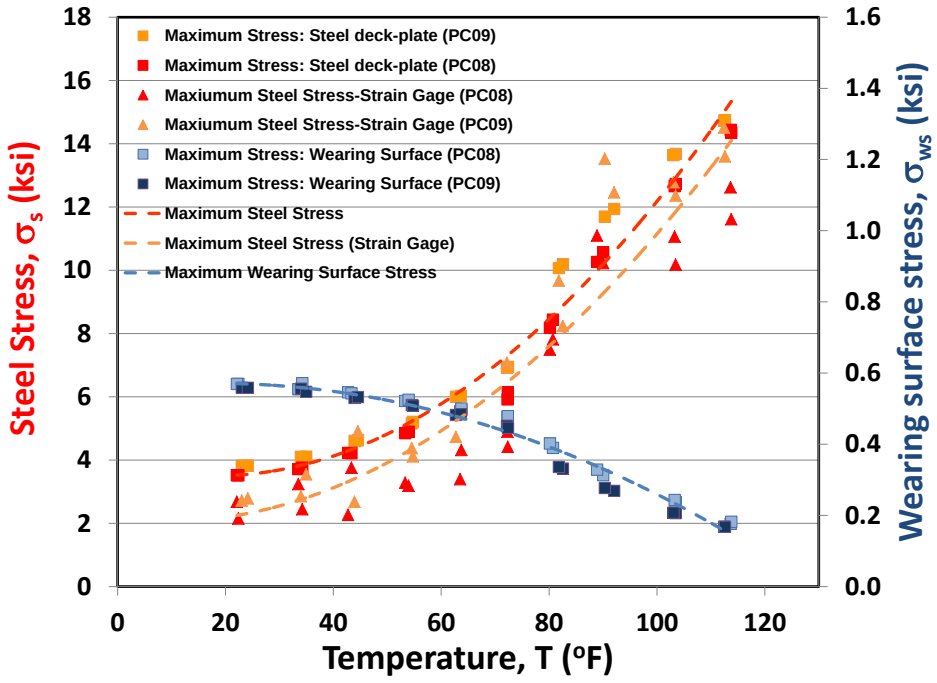

Fig. 5.13 *Steel and wearing surface stress as a function of wearing surface temperature (from PC composite specimens evaluated at the maximum load of 1,350 lbs.).*

The computed steel stress profiles illustrated in Fig. 5.12 and Fig. 5.13 have also been validated by using results from direct measurements of steel strains on several composite specimens.

5.3.3.5 Composite action, stress magnitudes and wearing surface design implications

Stress magnitudes as noted earlier, both in steel as well as the wearing surface material are influenced by the temperature dependent elastic modulus of the wearing surface. This is only one of the two important parameters under easy control of the bridge designers. The composite stiffness of the wearing surface and steel plate is also affected by the depth of the wearing surface. Even if one chooses a wearing surface material for a steel orthotropic deck, it is possible to engineer stresses in the wearing surface and the

steel deck plate, with a view to optimize fatigue life by controlling the depth of the wearing surface. Details of related analytical and experimental analyses of composite action are presented by Gopalaratnam (2009) and Gopalaratnam and Chamarthi (2012), as described earlier in Chapter 2. Fig. 5.14 and Fig. 5.15 shows plots of the steel stress and wearing surface stress, respectively, as functions of the wearing surface depth, d_{ws}, for different values of the modular ratio, n ($=E_s/E_{ws}$). The depth of the steel plate assumed for these computations is 5/8" and a steel elastic modulus of 30,000 ksi is assumed. The modular ratio for these plots is varied from n = 20 to 1,500 (equivalent wearing surface modulus from 1,500 ksi (cold) to 50 ksi (hot)). Steel stress monotonically decreases with increasing wearing surface depth.

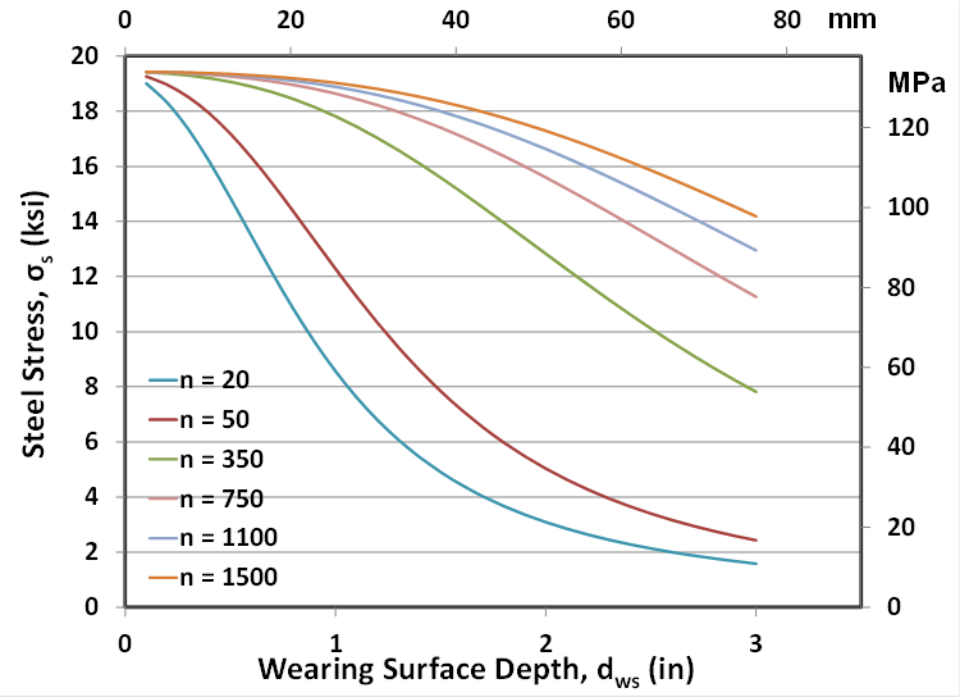

Fig. 5.14 *Analytical steel stress as a function of wearing surface depth for different modular ratios.*

At very small wearing surface depths the steel stress approaches 19 ksi. At larger wearing surface depths, a higher modulus wearing surface (or one at cold temperatures) can dramatically reduce steel stress from transverse bending of the deck (~2 – 3 ksi). At the larger wearing surface depths, a low modulus wearing surface (or one at hot temperatures) steel stress remains relatively high (~14 - 16 ksi, Fig. 5.14).

Fig. 5.15 illustrates the relationship between magnitude of wearing surface stress and its depth, as a function of modular ratios in the range 20-1,500. Unlike steel stress which decreases monotonically with increases in wearing surface depth, the wearing surface stress does not monotonically decrease with increases in wearing surface depth. Maximum stress magnitudes are highlighted with square markers in Fig. 5.15. For wearing surfaces with large elastic modulus (or ones subjected to cold temperatures), a smaller wearing surface depth could result in larger wearing surface stresses. For lower wearing surface moduli, the critical depth that produces maximum stress in the wearing surface has been observed to increase (Fig. 5.14).

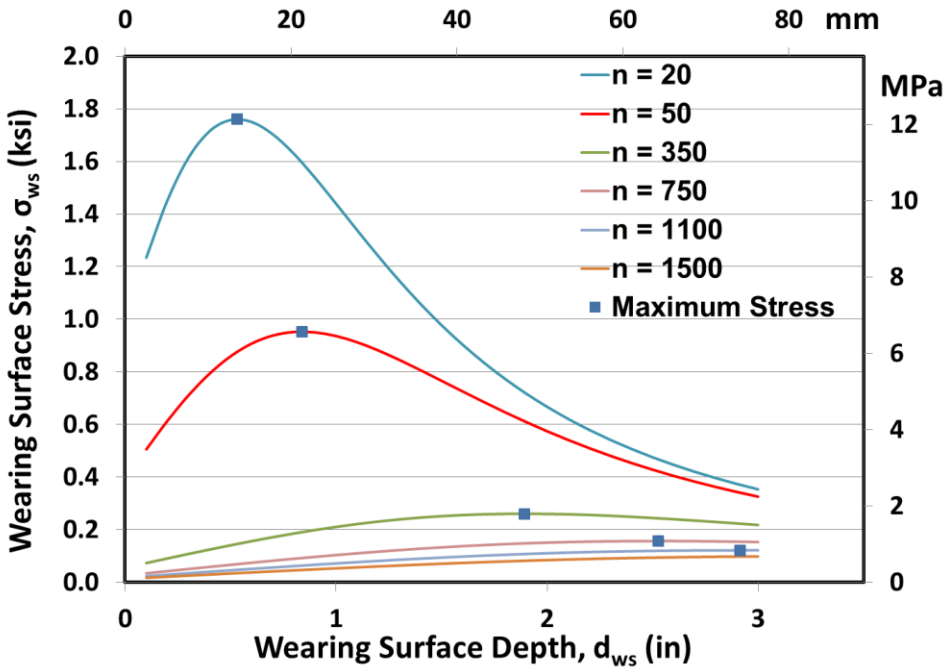

Fig. 5.15 *Analytical steel stress as a function of wearing surface depth for different modular ratios.*

5.4 Dynamic flexural response and rate sensitivity of wearing surface

Similar to the Static Deflection Ratio, the Dynamic Deflection Ratio, DDR, is also a non-dimensional parameter that is useful in characterizing the contribution of the wearing surface to the composite stiffness when subjected to dynamic loads. It is defined as the ratio of the span to the dynamic deflection of the flexural specimen at a prescribed flexural load. The dynamic deflection ratios were computed at the maximum fatigue load of 1,350 lbs. Fig. 5.16 shows the plot of DDR as a function of test temperature for BS, EAC-composite and PC-composite specimens at three test temperatures (25°F, 68°F, and 122°F). Dynamic deflections were measured when the specimens were subjected to a 10 Hz sinusoidal loading with the nominal upper and lower limit loads of 1,350 and 100 lbs., respectively. Fig. 5.16 shows that BS does not exhibit temperature dependent stiffness

characteristics (constant DDR values). Results from the composite specimens show the contribution to composite stiffness is obviously temperature dependent.

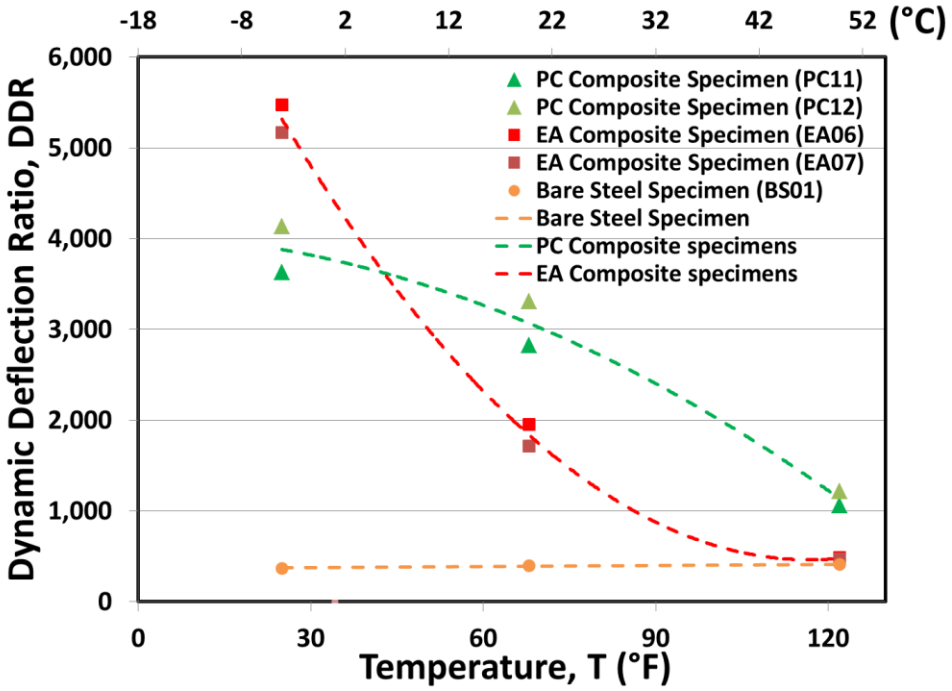

Fig. 5.16 *Dynamic deflection ratio as a function of test temperature for BS and EAC and PC composite specimens*

While the overall trends for DDR as a function of temperature, are similar to those discussed earlier in Section 5.3.2. DDR values however are higher than corresponding SDR values at room temperature largely because of the rate sensitivity of the materials exhibited by both the EAC and PC composite specimens.

Fig. 5.17 and Fig. 5.18 show the rate sensitivity of the apparent modulus, E_{ws}, for the two wearing surfaces (EAC and PC, respectively). The apparent modulus, as earlier for the static tests, is back computed from composite stiffness measured at the different temperatures assuming transformed uncracked elastic section. Results from tests conducted at loading rates of 0.0167, 1, 2, 5, 7.5, 10 and 15 Hz are plotted in these two

figures at the cold (32°F), room (70°F) and hot (120°F) temperatures. For the EAC composite specimens there is little rate sensitivity observed at the hot temperatures. This results from the relative small contribution of the wearing surface to composite stiffness at the hot temperature. At the cold temperature, EAC composite specimen does not exhibit rate sensitivity beyond 5 Hz. In the frequency range 0.0167 – 5 Hz, there appears to be measurable loading rate sensitivity.

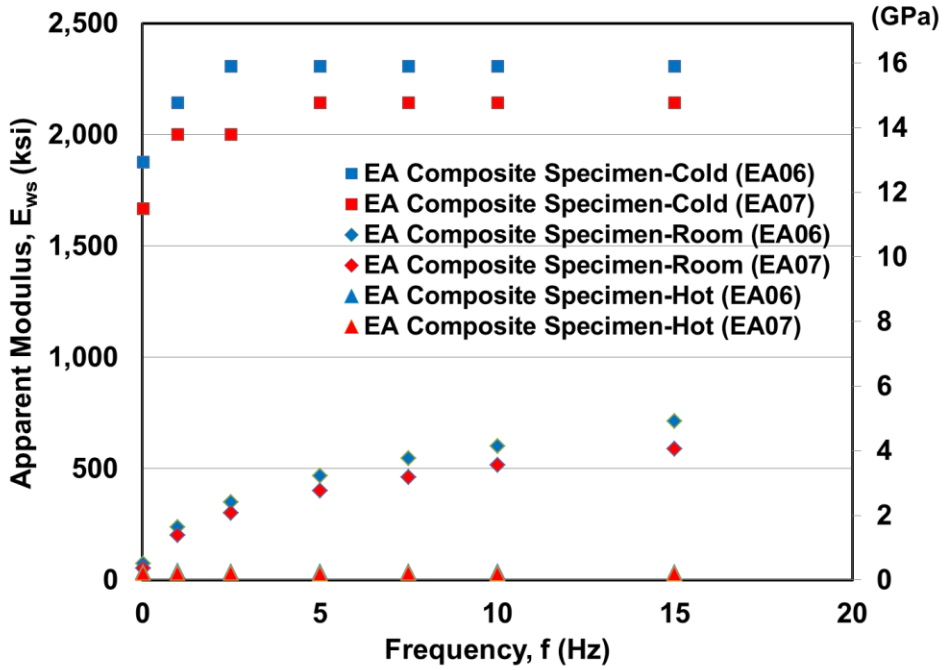

Fig. 5.17 *Dynamic values of the apparent modulus of the EAC wearing surface as a function of the loading rate at three different test temperatures.*

At room temperature, EAC exhibits rate sensitivity in the entire range tested (0.0167 – 15 Hz). The rate sensitivity at the lower loading rates appears to be nonlinear whereas at rates beyond 5 Hz, the rate sensitivity is nearly linear. These experimental

observations are likely to be helpful in the numerical modeling of deck stresses where contributions from the wearing surface to deck stiffness are not neglected.

Unlike the EAC wearing surface, the PC wearing surface shows no significant rate sensitivity beyond approximately 2.5 Hz for all the three test temperatures. At the lower test frequencies (0.0167 – 2.5 Hz) PC wearing surface does exhibit measurable rate sensitivity at all three temperatures. The ratio of the dynamic modulus to the static modulus in this range appears to be independent of the temperature (Fig. 5.18).

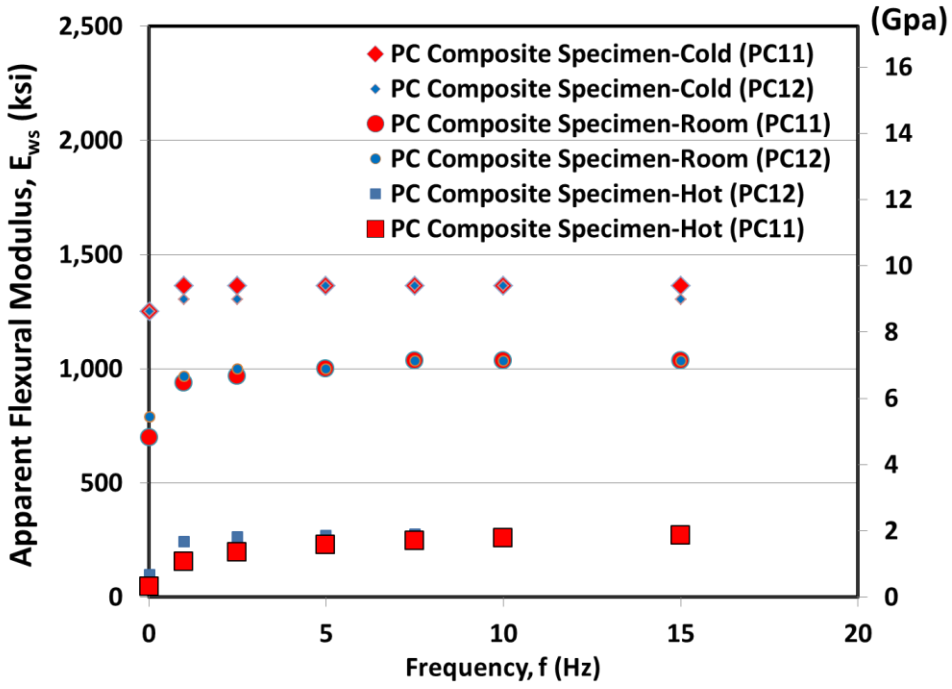

Fig. 5.18 *Dynamic values of the apparent modulus of the PC wearing surface as a function of the loading rate at three different test temperatures.*

5.5 Fatigue performance of EAC and PC wearing surfaces

Results from EAC and PC composite specimens subjected to flexural fatigue loading (per procedures described in Section 4.5) are discussed in the following four subsections and include performance at the cold, room and hot temperatures. A general summary of observations is also included to complete these discussions. Stiffness, maximum and minimum loads and maximum and minimum deflections were monitored continuously during these tests. Crack initiation was detected using multiple techniques including monitoring of the signal from the crack detection wire glued on the tension face of the wearing surface, digital image of the tension face, and changes in stiffness magnitudes with fatigue cycles. Tests were typically continued well beyond crack initiation with a view to monitor crack growth (size, patterns and width) for specimens that exhibited cracking prior to the limiting life. The limiting life of 10 million cycles was also imposed on specimens.

5.5.1 Fatigue performance at the cold temperature

The temperature desired for tests at the cold temperature (32ºF) was achieved by operating the cooling unit overnight so that the mass of test fixtures, test specimens and instrumentation all attained steady state temperature prior to the start of the fatigue loading. Stiffness from the fast cycle segments computed every 30 seconds (as average of 30 values of the ratio of the difference in maximum and minimum load to the difference in the maximum and minimum displacement, as described in Section 4.5) is plotted in Fig. 5.19afor the EAC composite specimens subjected to cold temperature fatigue tests. Virgin stiffness values for the four specimens range from 350-450 kip/in. Over the 10 million fatigue cycles, the stiffness values were observed to be nearly constant for all four

specimens, indicating that the EAC composite specimens were able to withstand the fatigue loading with no discernible cracking or damage. This observation has also been confirmed from several other independent parameters recorded as discussed later. The small increase in stiffness values for all four specimens after approximately 1.5 million fatigue cycles is attributed to the fact that a new circulation fan was introduced into the test chamber to ensure more uniform temperatures within the test chamber. This caused a drop in chamber temperature and resultant increase in the stiffnesses observed. Fig. 5.19b shows a plot of the normalized stiffness (ratio of current stiffness to that of the virgin specimen) values as a function of the number of fatigue cycles. This plot confirms the observations made from Fig. 5.19a while masking the variability in stiffness values between individual specimens, typical in heterogeneous composite specimens.

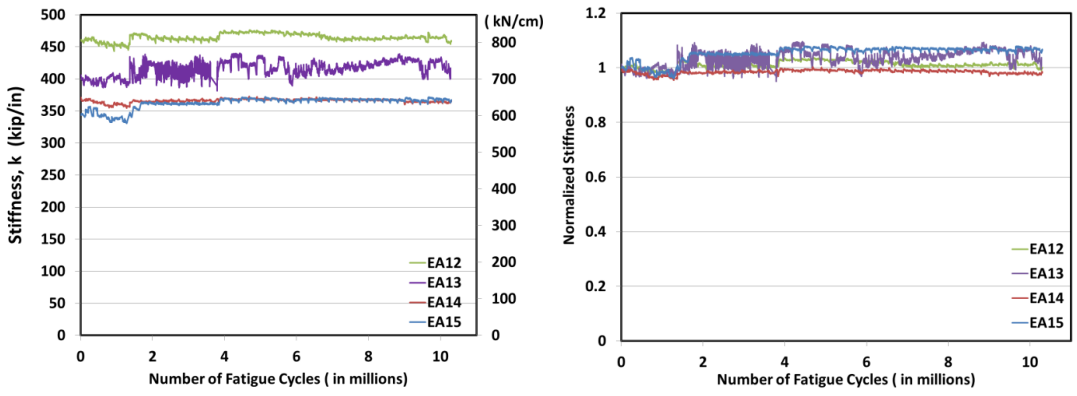

Fig. 5.19 *(a) Stiffness and (b) Normalized stiffness of the EAC composite specimens versus number of fatigue cycles at the cold temperature.*

Fig. 5.20 shows the signal from the crack detection wire as a function of the number of fatigue cycles for the EAC composite specimens tested. All four specimen signals are identical and hence the four plots are indistinguishable. The steady signal at 5 V indicates that there is no loss of continuity, implying no surface cracks are present on

the tension faces of the four test specimens. The two end-slip gage signals for the four specimens too did not indicate any slip from debonding or delamination. Photographs from the overhead cameras of the automated digital imaging system, too confirm that 10 million cycles of the cold temperature fatigue loading did not cause any visible cracking. Fig. 5.21 shows a plot of the maximum and minimum loads from the cold temperature fatigue tests on EAC composite specimens. Variations in the maximum load in the 1,350 lbs ± 75 lbs range observed in the figure results from a combination of effects from temperature fluctuations (auto defrost cycles needed to maintain temperature and mitigate ice buildup in the coils of the cooling system), relaxation of the viscoelastic wearing surface material from the displacement controlled tests, and automated readjustments in the maximum load built into the custom LabVIEW program developed for test control. The minimum load, like the stiffness, shows a modest bump at approximately 1.5 million fatigue cycles, with the introduction of the new circulation fan in the test chamber.

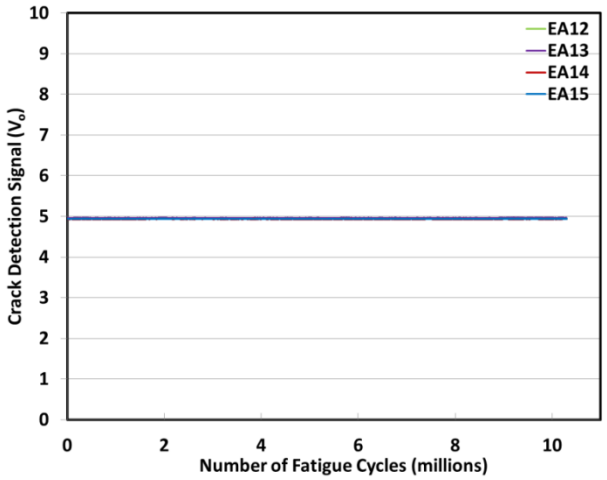

Fig. 5.20 *Crack detection wire signals from the EAC composite specimen fatigue tests at the cold temperature.*

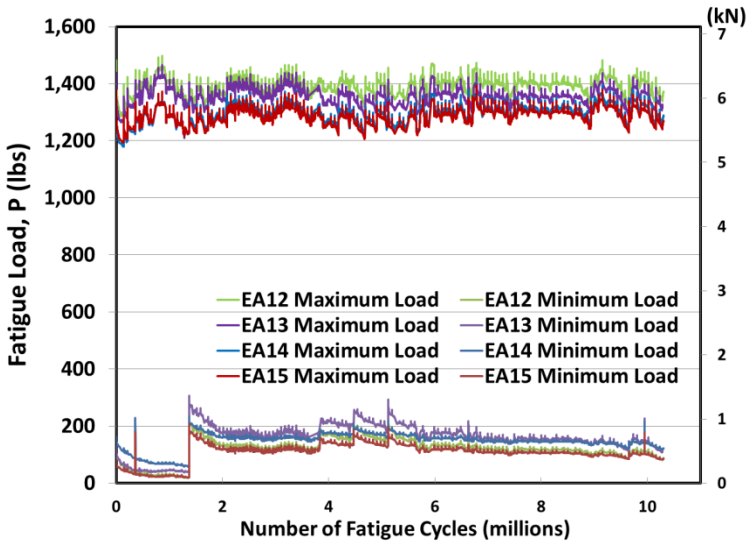

Fig. 5.21 *Maximum and minimum fatigue loads maintained during the fatigue test on EAC composite specimens at the cold temperature*

Fig. 5.22 shows a plot of the load deflection responses from the "slow-cycle" segments of the fatigue test at three different stages in life of the EA12 composite specimen. One load-deflection plot is from the virgin specimen, the second is after the specimen has been subjected to 5 million fatigue cycles, and the third is after the fatigue test at cold temperature has been terminated (after 10 million fatigue cycles). Similar to the previous observations, the slow-cycle stiffness (slope of the load-deflection response) shows no degradation even after 10 million fatigue cycles, validating the observation that the EAC composite specimens have withstood the 10 million cycles of fatigue loading at cold temperatures with little noticeable damage (tensile cracking and/or debonding/delamination). Post-test crack inspections as well as static failure test of these specimens (discussed in Section 5.6) too confirm this observation. The load-deflection plots from the slow-cycle loading of the EAC composite specimen also exhibit hysterisis observed previously in the static flexural tests.

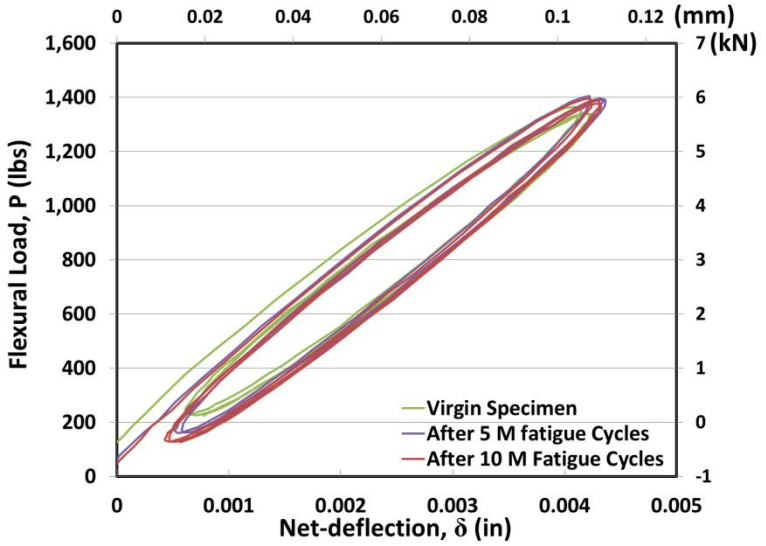

Fig. 5.22 *Load deflection response from slow-cycle loading at different times during the cold temperature fatigue test for the EA12 composite specimen showing no degradation in flexural stiffness.*

Fig. 5.23a and Fig. 5.23b show the stiffness and normalized stiffness, respectively, versus the number of fatigue cycles for PC composite specimens tested at the cold temperature. The variation in the virgin stiffness values ranges from 300-475 kip/in., which is more than the variations observed for the EAC composite specimens. This may be partly attributed to the variations in mixture proportions in the small scale fabrication of these laboratory specimens. Also, since the wearing surface stiffness depends on the stiffness of the low-modulus binder, mixtures with larger binder content, can be affected more readily by variations in mixture proportions (the binder content in PC was 12.5% versus 6.5% for the EAC wearing surface material). However, like EAC composite specimens, the PC composite specimens also exhibited no stiffness degradtaion with the number of fatigue cycles in these cold temperature tests. The drop in normalized stiffness (from 1.0 to 0.9-0.95 for the different specimens) during the first

million fatigue cycles can be attributed to relaxation of the wearing surface. Thereafter the stiffness is constant up to 10 million fatigue cycles.

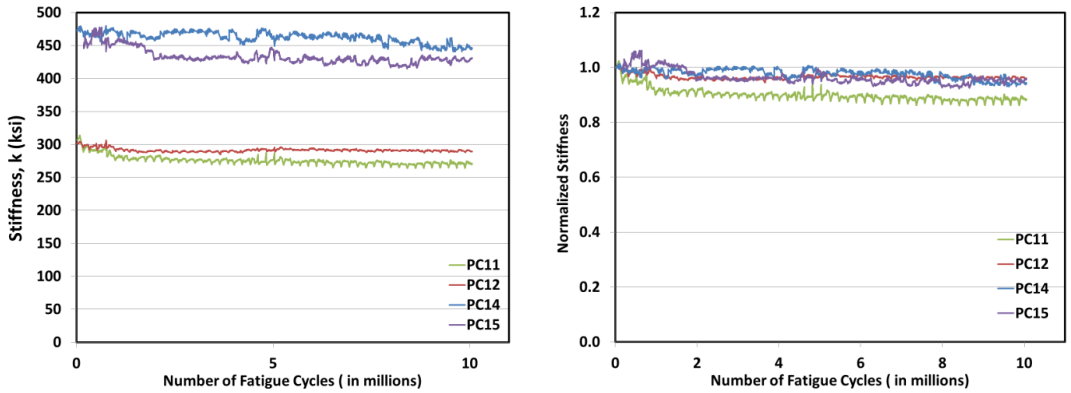

Fig. 5.23 *(a) Stiffness and (b) Normalized stiffness of the PC composite specimens versus number of fatigue cycles at the cold temperature.*

Like for the EAC composite specimens, the crack detection wire signals from all the four PC composite specimens were constant at 5 V indicating no loss of continuity, and implying no surface cracks were present on the tension face of the specimens. The two end-slip gage signals for each of the four specimens too did not indicate any slip from debonding or delamination. Photographs from the overhead cameras of the automated digital imaging system, too confirm that 10 million cycles of the cold temperature fatigue test did not cause any visible cracking.

Fig. 5.24 shows a plot of the load deflection response from the "slow-cycle" segments of the fatigue test at three different stages in the fatigue loading (virgin specimen, and specimens after 5 and 10 million fatigue cycles) for the PC12 composite specimen. Similar to the previous observations, the slow-cycle stiffness (slope of the load-deflection response) shows no degradation even after 10 million fatigue cycles,

validating the observation that the PC composite specimens have withstood the 10 million cycles of fatigue loading at cold temperatures with little noticeable damage (tensile cracking and/or debonding/delamination). Post-test crack inspections as well as static failure tests of these specimens (discussed in Section 5.6) too reinforce this observation. The load-deflection plots from the slow-cycle loading of the PC composite specimen exhibits significantly less hysteresis than that observed previously for the EAC composite specimens. This is consistent with observations from the static flexural test results for the PC composite specimens.

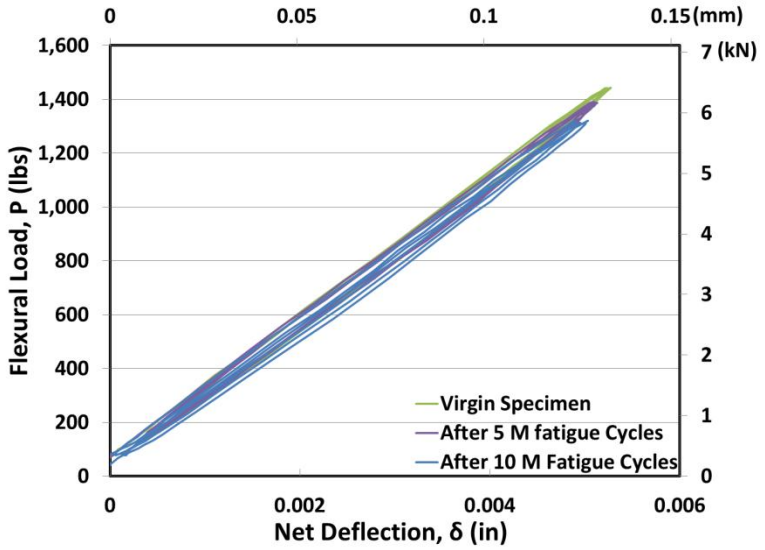

Fig. 5.24 *Load deflection response from slow-cycle loading at different times during the cold temperature fatigue test for the PC12 composite specimen showing no degradation in flexural stiffness.*

5.5.2 Fatigue performance at the room temperature

The EAC composite specimens were typically observed to exhibit the largest amount of hysteresis at room temperature (of tests at the cold, room and hot temperatures). Hysteresis has been associated earlier with viscoelastic nature of mechanical response observed in such polymeric and asphalt-based materials. This

behavior can also be observed in the stiffness versus number of fatigue cycles plots recorded for the EAC composite specimens at room temperature (Fig. 5.25). For logistical reasons, the room temperature fatigue tests had to be paused and resumed several times each week (the research laboratory also served as an undergraduate teaching laboratory and the tests were paused to mitigate noise during the classes). Fig. 5.25 highlights the relaxation effects recorded from these stop/start operations. Automated maximum load readjustment feature in the LabVIEW test control program described earlier, ensured that the maximum load was within ±75 lbs of the prescribed maximum fatigue load of 1,350 lbs at all times in the ram displacement controlled fatigue test.

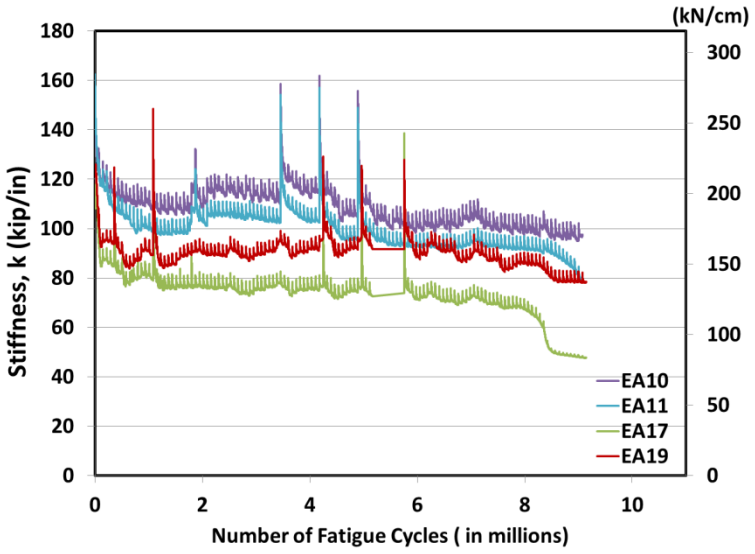

Fig. 5.25 *Stiffness of the EAC composite specimens versus number of fatigue cycles at the room temperature.*

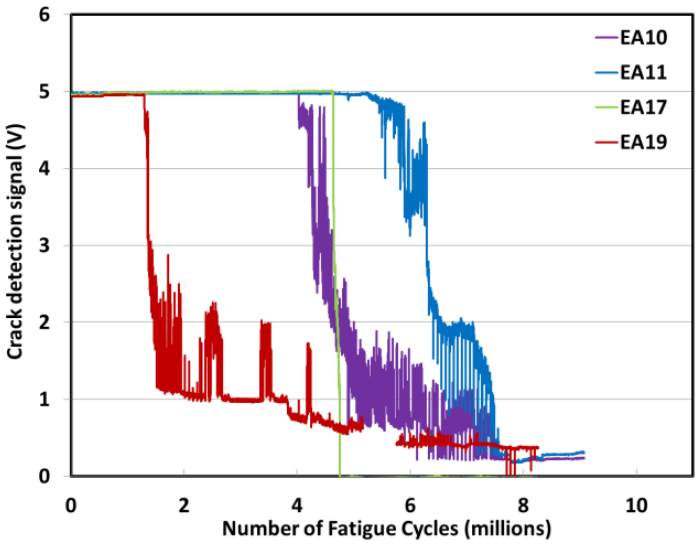

Fig. 5.26 *Crack detection wire signals from the EAC composite specimens for fatigue tests at room temperature.*

All four of the EAC composite specimens experienced cracking on the tension face as observed from the drop in stiffness with the number of fatigue cycles in these room temperature tests. Crack initiation and growth were confirmed using results from multiple independent measurements (crack detection wire signals, digital images during the fatigue test, drop in stiffness, and post-test crack inspections). Fig. 5.26 shows the variation of crack detection wire signals from the test. As noted earlier, any drop in voltage in this signal can be attributed to a loss of electrical continuity caused by surface cracking in the wearing surface. It can be readily observed from Fig. 5.26 that specimen EA10 cracked after 4.1 million fatigue cycles, EA11 cracked after 5.2 million fatigue cycles, EA17 cracked after 4.5 million cycles and specimen EA19 cracked after 1.3 million cycles. The post-cracking response from the crack detection wire signal can take one of two forms and is largely an artifact due to the combined effects of the discontinuity type and the data averaging algorithm used for this channel of information.

If there is intermittent and alternating discontinuity/continuity in the crack detection wire from the fatigue loading (opening and closing of the crack), the signal drops gradually from 5V to zero with a "noisy" transition (Type 1 response). If the loss of continuity is not intermittent (happens due to surface roughness in the vicinity of the crack, where crack closing may not result in reestablishing electrical continuity of the crack detection wire, the drop in signal from 5V is not gradual (Type 2 response). From Fig. 5.26, specimens EA10, EA11 and EA19 exhibit Type 1 post-cracking response, whereas specimen EA17 exhibits Type 2 response.

Fig. 5.27 shows the load deflection responses for specimen EA17 as a virgin specimen, and after 6 and 10 million cycles of fatigue loading. Note from Fig. 5.26 that a crack was first detected after approximately 5.1 million cycles of loading. The drop in stiffness (slope of the load deflection graph) between the virgin specimen and the specimen with 6 million cycles of fatigue loading is readily observed. Even while the fatigue tests were carried out until 10 million fatigue cycles, further degradation in the slope of the load deflection response is very minimal (Fig. 5.27-- see also drop in stiffness from Fig. 5.25).

Fig. 5.28 shows stiffness variation with the number of fatigue cycles for the PC composite specimens tested at the room temperature. Based on this plot as well as other results obtained from this test series, specimen PC17 was the first to crack after approximately 3.5 million cycles of fatigue loading. This was followed by specimen PC16 which experienced cracking after 5.2 million fatigue cycles. Specimen PC18 cracked after 9.9 million fatigue cycles and PC19 survived the 10 million cycles of fatigue loading without exhibiting any cracking or debonding/delamination. PC

composites tested under fatigue loads at room temperature appears to exhibit a 3-stage response where in the first stage there is a modest but gradual drop in stiffness, perhaps due to accumulation of very fine and distributed internal damage. The second stage results from a surface crack, with more rapid drop in stiffness. The stiffness drop is again gradual with increasing fatigue cycles in the third stage. This third stage can be attributed to a growth in the crack size (only one crack was observed in all PC specimens that exhibited cracking).

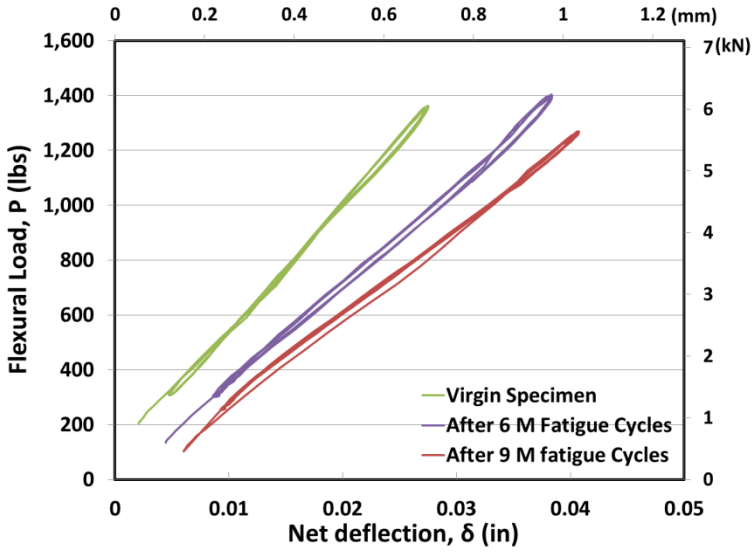

Fig. 5.27 *Load deflection response from slow-cycle loading for the EA17 composite specimen showing stiffness degradation at different times during the room temperature fatigue test.*

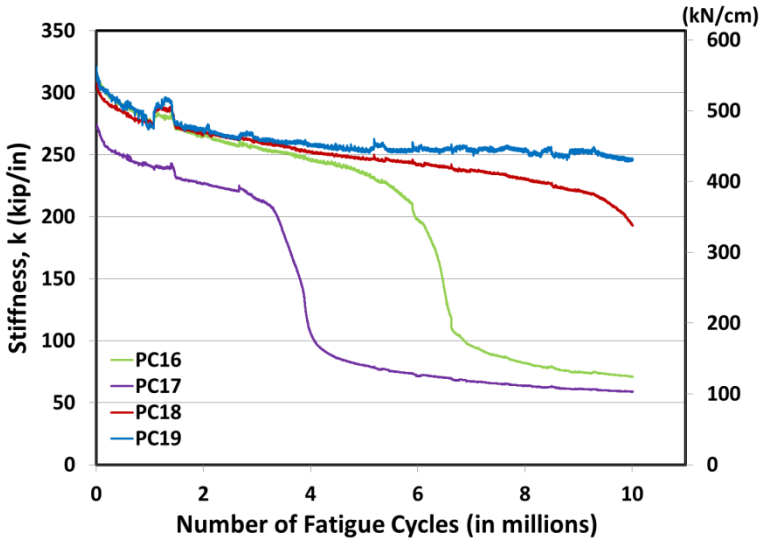

Fig. 5.28 *Stiffness of the PC composite specimens versus number of fatigue cycles at the room temperature.*

Note that the flexural stiffness of the bare steel plate is approximately 35 kip/in. Even after the 10 million fatigue cycles (the limit used in this investigation), two cracked PC composite specimens (PC16 and PC17) exhibited no debonding/delamination. The stiffness values on termination of the test were in excess of that from the bare steel plate. The small increase in stiffness experienced by all the specimens between 1 million and 1.4 million fatigue cycles was due to a malfunction in the temperature control program due to which the chamber temperature dipped to 60ºF (from the prescribed room temperature value of 70ºF).

Fig. 5.29 shows the crack detection wire signal response versus the number of fatigue cycles confirming previously reported fatigue lives at crack initiation in three of the four PC specimens. Again, it is obvious that PC 19 survived 10 million cycles of fatigue loading without any cracking or debonding/delamination. All PC specimens that experienced cracking exhibited Type 2 response “post-cracking” as far as the crack

detection wire signals history is concerned (i.e an abrupt drop in signal from the 5V virgin threshold). Unlike the EAC specimens that are smooth on the tension face due to vibratory compaction used to fabricate them, the PC specimen surface is very rough with embedded aggregates. There is no intermittent electric continuity in the crack detection wire due to the fatigue loading (once the specimen has cracked) and hence the abrupt drop in signal.

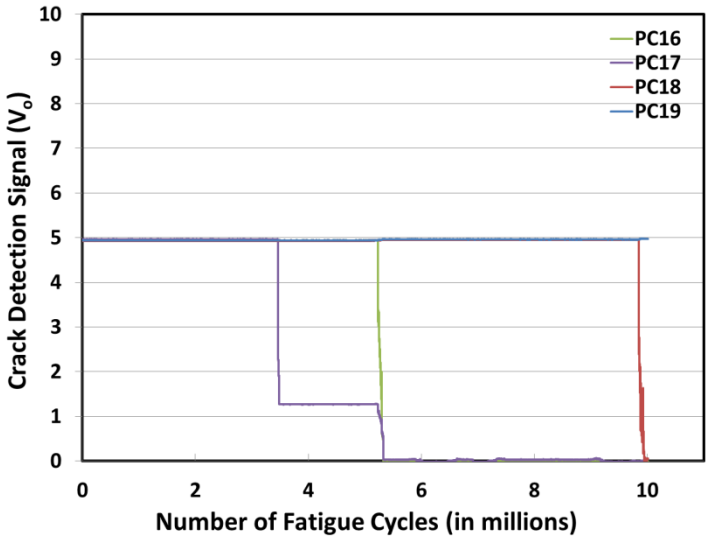

Fig. 5.29 *Crack detection wire signals from the PC composite specimens for fatigue tests at the room temperature.*

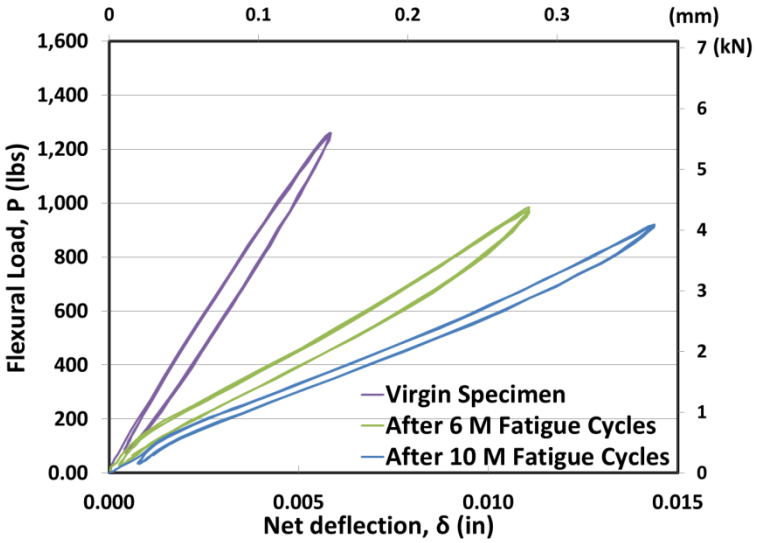

Fig. 5.30 *Load deflection response from slow-cycle loading for the PC16 composite specimen showing stiffness degradation at different times during the room temperature fatigue test.*

Fig. 5.30 shows the load deflection responses for the specimen PC16 as a virgin specimen, and after 6 and 10 million cycles of fatigue loading. Note from Fig. 5.28 that a crack was first detected after approximately 5.2 million cycles of loading. The drop in stiffness (slope of the load deflection graph) between the virgin specimen and the specimen with 6 million cycles of fatigue loading can be readily observed. Even while the fatigue tests were carried out until 10 million fatigue cycles, further degradation in the slope of the load deflection response is modest (Fig. 5.30-- see also drop in stiffness from Fig. 5.28).

5.5.3 Fatigue performance at the hot temperature

At the hot temperature, the contribution of the wearing surface to the composite stiffness is very small both for EAC and the PC wearing surface materials. This makes, crack detection exclusively from stiffness magnitudes, impossible. Fig. 5.31 for example,

shows the stiffness response of the EAC composite specimens versus the number of fatigue cycles. The virgin stiffness values are in the 40 - 43 kip/in, while the stiffnesses appear to be relatively constant, these specimen cracked after 1 million (EA22), 2.6 million (EA21) and 5.3 million (EA20) fatigue cycles. This is clearly evident from Fig. 5.32 where the crack detection wire signals are plotted versus the number of fatigue cycles. As noted, earlier, these EAC composite specimens too exhibit a Type 1 "post-cracking" response from the crack detection wire signal (gradual drop from 5 V due to intermittent electrical continuity during the remainder of the fatigue loading after crack initiation).

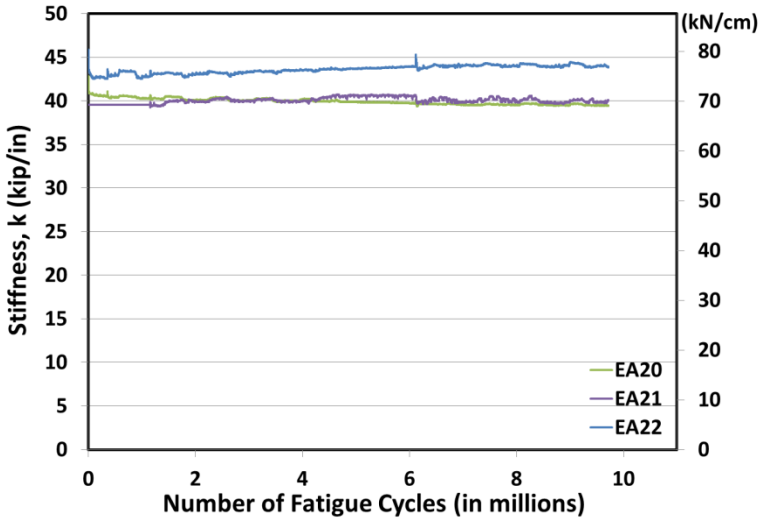

Fig. 5.31 *Stiffness of the EAC composite specimens versus number of fatigue cycles at the hot temperature.*

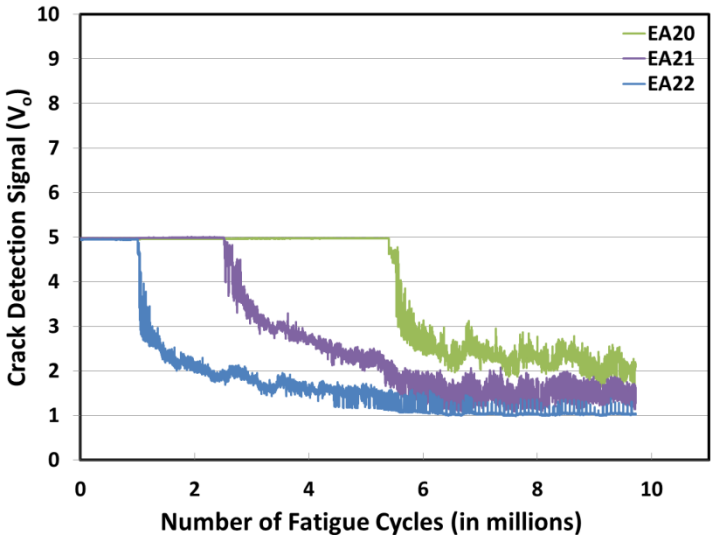

Fig. 5.32 *Crack detection wire signals from EAC composite specimens from the fatigue tests at hot temperature.*

The fatigue performance of the PC composite specimens at the hot temperature is shown in Fig. 5.33. The figure comprises plots from two separate tests. The first fatigue test series included specimens PC21-24. Based on crack detection wire signals, it was observed that these specimens cracked very early into the fatigue test. PC21 cracked after 6,100 fatigue cycles, PC22 after 5,100 fatigue cycles, PC23 after 2,200 cycles and PC24 after 11,300 cycles. The early cracking can also be observed as stiffness drops within the first few thousand cycles. Despite this, the tests were carried out until 5.5 million cycles. No noticeable further degradation in stiffness or reductions in the maximum loads sustained during this time suggested that there was little additional growth in the crack/damage. Post test crack inspections, as described later, also confirmed this observation. In order to verify if the early crack initiation in the four specimens resulted from initial accidental overloads or from specimen fabrication anomalies, two spare specimens available (PC13 and PC 20) were subjected to fatigue loading at the hot

temperature. These specimens too cracked after 10,000 and 11,000 fatigue cycles. This test too was continued until 6 million fatigue cycles, with little additional degradation of stiffness or damage from debonding or delamination. Post-test crack inspections again confirmed that but for the presence of a single 0.3 mm wide crack (not across the entire width of the specimen or through the thickness of the specimen) in each of these specimens, the specimens appeared to be in comparable shape to those previously tested under fatigue at room temperature.

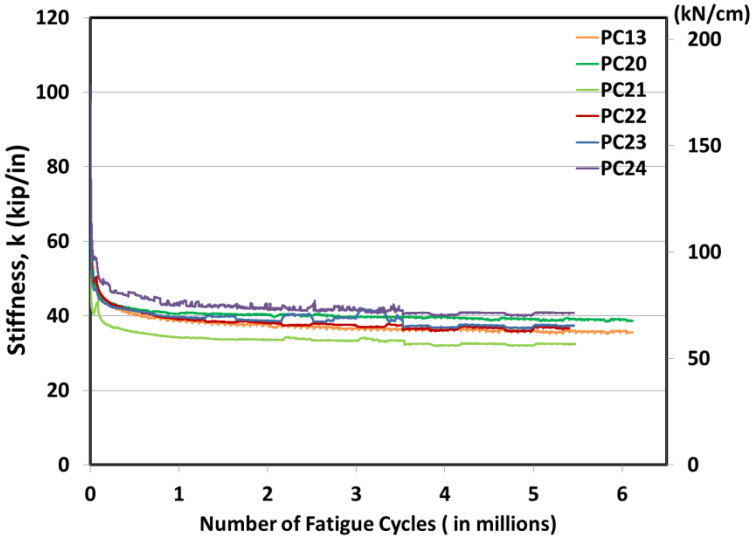

Fig. 5.33 *Stiffness of the PC composite specimens versus number of fatigue cycles at the hot temperature.*

5.5.4 Summary observations from the fatigue test series

Table 5-5 provides a summary of results from the fatigue test series listing the fatigue life when crack initiation was first detected. It also provides information of when the fatigue tests were terminated as well as typical maximum crack widths measured in the post-test crack inspection effort.

Both the EAC and PC composite specimens sustained 10 million cycles of the prescribed fatigue loading at the cold temperature without any cracking, debonding or delamination. Post-test crack inspection as well as performance in the post-fatigue static flexural failure tests confirmed this observation.

The PC composite specimens performed better in the room temperature fatigue tests with one of four replicate specimens surviving the 10 million fatigue cycles without any cracking/damage and one other exhibiting crack initiation only after 9.9 million fatigue cycles. Two others PC specimens exhibited crack initiation after 3.5 and 5.2 million fatigue cycles. The four EAC composite specimens cracked after 4.1, 4.5, 5.1 and 5.2 million fatigue cycles. Even when the cracked specimens were subjected to additional fatigue cycles (EAC tests terminated at 9 million cycles and PC test terminated at 10 million cycles), typical maximum post-test crack widths for loaded specimens were only in the 0.2 mm range.

The EAC composite specimens performed marginally better in the hot temperature fatigue tests than the PC composite specimens. Crack initiation was detected in EAC specimens after 1, 2.6 and 5.3 million cycles, whereas the six PC composite specimens all exhibited crack initiation after only 11,000 fatigue cycles. Typical maximum post-test crack widths of 0.2 mm for the EAC composite specimens and 0.3 mm for the PC composite specimen were observed.

Only a single crack was observed in each specimen (for those specimens that cracked in the fatigue test program). As discussed later in Sections 5.7 and 5.8, these cracks were not through the thickness exhibiting resistivity values in excess of 4 MΩ.

5.6 Response from monotonic static flexural failure tests

Monotonic static failure tests were completed prior to the fatigue test series. This was done so that the type of fatigue failure expected would be instructive for planning purposes, particularly since the fatigue tests, unlike the static failure tests were conducted in a temperature controlled test chamber. As noted earlier in Sections 3.8 and 4.6, the static flexural failure tests were conducted in a companion MTS test frame to allow for potentially larger test loads, if necessary, without concern for damaging the custom designed fatigue load cells. These tests were conducted one specimen at a time and at room temperature (70º-75°F, in an air-conditioned environment, but not temperature controlled test chamber). The tests were ram displacement controlled with a ramp command signal at the rate 0.00025 in/s. Tests were instrumented with net-deflection gage, two end slip gages, crack detection wire, foil strain gage to measure steel strain, thermocouple to measure wearing surface temperature, load and ram displacement.

After running static flexural failure tests on two virgin EAC and two PC composite specimens, the research team completed the cold temperature fatigue tests on four EAC and four PC composite specimens. All eight of these fatigue specimens survived the 10 million fatigue cycles without any discernible cracking, softening, delamination or degradation in stiffness (as described in Section 5.5 of Results from the Fatigue Tests). These specimens were then subjected to static flexural failure tests to further investigate damage from the cold temperature fatigue tests and their post-fatigue performance.

Fig. 5.34 shows the load deflection response of EAC composite specimens until the “first peak” load. The composite specimens, given the presence of steel plate, are

expected to peak yet again at loads higher than the “first peak” (at significantly larger deflections). Plots in figure include the two virgin specimens (EA04 and EA05) and the four post-fatigue test specimens (EA12, EA13, EA14, and EA15). The overall load deflection responses, initial stiffnesses, first peak loads and corresponding deflections all show consistent and comparable magnitudes for both the virgin and post-fatigue specimens. As observed from Fig. 5.34, the first peak loads ranged from 6,200 lbs. – 6,570 lbs. The virgin specimens averaged a “first peak” load of 6,400 lbs. and the post-fatigue specimens at 6,300 lbs. which confirms that the fatigue specimens tested at cold temperature experienced little damage, if any. It is relevant to note that these “first peak” loads are nearly an order of magnitude larger than those expected during service and at least 5 fold the maximum fatigue load used in the current fatigue test program. The steel plate is expected to be well past yield stress at this level of load (even while elastic analysis may not be applicable at this stage of loading, the elastic analysis prediction of maximum steel stress is approximately 65,000 psi). The maximum wearing surface stresses at the “first peak” loads (also computed using uncracked elastic analysis just for providing crude estimates of stresses) are in the 750 – 850 psi range).

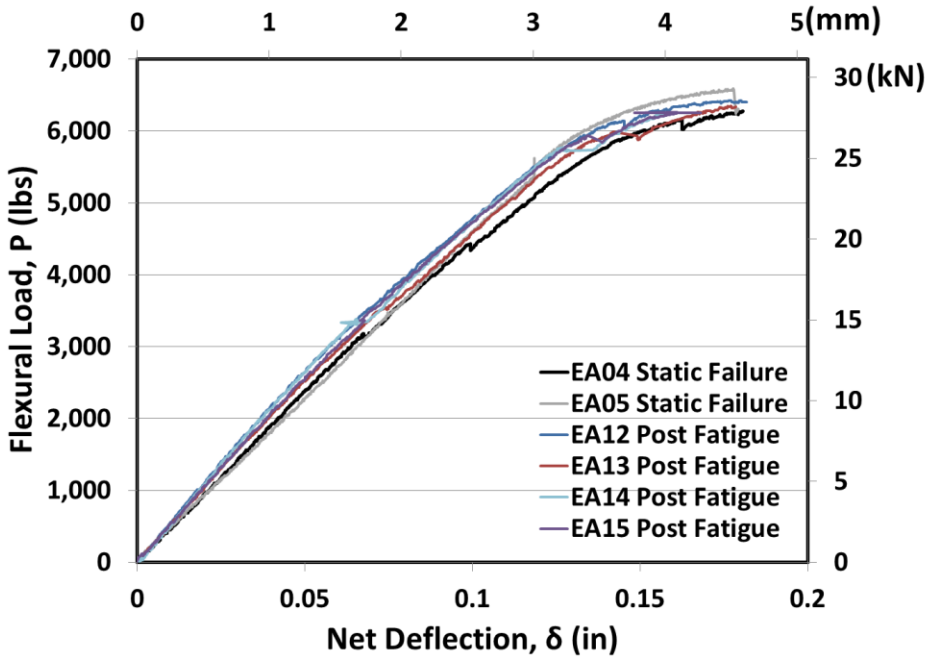

Fig. 5.34 *Load deflection response from static flexural failure tests (EAC Composite Specimens) at room temperature.*

The deflection at the "first peak" load for the EAC composite specimens are approximately 0.17 in. (compared to 0.020-0.025 at the maximum load of 1,350 lbs. used for the static, dynamic and fatigue test series). Even at such large deflections, no debonding or delamination was visually observed at the steel-wearing surface interface. The end slip gages too did not record discontinuities typically associated with interface slip or debonding.

The "first-peak" load can be most likely associated with catastrophic cracking in the wearing surface, also corroborated by visual observations, and data from the test. However, based on interpretation of results from numerous redundant instrumentation (crack detection wire, load-strain response, load deflection response etc.), it appears that crack initiation in EAC wearing surface occurred at a load of approximately 4,000 lbs

(see also deviation from linearity in Fig. 5.34), corresponding to a tensile stress in the wearing surface of approximately 530 psi in these room temperature tests.

Fig. 5.35 includes load deflection responses from PC composite specimens subjected to static flexural failure tests. Like for EAC specimens, plots from the virgin specimen tests (PC08 and PC09) as well as post-fatigue specimen tests (PC11, PC12, PC14 and PC15) are included in the same figure. The scatter in the initial stiffness, "first-peak" loads, and corresponding deflection are noticeably larger than for the EAC composite specimens, consistent with similar observations from the other static and flexural fatigue tests.

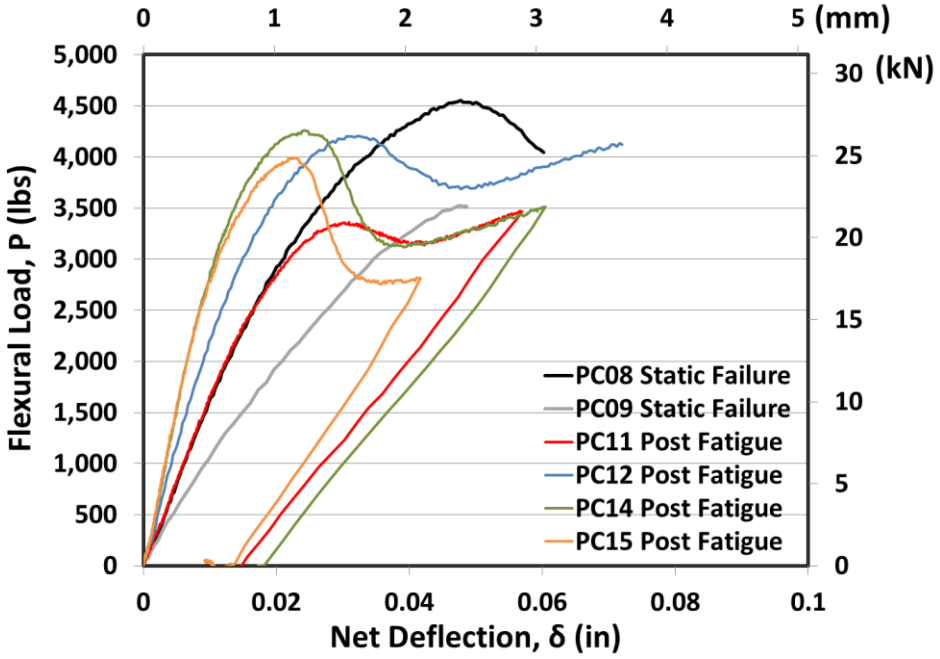

Fig. 5.35 *Load deflection response from static flexural failure tests (PC Composite Specimens) at room temperature.*

As the PC composite specimens were stiffer than the EAC composite specimens at room temperature, it was possible to load them to deflections larger than those at "first-

peak" loads to demonstrate increasing loads at larger deflections. It was also possible to record unloading data on a few select specimens to make observations on the residual stiffness for a cracked PC composite specimen. The "first-peak" loads for the PC composite specimens were in the 3,330 lbs. – 4,550 lbs. range. The "first-peak" loads for the virgin specimen averaged 4,050 lbs versus that for the post-fatigue test specimens at 3,925 lbs., again providing evidence that the cold-temperature fatigue tests did little damage to the PC composite specimens. Even while these loads are smaller than observed for EAC composite specimens, the corresponding stresses are in the 1,425 psi (virgin specimen average) and 1,375 psi (post-fatigue test specimens) resulting from significantly higher wearing surface modulus at room temperatures for the PC compared to the EAC material. The "first-peak" loads for the PC composite specimens were approximately 3 times the magnitude of the maximum fatigue loads (1,350 lbs.) used in this research and approximately 6 times the design service loads. The deflection at the "first peak" load for the PC composite specimens is in the range 0.02-0.05 in. (compared to 0.01-0.013 at the maximum load of 1,350 lbs. used for the static, dynamic and fatigue test series). Even at these deflections, no debonding or delamination was visually observed at the steel-wearing surface interface. The end slip gages too did not record discontinuities typically associated with interface slip or debonding.

The "first-peak" load can be most likely associated with catastrophic cracking in the wearing surface, also corroborated by visual observations, and data from the test. However, it appears that crack initiation in PC wearing surface occurred at a load of approximately 2,500 lbs (see also deviation from linearity in Fig. 5.35), corresponding to

a tensile stress in the wearing surface of approximately 875 psi in these room temperature tests.

The residual flexural stiffness (slope of the unloading response) computed from three of the specimens where data was recorded during unloading (PC11, PC14 and PC15) averaged 84,000 lb/in. (Fig. 5.35). This value suggests that, even while cracked, the PC wearing surface can contribute significantly to stiffening the deck plate. It is useful to note that the BS stiffness is approximately 35,000 lb/in and that of the uncracked PC composite specimen is 110,000 lb/in (at room temperature).

Table 5.4 includes post-test crack width measurements after the static failure tests conducted on virgin as well as previously tested (cold temperature fatigue tests where none of the specimens had cracked even after 10 million cycles of fatigue loading). EAC composite specimens exhibited larger crack widths (0.5 – 1 mm) compared to PC specimens (0.2-0.3 mm) partially because of their lower modulus at room temperatures and partly because they also withstood higher loads at “first peak”.

Table 5-4 Summary of typical maximum crack widths from the static flexural failure tests

Test type	Specimen ID	Typical maximum crack widths (mm)	Test type	Specimen ID	Typical maximum crack widths (mm)
Static flexural failure test	EA04	1	Post cold fatigue static flexural failure test	EA13	0.5
	EA05	0.8		EA14	0.5
	PC08	0.2		EA15	0.5
	PC09	0.3		PC11	0.2
				PC12	0.2
				PC14	0.3
				PC15	0.2

5.7 Crack detection and mapping effort

As described earlier in Chapter 4, since it was not possible to undertake a thorough inspection of cracks while the specimens were still in the test chamber, crack inspection was accomplished using a specially developed set-up to detect cracks, measure typical maximum widths, and map crack patterns and distribution while the specimen was loaded (to the same maximum level of deflections they were subjected in the actual test).

No cracks were readily visible in any of the composite specimens (known to be cracked from prior testing) when they were in an unloaded state. When these were loaded to the maximum deflection (replicating the actual tests), some cracks required a well-lit magnifying glass even to be detected. None of the cracks appeared to be of full depth, even when the specimens cracked early (3-5 million fatigue cycles) and fatigue tests were carried out to the full 10 million fatigue cycle limit. All of these observations bode well for the service performance of either of the wearing surface materials tested. A summary of typical maximum crack widths was included earlier in Table 5-4 for the specimens tested up to failure in static flexure, and in Table 5-5 for all the fatigue tests and will not be duplicated here.

A typical set of data from the crack detection and mapping effort has been compiled and presented in Fig. 5.36– Fig. 5.39 for static flexural failure (EAC and PC composite specimens) and room temperature flexural fatigue specimens (EAC and PC composite specimens), respectively.

Table 5-5 Summary of results from the fatigue tests at different test temperatures

Test Conditions	Specimen ID	Detection of Crack Initiation[1]	Test Terminated[2] (Cycles)	Typical Maximum Crack Width[3] (mm)
Fatigue (Cold)	EA12	None detected	10 M	NA
	EA13	None detected	10 M	NA
	EA14	None detected	10 M	NA
	EA15	None detected	10 M	NA
	PC11	None detected	10 M	NA
	PC12	None detected	10 M	NA
	PC14	None detected	10 M	NA
	PC15	None detected	10 M	NA
Fatigue (Room)	EA10	4.1 M	9 M	0.2
	EA11	5.2M	9 M	0.2
	EA17	4.5M	9 M	0.2
	EA18	5.1M	9 M	0.2
	EA19	1.3 M	9 M	0.2
	PC16	5.2M	10 M	0.2
	PC17	3.5 M	10 M	0.2
	PC18	9.9M	10 M	0.2
	PC19	None detected	10 M	NA
Fatigue (Hot)	EA20	5.3M	10 M	0.2
	EA21	2.6M	10 M	0.2
	EA22	1.0M	10 M	0.2
	PC13	10.0 K	6 M	0.3
	PC20	11.0 K	6 M	0.3
	PC21	6.1 K	5.5 M	0.3
	PC22	5.1 K	5.5 M	0.3
	PC23	2.2 K	5.5 M	0.3
	PC24	11.3 K	5.5 M	0.4

1 *Using all techniques including crack detection wire signal, digital images during fatigue tests, stiffness and load data, and post-test crack inspection.*

2 *Tests were continued beyond crack initiation to study its growth until fatigue cycle limit noted in the column.*

3 *Crack widths are based on measurements with a crack width gage during post-test inspections.*

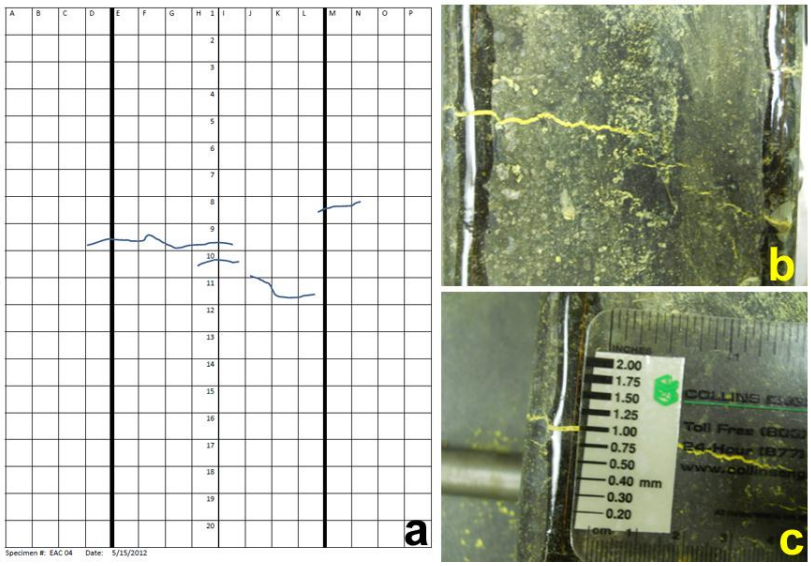

Fig. 5.36 (a, b) Crack patterns and (c) representative crack widths (EA04 Static Failure Test)

In each of these figures, Part (a) documents the manual mapping of crack profile and location. Each of the smallest square grids is of scale 0.5" x 0.5". The central portion between the solid vertical lines represents the top surface (tension face, 4" wide) of the wearing surface.

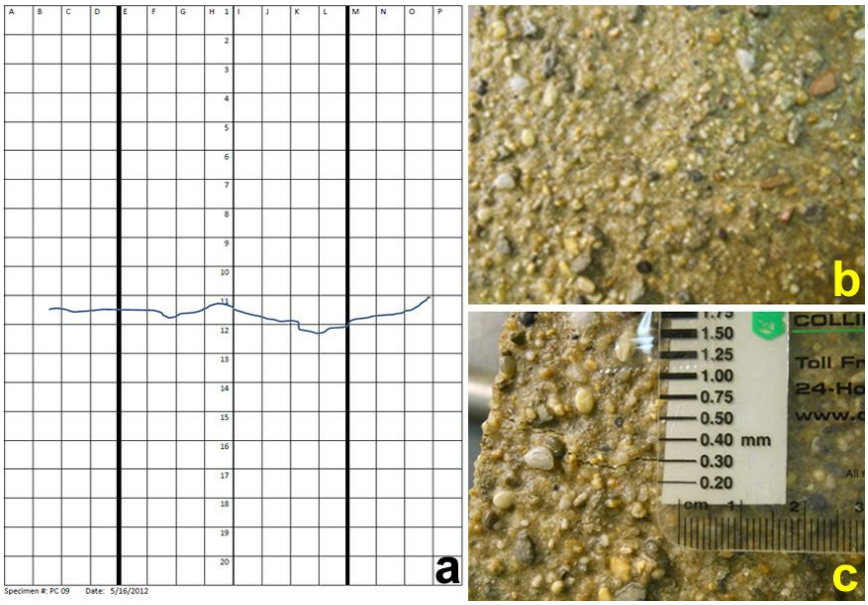

Fig. 5.37 (a, b) Crack patterns and (c) representative crack widths (PC09 Static Failure Test)

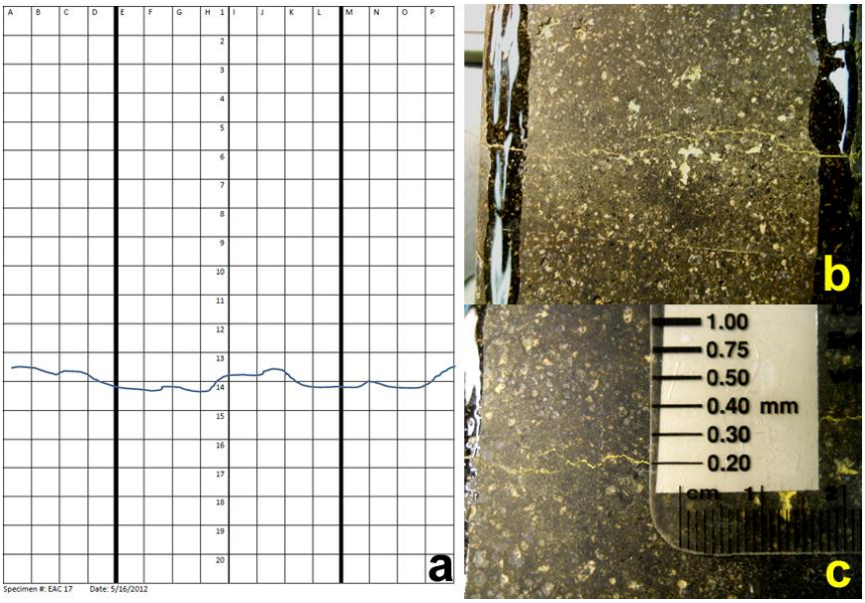

Fig. 5.38 (a, b) Crack patterns and (c) representative crack widths (EA17 Fatigue test, 70ºF)

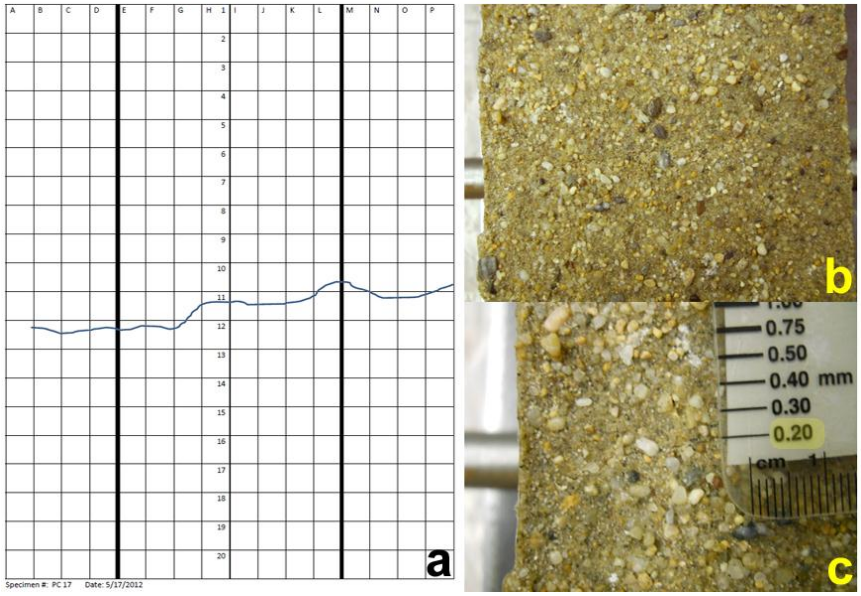

Fig. 5.39 (a, b) Crack patterns and (c) representative crack widths (PC17 Fatigue test, 70ºF)

The grid patterns to the left and right of this top surface are maps along the 2" nominal depth on either side of the specimen. The template shows only the middle 10" of specimen length (out of the total specimen length of 18") as the end sections are not critical as far as potential cracking is concerned. Part (b) in these figures is a photograph showing the full 4" top face which includes the cracks shown in (a). Part (c) is a close-up of the crack showing typical maximum widths observed for the specimen.

Only one crack was observed for all the specimens tested in fatigue. Typical maximum crack widths for all the fatigue specimens (that cracked during the fatigue tests) were in the 0.2-0.3 mm range. No cracks were detected in the fatigue tests conducted on both EAC and PC composite specimens at the cold temperature. Multiple cracks, though not always through the entire width were observed for the EAC composite (Fig. 5.36). Cracks in the PC specimens in many cases were along the entire width (Fig. 5.37 and Fig. 5.39).

The maximum crack widths for the EAC specimens tested in the static failure tests were in the 0.8 – 1 mm range and noticeably wider than those for the PC specimens (0.2 – 0.3 mm range) in identical tests. This can be attributed to the lower modulus at room temperature for the EAC material and the larger deflections necessary to cause static failure.

5.8 Results from the resistivity tests

Table 5-6 includes a summary of results from the resistivity tests. This test was not among those originally proposed for the research program. Since cracks from the fatigue testing were observed to be of small width, and that too detectable only when the specimen was loaded, it was essential to verify if fine cracks were inadvertently not being detected. The resistivity test [ASTM C3633-98] which is intended for the measurement of the electrical resistivity of water-barrier membrane-pavement systems when applied to concrete bridge decks, has served a very useful purpose in past research on qualitative measures of severity of cracking in wearing surfaces on a steel bridge deck [Gopalaratnam et al., 1993, FHWA, 2012]. Low resistance (less than 10,000 ohms) indicates the wearing surface has a through-thickness crack in the wearing surface. A minimum resistance of 750,000 ohms has been specified in past projects as an acceptable value ensuring against water infiltration. Although there is little theoretical basis for this specific threshold resistivity, readings in the MΩ range suggest that the cracks are not through the entire depth or that the bond coat still remains uncracked (primary corrosion protection for the steel deck)

Table 5-6 Summary results from resistivity tests on cracked composite specimens

Specimen ID	Test Classification	Initial Reading (MΩ)	2nd Reading[1] (MΩ)	3rd Reading[1] (MΩ)	4th Reading[1] (MΩ)
EA08	Fatigue (70ºF)	7.0	6.9	6.8	6.7
EA13[2]	Fatigue (32ºF) + Static Failure	27.0	26.0	26.0	29.0
EA21	Fatigue (120ºF)	49.0	60.0	51.0	60.0
PC16	Fatigue (70ºF)	7.5	7.4	7.3	6.8
PC11[2]	Fatigue (32ºF) + Static Failure	5.8	5.2	5.0	5.0
PC21	Fatigue (120ºF)	4.4	4.2	4.2	4.2

1. *The initial reading was taken immediately after ponding the wearing surface with detergent water. The 2nd, 3rd and 4th readings were recorded after 1, 2 and 3 hours of initial ponding, rewetting each time prior to taking the reading.*
2. *Specimens subjected to cold temperatures did not fail even after being subjected to 10 million fatigue cycles. These specimens were then used to additionally conduct static failure tests.*

Table 5-6 includes a representative set of resistivity test results from EAC and PC composite specimens tested in fatigue (at room and hot temperatures) that were known to be cracked. Also included in the table are results from specimens that had not cracked in the cold temperature fatigue tests but were subsequently subjected to static failure test (confirmed cracked specimens). The lowest resistivity results recorded for any test was in the 4+ MΩ range, even after 3 hours of ponding detergent water over the cracked wearing surface. This indicates that there is no electrical conductivity between the top of the saturated (cracked) wearing surface and the steel plate, suggesting that the cracks are not through the entire depth or the bond coat still remains uncracked despite the mechanical testing that preceded the resistivity tests. As long as the resistivity readings are in the MΩ range, variations in the 4-60 MΩ (as in Table 5-6) do not provide additional information on the extent of cracking in the wearing surface.

5.9 Tensile pull-out strength

Since both wearing surface materials (EAC and PC) had excellent bond to the steel plate, it was a challenge to find a glue strong enough to pull out cores of the wearing surface from the steel plate. Due to the nature of their fabrication the EAC specimens had a relatively smoothly compacted top surface. This made getting good bond with the glue (to bond the pipe cap) more difficult without special surface preparation or additional mechanical modifications. Various glues were tried, including a polyester binder (the binder used to fabricate the PC specimens), Devcon 5-minute epoxy, Loctite HD (High Density), Loctite MC (Metal to Concrete), Gorilla glue, and Transpo T41 epoxy. Additionally for the EAC pull-out specimens additional modifications tried include, surface grooving, use of small diameter-shallow depth angular holes filled with glue (to increase bonded area and engage additional bearing forces during pull-out), and three different kinds of anchors (complementary to the glue) including wedge anchors, bolt anchors and sleeve anchors. The classification of various types of pull-out failures is illustrated in Fig. 5.40.Not all failure types noted in the schematic would provide the basis for computation of the tensile bond strength of the wearing surface. Failure Type 4 provides a good measure of the tensile strength of the wearing surface (particularly when it is smaller in magnitude than its tensile bond strength to steel), and Failure Type 5 or 6 provide a good measure of the tensile bond strength of the wearing surface to steel. Failure Types 1-3 are not desirable as they can only provide “lower bounds” of the tensile bond strength of the wearing surface to steel.

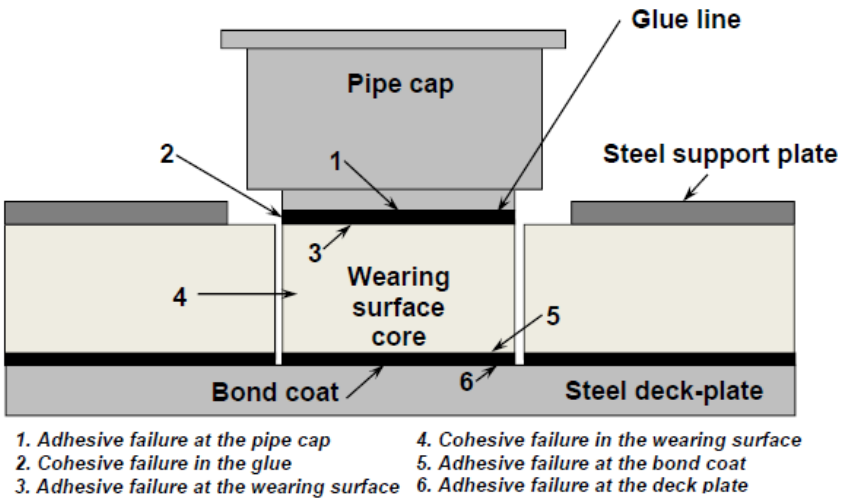

Fig. 5.40 Failure classifications for the pull-out of wearing surface cores from steel plate

Table 5-7 includes a summary of results from the tensile pull-out tests. As noted in the footnote to the table, only those rows that are shaded represent successful tensile pull-out tests. All of these results are for PC composite specimens at the cold, room and hot temperatures. None of the glues or additional modifications used resulted in a successful tensile pull-out test for EAC composite specimens. So the tests were only completed at room temperature and even these results would only provide a "lower bound" estimate of the tensile pull-out strength.

The tensile pull-out load versus time response for EAC cores at room temperature are illustrated in Fig. 5.41. All the plots are shown as dashed lines in this figure as these tests did not result in successful pull-out of the core from the steel plate. The glue and the additional modifications used are highlighted in the two right most columns of Table 5-7.

The highest loads were obtained when Loctite HD glue was used in conjunction with bolt anchors embedded about 1.75" deep into the EAC core. Failure in these cores was due to cohesive failure in the wearing surface at the level of the bolt head. A "lower bound" estimate of the tensile bond strength was computed as: 621 psi (average of 639

and 603 psi, see Table 5-7). Fig. 5.42 shows a failed EAC core, also showing the bolt anchor head and the cohesive failure of the EAC core at that level

Table 5-7 Summary of results from the tensile pull-out tests

Spec. No.	Core ID	Maximum Load (lbs)	Bond Strength[1] (psi)	Temp. (^{o}F)	Failure Type	Bonding Agent	Additional Modifications
EA01	A	937	298	75	1, 2, 3[2]	Devcon 5 Min	Wedge Anchor
EA01	B	1,089	347	75	1, 2, 3[2]	Transpo T41	Sleeve Anchor
EA01	C	1,105	352	75	1, 2, 3[2]	Transpo T41	Sleeve Anchor
EA01	D	1,334	425	75	1, 2, 3[2]	Transpo T41	9 Holes[3]
EA01	E	1,779	567	75	1, 2, 3[2]	Loctite HD	None
EA01	F	1,672	532	75	3	Loctite MC	None
EA02	B	2,008	639	75	4[4]	Loctite HD	Bolt
EA02	F	1,892	603	75	4[4]	Loctite HD	Bolt
PC06	A	3,730	1,188	32	5	Transpo T41	None
PC06	B	2,433	775	32	1, 2, 3[2]	Transpo T41	None
PC07	B	2,667	849	32	1, 2, 3[2]	Transpo T41	None
PC07	F	2,789	888	32	1, 2, 3[2]	Transpo T41	None
PC06	C	3,102	988	75	5	Loctite MC	None
PC06	D	3,036	967	75	1, 2, 3[2]	Loctite MC	None
PC06	E	3,137	999	75	5	Loctite MC	None
PC06	F	1,397	445	122	5	Transpo T41	None
PC07	A	886	282	122	1, 2, 3[2]	Transpo T41	None
PC07	C	1,335	425	122	5	Transpo T41	None
PC07	E	1,199	382	122	5	Transpo T41	None

1. *Tensile bond strength only for the successful tests (shaded rows). For all other rows values in this column are the "lower bounds" for the tensile bond strength.*
2. *Failure comprising all three types (1, 2 and 3) of failure at the same time*
3. *Inclined holes filled with glue ensured increased bonded area and additional load transfer via bearing.*
4. *Failed at the head of the embedded bolt – not considered a successful pull-out test.*

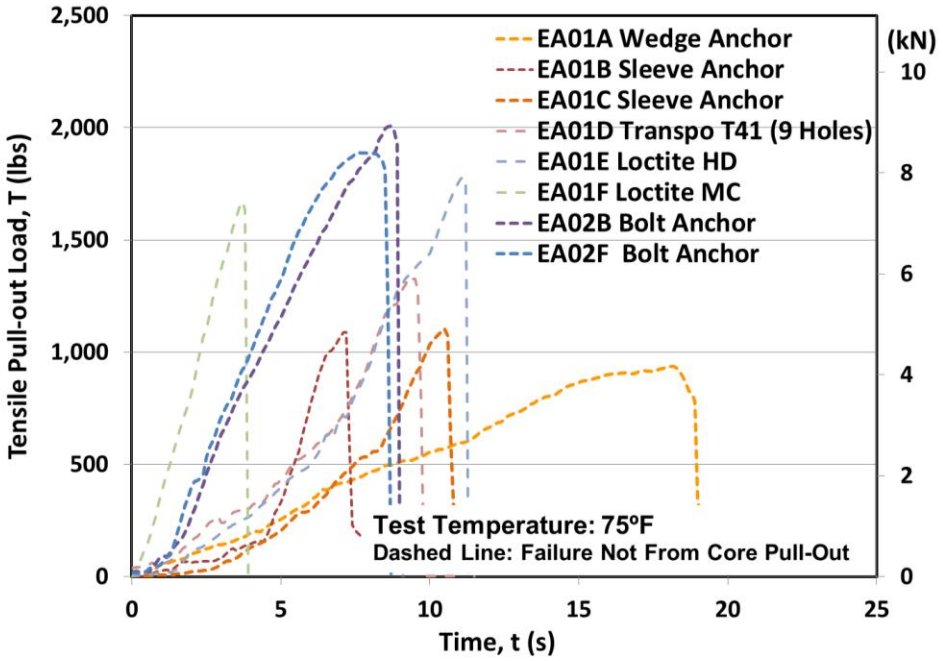

Fig. 5.41 Pull-out of EAC cores from steel plate (wearing surface temperature: 75ºF)

The tensile pull-out load versus time response for PC cores at room, cold and hot temperatures are illustrated in Fig. 5.43-Fig. 5.45. The plots shown as solid lines resulted from successful pull-out tests and those shown as dashed lines represent tests that did not result in successful pull-out of the core from the steel plate. The average tensile bond strength (from the successful pull-out tests) were 1,188 psi, 994 psi and 417 psi, respectively, at 32°F, 75ºF and 122°F.

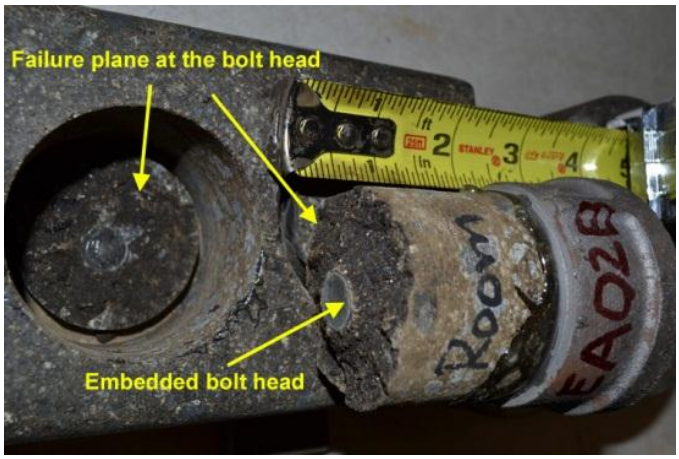

Fig. 5.42 *EAC Core pull-out test not successful. Photo shows failure at level of head of bolt anchor*

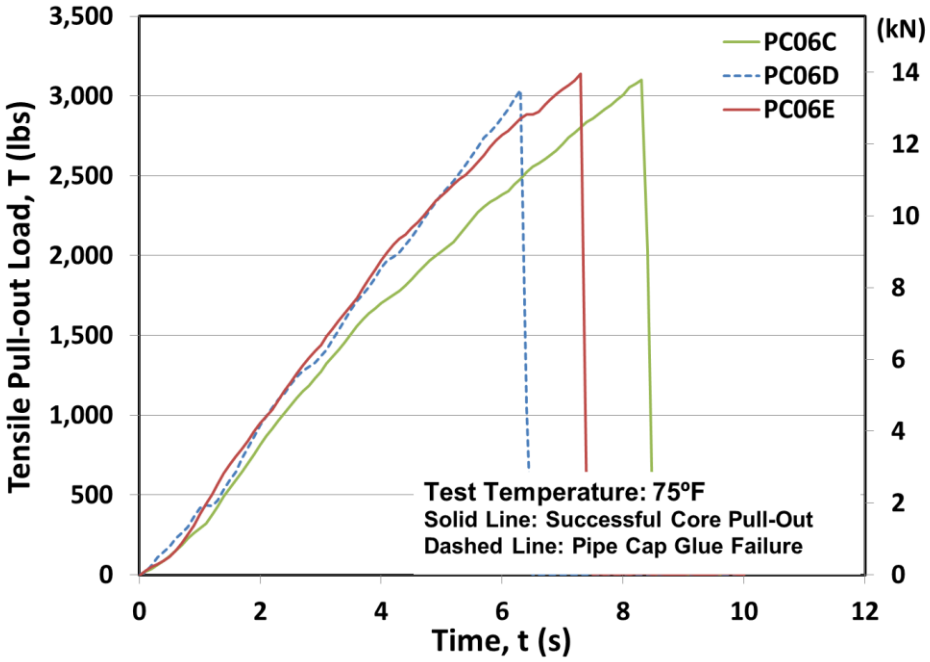

Fig. 5.43 Pull-out of PC cores from steel plate (wearing surface temperature: 75°F)

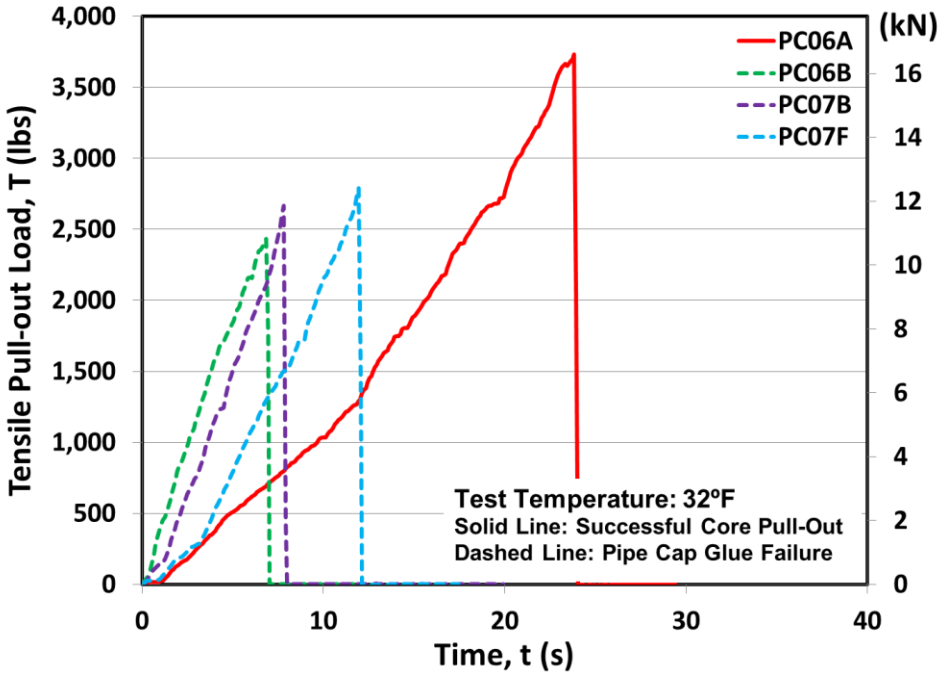

Fig. 5.44 Pull-out of PC cores from steel plate (wearing surface temperature: 32°F)

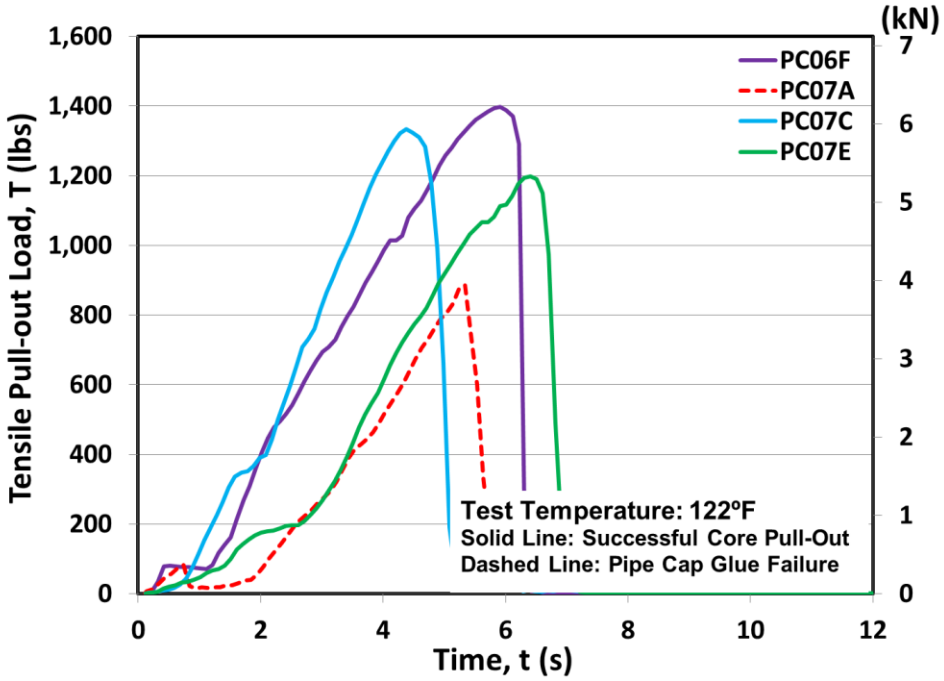

Fig. 5.45 Pull-out of PC cores from steel plate (wearing surface temperature: 122ºF)

Fig. 5.46 PC Core pulled out in the tensile test exhibiting Type 5 failure.

All the successful core pull-out tests for the PC composite specimens resulted from Type 5 failure (adhesive failure at the bond coat). This type of failure is illustrated in Fig. 5.46 where the bond coat can be seen to be still adhering to the steel plate.

6 Conclusion and Recommendations

Conclusions and recommendations are presented in a cohesive manner rather than in independent sections because the recommendations to be more readily tied to summary observations from this research. These observations and discussions are presented in thematic sections that allow expounding the important practical performance implications of the wearing surface materials evaluated.

6.1 Composite action

Both experimental and analytical results developed in this investigation have been used to demonstrate that wearing surface for orthotropic steel decks can contribute significantly to deck stiffness depending upon the elastic modulus of the material and the thickness of the wearing surface used. When composite action of the wearing surface and the steel deck is considered, stresses in the steel deck due to transverse bending, can be significantly reduced. The reduced stress can serve to enhance the fatigue life of the steel deck. It is recommended that orthotropic deck design should incorporate the wearing surface as an integral component of the design to take advantage of this quantifiable response.

Both the EAC and PC wearing surfaces evaluated in this investigation exhibit viscoelastic characteristics. Unlike for very thin polymer wearing surface systems, the wearing surface thickness in this study (2" nominal thickness), makes the viscoelastic response of the “wearing surface – steel deck composite” more pronounced. This is due to the increased influence of the (thick) wearing surface on composite stiffness. Both the viscous and elastic properties of these two wearing surface materials are influenced

significantly by temperature and to a lesser extent by the rate of loading as detailed elsewhere in this report.

6.2 Apparent elastic modulus of EAC and PC wearing surface materials

The apparent elastic modulus of the EAC wearing surface is relatively low (~40-70 ksi) and not as sensitive to temperature in the 60º-120ºF range. However, at colder temperatures (20º-35ºF range), the apparent elastic modulus, is significantly more sensitive to temperature reaching values in the 1,000-1,500 ksi range. The PC wearing surface is nearly linearly sensitive to temperature, varying from approximately 50 ksi at 120ºF to 1,000 ksi at 20ºF. While at the colder and hotter temperatures the EAC and PC materials exhibit nearly comparable modulus values, in the intermediate temperature range (50º – 90ºF), reflective of more common service temperatures, PC modulus is 4-8 fold of the EAC modulus. This has implications with regard to deflections, wearing surface and steel stresses, and as a result on fatigue performance in service as discussed earlier in Chapter 5 and elsewhere in this chapter. When cracks are present in the wearing surface, crack openings under load are also influenced by composite stiffness values.

6.3 Effect of wearing surface depth and local variations in depth

All tests in this investigation were performed on a nominal wearing surface depth of 2". It has been shown analytically, that while transverse bending maximum stresses in steel monotonically decreases with increases in wearing surface depth, the maximum wearing surface stress does not monotonically decrease with increases in wearing surface depth. Ensuring good depth control while placing the wearing surface will lead to better control of stresses in the wearing surface. Also, since it is expected that the San Mateo

Hayward bridge deck plate will contain bolted connections, more care towards wearing surface depth control at these locations is important to mitigate potential local cracking.

6.4 Fatigue performance

Both the wearing surface systems performed well at cold temperatures, surviving 10 million fatigue cycles without any cracking or other types of deterioration (slip, debonding, and delamination) at maximum fatigue load levels that are significantly more severe than design service loads expected. Both wearing surfaces experienced cracking at room and hot temperatures. It is likely that cracking in both these materials is governed more by strain magnitudes (rather than tensile strength) given the fatigue performance observed at the three test temperatures. Since tensile characteristics of these materials as a function of test temperatures was not readily available in the published literature and were beyond the scope of this investigation, this observation cannot be conclusively established. The PC wearing surface performed better (one specimen experiencing no cracking at all and one where cracks were initiated at 9.8 million fatigue cycles) than the EAC wearing surface in the room temperature tests, while the EAC wearing surface performed better than the PC wearing surface in the hot temperature tests (crack initiations were consistently very early in the fatigue loading for the PC specimens). Even while cracking occurred well within the limiting 10 million fatigue cycles, when tests on cracked specimens were carried out to the full 10 million fatigue cycles, these cracks did not result in wearing surface delamination or local debonding. In most instances these cracks were not visible in an unloaded state. When loaded to replicate the maximum flexural loads during post fatigue crack inspection, typical maximum crack widths of 0.2-

0.4 mm were measured. Even while the service loading may be lower than those used in these fatigue test, cracking is likely in the service performance of both EAC and PC wearing surface materials and it is prudent to have a crack maintenance program in place.

6.5 Hysteresis and loading rate effects

Both the EAC and PC composite specimens exhibited more pronounced hysteresis in the load-deflection response in the 60º-80ºF temperature range than at the colder or hotter temperatures. This phenomenological response has been predicted using an idealized tensile rheological model of the elastic steel and viscoelastic wearing surface composite. EAC exhibited more hysteresis than the PC material. The effect of loading rate on the apparent elastic modulus, also closely related to the viscous behavior of the wearing surface, was more pronounced at the slower rates of loading (typically less than 2.5 Hz) for both the EAC and PC materials. The change in apparent elastic modulus with loading rate was very minimal in the 2.5 – 15 Hz range of dynamic loading, at all three test temperatures for the PC composite specimens and at the cold and hot temperatures for the EAC composite specimens. EAC composite specimens continued to exhibit measurable increases in the apparent elastic modulus with increases in the loading rate in the 2.5 - 15 Hz range. These observations are unlikely to affect the service performance of these two wearing surface systems in any significant manner.

6.6 Tensile pull-out strength and use in quality control:

The average tensile bond strengths from successful pull-out of PC cores form the steel plate were 1,188 psi, 994 psi and 417 psi, at 32ºF, 75ºF and 122ºF, respectively. All these pull-out failures occurred due to an adhesive failure at the bond coat (i.e. at the

interface between the bond coat and the wearing surface). Despite fairly exhaustive attempts at identifying a glue, and/or additional mechanical modifications to pull out EAC cores from the steel plate, no successful cores of EAC were pulled out. Failures in EAC often happened at the glue line or cohesively in the wearing surface at smallest net cross-sections when mechanical anchors were used. The smoother well compacted top surface of these specimens did not allow good bonding of the pipe cap used in the pull-out test. Despite this, a lower bound of the tensile pull-out strength at room temperature could be estimated as 639 psi. Since no successful pull-out tests were completed at the room temperature, these tests were not attempted at the cold or hot temperatures. The above strength values far exceed the 200-250 psi specified for pull-out of wearing surface cores from the steel plate for previous wearing surface placement on orthotropic steel decks. Also, in any case, these tensile pull-out tests serve primarily for quality control purposes, both for initial wearing surface placement, as well as to identify potential areas where the wearing surface may have debonded from the deck due to local damage.

6.7 Cracking characteristics and need for maintenance:

EAC and PC specimens that cracked in the fatigue tests (room and hot temperatures only) typically had one single crack. Even when these cracks were loaded for several million additional fatigue cycles, these cracks did not appear to grow through the full depth of the wearing surface. This was confirmed by resistivity tests where even after 3 hours of ponding of detergent water on the cracked surface, resistivity values in excess of 4MΩ. The cracks in most of these specimens were not visible to the naked eye in an unloaded state. When loads replicating the maximum loads that these specimens

experienced in the test program were applied, typical maximum crack widths of 0.2 -0.4 mm were observed. Typical maximum crack widths of up to 1 mm were recorded for EAC composite specimens after static flexural failure testing. Crack widths of up to 0.3-0.4 mm were recorded for the PC composite specimens after static failure tests. It should be however be noted that higher loads (~6,300 lbs) were needed to reach the first-peak load for the EAC composite compared to the PC composite specimens (~4,050 lbs). Even at such large loads, no debonding or delamination of either wearing surface was observed. As noted earlier cracking is likely, even if localized, in the service performance of both EAC and PC wearing surface materials it is prudent to have an active crack maintenance program.

6.8 Consistency of mixture proportions and material properties

Results from this research demonstrate that there are measurable variations in material property and associated mechanical performance in the small scale fabrication of composite specimens. These variations were observed to be more significant for the PC material when compared to the EAC material. This can be attributed, in part, to the differences in the techniques used to mix and place the wearing surface materials, and in part to differences in the binder content and the significant influence of binder on the mechanical and physical properties of the resultant concrete. While these variations are likely to be greatly reduced in the larger volume field application of these wearing surfaces, it is recommended that rigorous controls of the mixture proportions immediately prior to placement be developed along with tight tolerances for placement conditions (temperature, humidity and level of cleanliness).

6.9 Field evaluation of test patches subjected to service conditions and loads

Test placement of the two wearing surfaces on one or adjacent lanes (20+ ft.) will serve to additionally complement information from this research. The 2" thick EAC has served Caltrans well as the original wearing surface for several decades without significant maintenance issues. The comparative study in this exhaustive laboratory investigation has shown that the 2" thick PC material, for which Caltrans has several decades of successful experience as overlays on concrete decks, could perform equally well on orthotropic steel decks. The field evaluation would provide valuable data on performance of these materials at locations where the deck plate is bolted. The smaller depths of the wearing surface over bolt heads as well as local stress concentrations at these locations may result in local cracking that could not be simulated in the laboratory tests. The field test placement would have the added advantage of subjecting the test patches to actual service loads and environmental conditions.

References

AISC (1963). Design Manual for Orthotropic Steel Plate Deck Bridges, American Institute of Steel Construction. Chicago, IL.

American Concrete Institute Committee 503 (ACI503R-93 – Reapproved 2008), "Use of Epoxy Compounds with Concrete," (Appendix A).

Barrett, D. (2003), "Fatigue Performance of Polymer Concrete Wearing Surfaces," M. S. Thesis, University of Missouri-Columbia, May 2003, 90 pp.

Braam, R., Kolstein, H., Romeijn, A, and Buitelaar, P. (2008), "Concrete Overlays to Improve the Fatigue Life of Movable Orthotropic Steel Bridges". Proceedings 2008 International Orthotropic bridge Conference, Sacramento, CA

Buitelaar, P. and Braam, R. (2008), "Application of Reinforced High Performance Concrete Overlays on Orthotropic Steel Bridge Decks – Theory and Practice", Proceedings 2008 International Orthotropic bridge Conference, Sacramento, CA

Cao, Wei-Min, "Polymer Concrete Wearing Surface System for Orthotropic Steel Plate Bridges", M.S. Thesis, University of Missouri – Columbia. Columbia, Missouri. May 1998.

Cullimore, M.S.G., Flett, I.D., and Smith, J.W. (1983), "Flexure of Steel Bridge Deck Plate with Asphalt Surfacing, IABSE Periodica, Vol. 1.

Gopalaratnam, V. S., (2009) "Stresses and Composite Action of the Wearing Surface in Orthotropic Steel Bridge Decks", University of Missouri Report,

Gopalaratnam, V. S., Baldwin, Jr., J.W., and Hartnagel, B.A. (1993-1995), Performance of Polymer Concrete Wearing Surface System on the Poplar Street Bridge Inspection Reports I-III, Report 92-5. Submitted to the Missouri Highway and Transportation Department.

Gopalaratnam, V.S., Baldwin Jr., J.W., and T. R. Krull (1993b) Application of Polymer Concrete Wearing Surface on the Poplar Street Bridge Deck: Construction Report," Final Report 92-5. Submitted to the Missouri Highway and Transportation Department, 30 pp.

Gopalaratnam, V.S., Baldwin Jr., J.W., Hartnagel, B.A., and Rigdon, R.A. (1993a), "Evaluation of Wearing Surface Systems for Orthotropic Steel-Plate-Bridge Decks," Final Report 89-2. Submitted to the Missouri Highway and Transportation Department, 64 pp.

Gopalaratnam, Vellore S., James W. Baldwin Jr., Bryan A. Hartnagel., Theodore R Krull., "Performance of Polymer Concrete wearing surface system on the Poplar

Street Bridge", Reports prepared for Missouri Highway and Transportation Department.

Gopalaratnam, V. S., J. W. Baldwin, Jr., and W.-M. Cao., "Temperature Dependent Performance of Polymer Concrete Wearing Surface System on the Poplar Street Bridge". Final Report RDT 99-001. Missouri Department of Transportation, Research, Development and Technology Division, Jefferson City, Jan. 1999.

Hartnagel, B.A., Gopalaratnam, V.S., and Baldwin Jr., J.W. (1991), "Challenges in Long-Term Deck Strain Measurements on Orthotropic Steel-Plate Decks," Proceedings of the 9th national Conference on Microcomputers in Civil Engineering, University of Central Florida, October 1991, pp. 101-105.

Hartnagel, Bryan A., "Long Term Deck Strain Measurements on an Orthotropic Steel-Plate Bridge Deck. M.S. Thesis, University of Missouri – Columbia. Columbia, Missouri. May 1993.

Hemeau, G., Puch, C., Ajour, A-M. (1981), Comportment a la fatigue en flexion sous moment negative, Bulletin de Liaison des Laboratoires des Ponts et Chaussees, Paris (in French).

Jong, F.B.P. de, Kolstein, M.H. (2004). "Strengthening a Bridge Deck with High Performance Concrete." Proc. of 2004 Orthotropic Bridge Conference, ASCE, Sacramento, CA, Aug. 25-27.

Jong, F.B.P. de, Kolstein, M.H. (2004). "Strengthening a Bridge Deck with High Performance Concrete." Proc. of 2004 Orthotropic Bridge Conference, ASCE, Sacramento, CA, Aug. 25-27.

Kolstein, H. and Sliederecht (2008), "Reduction of traffic induced stresses using reinforced high strength concrete, Proceedings 2008 International Orthotropic bridge Conference, Sacramento, CA, 11 pp.

Kolstein, H., and Wardenier, J. (1997), "Stress Reduction Due to Surfacing on Orthotropic Steel Decks," IABSE Workshop Proceedings, Lausanne, 1997.

Kolstein, H., Wardenier, J., "Stress reduction due to surfacing on orthotropic steel decks", IABSE Reports, 1997, ISSUE 76, pages 109-118

Kozy, B., Connor, R., Paterson, D., and Mertz, D. (2011). "Proposed revisions to the AASHTO LRFD Bridge Design Specifications for orthotropic steel deck bridges." J. Bridge Eng., 2011.16:759-767

Maggenti, R., (2001), "Polyester Concrete in bridge Deck overlays report", SFOBB East Spans Safety Project Skyway Structure, O4-ALA/SF-80-VAR

Mangus, Alfred R., and Sun, Shawn (2000). "Orthotropic Deck Bridges," Bridge Engineering Handbook, Chapter 14, edited by Chen, Wai-Fah and Duan, Lian. CRC Press LLC, Boca Raton, Florida

Manual for design, construction, and maintenance of orthotropic steel deck bridges, US Department of transportation federal highway administration.

Report on flexural testing of Epoxy Asphalt for Golden Gate Bridge deck renovation from the Office of Transportation Laboratory (1981), Department of transportation, State of California.

Rigdon, R.L., Gopalaratnam, V.S., and Baldwin Jr., J.W. (1991), "Automated Temperature Varying Flexural Fatigue Tests for Steel-Polymer Concrete Composite Specimens," Proceedings of the 9th national Conference on Microcomputers in Civil Engineering, University of Central Florida, October 1991

Rigdon, Robert L., "Wearing Surfaces for Orthotropic Steel Plate Bridges." M.S. Thesis, Univeristy of Missouri – Columbia. Columbia, Missouri. August 1990.

Seim, C., Ingham, T., (2004), "Influence of Wearing Surfacing on Performance of Orthotropic Steel Plate Decks", Transportation Research Record: Journal of the Transportation Research Board, No. 1892, TRB, National Research Council, Washington, D.C., 2004, pp. 98–106.

Seim, C., Manzanarez, R. (2004), "A Performance based surfacing for the orthotropic deck of the new San Francisco-Oakland bay bridge". 2004 Orthotropic bridge conference Sacramento, California, USA

Smith, J.W, Cullimore, M.S.G. (1987), "Stress reduction due to surfacing on a steel bridge deck" Steel Structures-Advances, Design and Construction; Cardiff; UK; 8-10 July 1987. pp. 806-814. 1987

Sogioka, K.,(2009), "Life cycle evaluation of fatigue mitigation for orthotropic steel bridge decks", PhD Thesis, Civil and Natural Resources Engineering, University of Canterbury

Touran, A., and Okereke, A. (1991), "Performance of Orthotropic Bridge Decks", ASCE Journal of Performance of Constructed Facilities, 5(2), May 1991

Weidlinger Associates, Inc. (2002) "Bronx-Whitestone Bridge Deck Replacement Project," Personal correspondence,

Wolchuck, R., (1999) "Steel orthotropic decks: developments in the 1990's", Transportation Research Record: Journal of the Transportation Research Board, Volume 1688 / 1999, pp. 30-37

Wolchuk, R. (2002), “Structural behavior of surfacings on steel orthotropic decks and considerations for practical design” Structural Engineering International, Volume 12, Number 2, 1 May 2002 , pp. 124-129(6)

Wolchuk, R., (2006), “Prefabricating Standard Orthotropic Steel Decks,” Modern Steel Construction, December 2006

Appendix

Geometric and Physical Properties of Wearing Surface Materials

Table A1 Properties of Epoxy Asphalt Concrete (EAC) specimens

Specimen ID	Weight (lbs)	Total depth of the Specimen (in)	Width of the Wearing Surface (in)	Density of Wearing Surface (pcf)
EA01[1]	26.6	2.604	4.038	160
EA02[1]	26.9	2.604	4.033	160
EA03[1]	27.1	2.607	4.035	159
EA04[2]	28.4	2.655	4.040	160
EA05[3]	28.4	2.655	4.030	162
EA06	28.4	2.619	4.047	163
EA07	28.4	2.623	4.051	163
EA08	28.4	2.591	4.038	163
EA09	28.4	2.595	4.047	163
EA10	28.4	2.618	4.041	163
EA11	28.6	2.612	4.051	159
EA12	28.6	2.590	4.047	159
EA13	28.6	2.609	4.033	159
EA14	28.6	2.592	4.044	159
EA15	28.4	2.603	4.028	163
EA16	28.4	2.607	4.030	163
EA17	28.4	2.625	4.034	163
EA18	28.4	2.621	4.031	163
EA19	28.4	2.624	4.015	163
EA20	28.4	2.615	4.014	163
EA21	28.4	2.615	4.024	163
EA22	28.4	2.612	4.034	163
Average	28.2	2.6	4.0	161.4
Standard Deviation	0.564	0.017	0.010	1.683
Coeff. of Variation (%)	1.999	0.656	0.251	1.043

[1] Measurements made after the coring operation.

[2] Values provided by Chem Co were reported due to the lack of availability of specimens during measurements

[3] Average values reported because of the lack of availability of specimens during the measurements

Table A2 Properties of Polyester Concrete (PC) specimens

Specimen ID	Weight (lbs)	Total depth of the Specimen (in)	Width of the Wearing Surface (in)	Density of Wearing Surface (pcf)
PC01	25.2	2.553	4.048	140
PC02	26.8	2.629	4.057	138
PC03	26.4	2.607	3.995	138
PC04	27.0	2.684	4.036	140
PC05	27.2	2.692	4.074	137
PC06[4]	27.2	2.713	4.017	149
PC07[4]	27.2	2.713	4.017	149
PC08[5]	27.2	2.774	4.038	149
PC09[5]	27.5	2.805	4.010	149
PC10	27.4	2.686	3.988	145
PC11	27.0	2.617	4.008	140
PC12	27.6	2.762	4.017	148
PC13	27.2	2.741	4.006	137
PC14	27.9	2.763	4.012	140
PC15	27.6	2.737	4.031	139
PC16	27.1	2.722	4.033	141
PC17	27.3	2.721	3.993	138
PC18	27.5	2.797	4.004	141
PC19	27.5	2.748	4.001	138
PC20[5]	27.2	2.660	3.997	149
PC21	27.2	2.704	4.002	140
PC22	27.7	2.802	4.023	140
PC23	27.3	2.740	3.990	141
PC24	27.4	2.752	4.017	140
Average	27.2	2.7	4.0	141.8
Standard Deviation	0.523	0.064	0.022	4.222
Coeff. of Variation (%)	1.924	2.375	0.544	2.978

[1] Measurements made after the coring operation.

[2] Values provided by ChemCo were reported due to the lack of availability of specimens during measurements

[3] Average values reported because of the lack of availability of specimens during the measurements

Table A3 Grading table of B39 aggregate used for Polyester Concrete mix

Screen Size	% Passing
9.5mm	100
4.75mm	70
2.36mm	50
1.18mm	44
600um	30
300um	5-20
150um	1
75um	T

Fig. A1 Aggregate grading chart for EAC Specimens

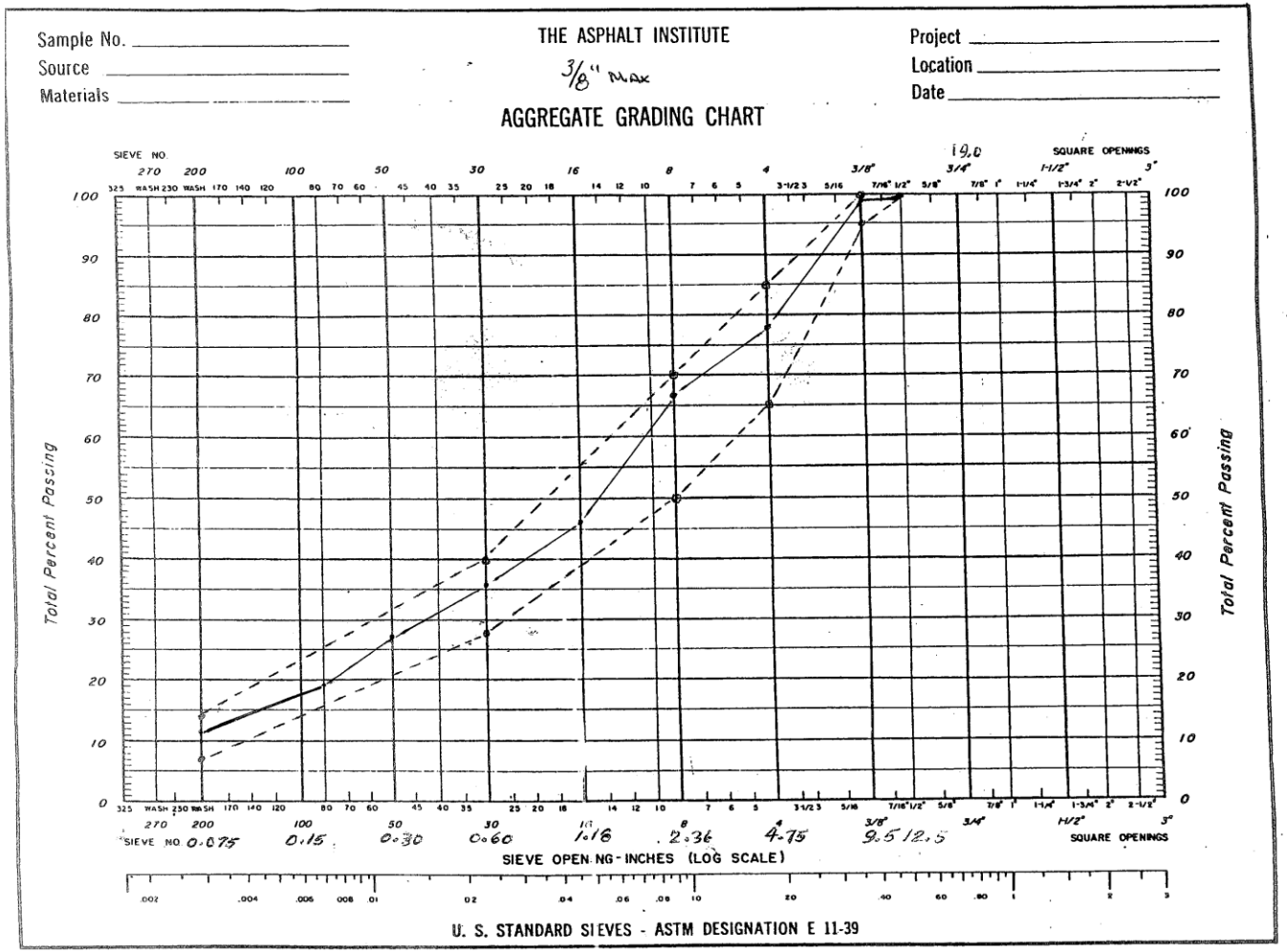

Table A4 Polyester Concrete Mix proportions of different batches used

Specimen ID's	Rock (lb)	Sand (lb)	Resin (lb)	DDM9 (gm)
PC01 to PC05	16.6	33.4	6.10	55.6
	11.0	22.0	4.04	27.5
PC06 to PC11	11.0	22.0	4.00	27.6
	11.0	22.0	4.00	26.0
PC12 to PC17	11.0	22.0	4.00	27.0
	11.0	22.0	4.00	27.2
PC18 to PC24	13.2	26.4	4.86	33.1
	13.2	26.4	4.90	33.1
	13.2	26.4	4.90	33.2

Table A5 Calibration factors of flexural load cells

Calibration factors	**10**	**1**	**0.1**	**0.01**	**Average**
Load Cell 1	278.208	278.046	277.977	277.812	278.011
Load Cell 2	272.509	272.039	271.727	271.398	271.918
Load Cell 3	282.227	281.797	281.681	281.414	-281.78
Load Cell 4	284.052	282.821	282.315	281.942	282.782

Table A6 Calibration factors for different clip gages used in various flexural tests

Clip Gauge ID	Calibration factor[1]
Clip Gauge 01	0.003515
Clip Gauge 02	0.004049
Clip Gauge 03	0.003579
Clip Gauge 04	0.003527
Clip Gauge 05	0.003998
Clip Gauge 06	0.003743
Clip Gauge 07	0.003778
Clip Gauge 08	0.003663
Clip Gauge 09	0.003840
Clip Gauge 10	0.003515
Clip Gauge 11	0.004181
Clip Gauge 12	0.004128
Clip Gauge 13	0.003964
Clip Gauge 14	0.003857
Clip Gauge 15	0.003352
Clip Gauge 16	0.003788
Clip Gauge 17	0.003837
Clip Gauge 18	0.003764
Clip Gauge 19	0.003933
Clip Gauge 20	0.003722